Corrosion and Transport Processes in Cracks

by

R. R. Shuck*

May 1971

*Now at Republic Steel Corporation Research Center, P. O. Box 7806, Cleveland, Ohio 44131.

This research was supported by the Advanced Research Project Agency, Order #878, Department of Defense under N00014-67-A-0314-0008, and also by NASA Research Grant NGR 39-002-023. Distribution of this document is unlimited and reproduction in whole or in part is permitted for any purpose of the U. S. Government.

ACKNOWLEDGMENTS

Many people have at one time or another made substantial contributions to the effort which has resulted in this thesis. I am indebted to Professor J. L. Swedlow for his guidance over the past five years. Discussions with Professors H. W. Paxton and F. Osterle helped to mold and focus the ideas presented here. Of special value have been the many long discussions into the early morning hours with my brother David.

Acknowledgments are also due to the many organizations which have provided fellowship support and funding for computer time: National Aeronautics and Space Administration; Advanced Research Projects Agency of the U. S. Department of Defense; Inland Steel Corporation; and the Office of Education of the U. S. Department of Health, Education, and Welfare.

I am especially grateful to my wife and to my mother and father for their encouragement, confidence, and support.

ABSTRACT

A numerical method for solving the electrochemical transport equations subject to an arbitrary set of charge-transfer boundary conditions is presented. The method is based on a two-dimensional time-dependent formulation of the equations derived from dilute solution theory. It is applied to a study of corrosion and transport processes in crack-like regions. The results show that the average species fluxes normal to the metal-electrolyte interface, the crack length, and the crack aspect ratio are the most important factors affecting the electrolyte composition. Other factors, such as the crack shape, the form of the boundary conditions, and the transport mode, also affect the composition; but, these factors are of secondary importance.

TABLE OF CONTENTS

I. INTRODUCTION

The transport of ions in electrolytic solutions plays an important role in every electrochemical process. Just how important is determined by several factors, but electrode geometry is the primary one. When the geometry is simple, as in the electroplating of continuous steel strip, ion transport is important only at high current densities. When the electrode geometry is more complex, as in the plating of bolts and nuts and baby shoes, the distribution of the plating current is strongly affected by the shape of the part, and transport in the bulk electrolyte is important even at low current densities. For decorative or ornamental plating, the uniformity of the current distribution may be unimportant; but for precision parts plated to obtain specific engineering properties, control of the plating thickness is necessary to control both product quality and production costs.

In this work we are concerned with ion transport as it affects the electrochemical corrosion of metals. The geometry considered is a surface discontinuity such as a pit, crack, or crevice on an otherwise smooth electrode surface. The importance of this geometry in metal corrosion may be seen by inspection of any bridge in Pittsburgh. The attack is relatively mild and fairly uniform along the expanse of the main structural members, and concentrated around the joints, brackets, and cover plates. The attack may be particularly severe around bolts and rivets. In general, any point where two parts join, forming a crack or crevice, is a point of accelerated corrosive attack.

The rate of attack in a pit or crevice is often large and may be difficult to control. The overall corrosion current typically increases by more than an order of magnitude

at the onset of pitting corrosion [1].* Depending on pit size and distribution, the current density in the pits themselves may increase by more than two orders of magnitude. Crevice corrosion may be associated with equally large currents. This is a major nuisance in polarization experiments, since specimens must be mounted with extreme care to control such corrosion and obtain uniform current densities [2].

Why surface discontinuities such as cracks increase the corrosion rate is poorly understood. In part, this is due to not knowing the electrolyte composition in such a region. Sampling the electrolyte in a crack poses some difficult experimental problems, so most of the composition estimates have been based on indirect observations. The work reported by B. F. Brown, C. T. Fujii and E. P. Dahlberg [3] is a notable exception. By the rapid freezing of specimens, they obtained samples of the electrolyte in propagating stress corrosion cracks tested in neutral salt solutions. They found the pH to be substantially less than that of the bulk electrolyte for all of the metals tested.

While the rapid freezing technique is promising, the small volume to be sampled constitutes a formidable obstacle to the experimental study of solution chemistry in crack-like regions. Size imposes no restrictions, however, on a theoretical study of such problems. There are well-developed theories describing both ion transport and electrochemical reaction rates. The theories have been successfully applied in a variety of electrochemical transport problems [4] and in the kinetic analysis of many charge-transfer reactions [5]. These facts suggest that the theory might be successfully applied to the study of solution chemistry in crack-like regions.

---

* Numbers in brackets designate References.

The theoretical study of corrosion and transport in crack-like regions has received little previous attention. J. G. Hines [6] derived a formula for the steady-state potential drop in a wedge-shaped crack assuming constant electrolyte resistivity and negligible transport by diffusion. Somewhat more sophisticated analyses have been presented by D. A. Vermilyea and C. S. Tedmin, Jr. [7] and by W. D. France, Jr. and N. D. Greene, Jr. [8]. However, both of these analyses are based on highly simplified models of electrolyte behavior.

T. R. Beck [9, 10] has presented a model of the electrochemistry of stress corrosion cracking in titanium alloys. Beck's 'MKT' model is the most comprehensive theoretical analysis published to date. The crack is treated as a one-dimensional continuum, and the system is assumed to be at steady state. Convective transport is neglected. The electrolyte contains three ions, two singly-charged salt ions and the hydrogen ion. The reactions at the metal-electrolyte interface are based on those observed experimentally. The transport equations are solved numerically using as additional boundary data experimentally observed values of current density and potential.

R. C. Alkire, E. A. Grens II, and C. W. Tobias [11] recently presented an analysis which is potentially more powerful than the method used by Beck. Although the method was developed to study porous electrodes, it is directly applicable to a pit-like region and with simple modification may be applied to a crack-like region. Like Beck's, theirs is a one-dimensional, quasi-steady state analysis. In their formulation, however, there is no intrinsic limitation to the number of ions and no boundary data other than reaction kinetics are required. The results presented to date are fragmentary and the work is continuing.

All of the studies above are based on a simplified

formulation of the transport equations, but they have been extremely useful in helping to understand corrosion in crack-like regions. In particular, the model developed by Beck has been a powerful tool in developing an understanding of the role of electrochemistry in stress corrosion cracking.

The successful application of electrochemical transport theory to the study of electrochemical phenomena, including those in crack-like regions, and the relative difficulty involved in the experimental study of such phenomena provided the motivation for the present work. The work consists of two parts. In the first, the transport equations are presented and the method developed for their solution is discussed. The method is based on the use of an Alternating-Direction Implicit (ADI) technique to obtain the time-dependent solution to a two-dimensional formulation of the ion transport equations. The boundary data may be of quite general form. Concentration, concentration gradient, ion flux, or charge-transfer boundary conditions may be used.

In the second part, the solution technique is employed in a systematic analysis of the factors influencing solution chemistry and ion transport in crack-like regions. These results are then extended using a one-dimensional formulation of the ion transport equations. Finally, certain aspects of stress corrosion cracking are discussed in the perspective of the results obtained from the transport analysis.

II. TRANSPORT IN ELECTROLYTIC SOLUTIONS

In this section the equations describing mass transport in electrolytic solutions are presented. The equations are based on the theory of dilute electrolytes. Several additional assumptions are then introduced; these are discussed and their implications considered. Boundary conditions are then examined, and, because it plays a key role in the theory, the electroneutrality equation is discussed in some detail. The section concludes with a discussion of the behavior of the field equations and boundary conditions under the class of coordinate transformations used in the numerical calculations.

The Field Equations

The difference between an electrolyte and an ordinary solution is that the dissolved species may exist as charged particles or ions rather than as uncharged atoms or molecules. The solvent itself is electrically neutral but has a sufficiently large dielectric constant to make the existence of the solute in the form of ions energetically favorable. The solvent may be a solid, liquid, or gas. In this work, however, it is assumed that the solvent is water.

The first element required to describe mass transport is a relation between mass flux and the forces which induce that flux. In this work, the flux equation based on the theory of dilute electrolytes (the Nernst-Planck equation) is used. In developing this equation it is assumed that the total flux can be expressed as the sum of the fluxes due to migration in an electrostatic field, simple diffusion, and solvent convection. The equation is written

$$\underline{J_i} = -z_i m_i \mathfrak{F} c_i \nabla \Phi - D_i \nabla c_i + c_i \underline{v} \qquad (1)$$

where

$\underset{\sim}{J_i}$ = mass flux of ith dissolved species (mole/cm^2-sec)

z_i = valence or charge number of ith species (equiv/mole)

m_i = mobility of ith species (mole-cm^2/joule-sec)

$\mathfrak{F}$ = Faraday's constant (96,520 coul/equiv)

C_i = concentration of ith species (mole/cm^3)

Φ = electrostatic potential (volts)

D_i = diffusion coefficient of ith species (cm^2/sec)

$\underset{\sim}{v}$ = solvent velocity (cm/sec)

∇ = 'del' operator = $\underset{\sim}{i}\frac{\partial}{\partial x} + \underset{\sim}{j}\frac{\partial}{\partial y} + \underset{\sim}{k}\frac{\partial}{\partial z}$

and $\underset{\sim}{i}$, $\underset{\sim}{j}$, and $\underset{\sim}{k}$ are the unit vectors in the three cartesian coordinate directions, x, y, and z.

Following the usual convention, the gradient of the electrostatic potential is the negative of the electric field strength. The mobility, m_j, may be interpreted as the average velocity, in meters per second, of the ith dissolved species when acted on by a force of one newton per mole regardless of the origin of that force. The mobility and diffusion coefficient are related by the generalized Nernst-Einstein equation.

$$D_i = m_i RT\left[1 + \frac{d(\ln \gamma_i)}{d(\ln C_i)}\right] \qquad (2)$$

where

R = universal gas constant (8.317 joule/mole-$^\circ$K)

T = absolute temperature ($^\circ$K)

γ_i = activity coefficient of ith species (dimensionless)

Each dissolved species also satisfies an equation of continuity or mass conservation.

$$\frac{\partial C_i}{\partial t} = -\nabla \cdot \underline{J}_i + G_i \qquad (3)$$

where

t = time (sec)

G_i = rate of generation of ith species (mole/cm^3-sec)

The quantity G_i in equation (3) may be positive, negative, or zero. If the ith dissolved species enters a homogeneous chemical reaction as a product, G_i is positive; if it enters as a reactant, G_i is negative; otherwise it is zero.

If a homogeneous reaction is to be included in the analysis, a relation between the rates of generation of the participating species and their concentrations must be found. Consider, for example, a simple association-dissociation reaction of the form

$$S_L + S_M \rightleftharpoons S_N \qquad (4)$$

Equation (4) states that one mole of species L combines with one mole of species M to form one mole of species N. The rates of generation of the participating species may be expressed with sufficient accuracy by an equation of the form

$$-G_L = -G_M = G_N = k_a C_L C_M - k_d C_N \qquad (5)$$

where

k_a = forward rate constant (1/mole-cm^3-sec)

k_d = backward rate constant (1/cm^3-sec)

While the rate constants, k_a and k_d, have the dimensions indicated, the units are usually suppressed when there is no ambiguity in their meaning. The forward and backward rate constants are related to the equilibrium constant, K_{eq}, by the equation

$$K_{eq} = \left(\frac{C_N}{C_L C_M}\right)_{C_N=0} = \frac{k_a}{k_d} \qquad (6)$$

In this work the solvent is assumed to be electrically neutral and non-conducting. (The small conductivity of pure water is due to the presence of hydrogen and hydroxyl ions resulting from the equilibrium, $H^+ + OH^- = H_2O$.) Thus, every homogeneous reaction must satisfy the requirement of charge neutrality. In the reaction described by equation (4), for example, the charge numbers of species L, M, and N satisfy the equation

$$Z_L + Z_M = Z_N \qquad (7)$$

If, for the moment, the convective term in the flux equation is set equal to zero, one more equation is required to complete the set of field equations. That equation is a relation between the electrostatic potential and the charge density. The most accurate physical description is provided by Gauss' law. For a medium with a constant dielectric strength, this may be written as

$$\nabla^2 \Phi = -\frac{\mathcal{F}}{\epsilon} \sum_{i=1}^{N_s} Z_i C_i \qquad (8)$$

where

ϵ = dielectric constant (coul/volt-cm)
(7.083×10^{-12} for H_2O)

N_s = total number of dissolved species in the electrolyte

As an alternative, it may be assumed that the charge density is everywhere zero. This assumption is a good approximation for electrolytes that are sufficiently concentrated. The condition of zero charge density or electroneutrality is written

$$\sum_{i=1}^{N_s} Z_i C_i = 0 \qquad (9)$$

It should be emphasized that either one of equations (8) and (9) may be used but not both. The use of equation (9) does not imply that the electrostatic potential satisfies Laplace's equation ($\nabla^2 \Phi = 0$). In this work the electroneutrality equation is employed. The relative merits of this formulation are considered below.

To the equations already discussed must be added those describing the motion of the solvent. These are a continuity equation, a momentum equation, and an equation of state. The continuity equation for the solvent is

$$\frac{\partial \rho}{\partial t} + \nabla \cdot (\rho \underline{v}) = 0 \qquad (10)$$

where

ρ = density of the solvent (gram/cm^3)

For a Newtonian fluid with constant viscosity, conservation of momentum is expressed by the Navier-Stokes equation

$$\rho \frac{D\underline{v}}{Dt} = -\nabla P + \underline{\chi} + \mu \nabla^2 \underline{v} \qquad (11)$$

where

P = hydrostatic pressure (dyne/cm^2)

$\underline{\chi}$ = body force per unit volume (dyne/cm^3)

μ = coefficient of viscosity (dyne-sec/cm^2)

$\frac{D}{Dt}$ = material derivative ($\frac{\partial}{\partial t} + \underline{v} \cdot \nabla$)

There is no a priori constraint on the form of the body force, $\underline{\chi}$, in equation (11). Typically, however, one is concerned with forces which are expressible as the gradient of a potential, for example, the gravitational force. It is convenient to separate the body force into two components: that arising from a non-zero charge density in the solution, and that due to all other causes. Thus, the body force may be written as

$$\underline{\chi} = -10^7 \mathfrak{F} \left(\sum_{i=1}^{N_c} Z_i C_i \right) \nabla \Phi + \underline{\chi}^* \qquad (12)$$

where

χ^* = body force from all sources other than charge (dyne/cm^3)

The factor, 10^7, appearing in the equation results from the conversion of energy units from joules to ergs. Using

equation (8), equation (12) may also be written

$$\underline{\chi} = 10^{7}\epsilon\left[\nabla^{2}\Phi\right]\nabla\Phi + \underline{\chi}^{*} \tag{13}$$

Examination of equations (11) and (13) reveals that the motion of the solvent is coupled to the motion of the solute species through the electrostatic body force. This coupling is fundamental to the description of phenomena such as mass transport through membranes and capillaries.

The equation of state is an expression relating the solvent density to its temperature and pressure. For an aqueous electrolyte at room temperature, subjected to small gradients of temperature and pressure, the solvent may be assumed incompressible. Making this assumption, the equation of state is

$$\rho = \rho_{0} = \text{constant} \tag{14}$$

The concept of electrical current is closely related to the ideas of mass transport in electrolytic solutions. It is frequently useful, and occasionally necessary, to express mass fluxes in terms of current densities. Since a current is simply a net flux of charge and the solvent is non-conducting, the current density may be written as

$$\underline{I} = \mathfrak{F}\sum_{i=1}^{N_{s}} z_{i}\underline{J}_{i} \tag{15}$$

where

$\underline{I}$ = current density (amp/cm^{2})

Equation (15) may be rewritten using equation (1) to

express the fluxes and equation (9) to eliminate the coefficient multiplying the solvent velocity. The result is

$$\underline{I} = -\left[\mathcal{F}^2 \sum_{i=1}^{N_s} z_i m_i c_i\right] \nabla\Phi - \nabla\left[\mathcal{F} \sum_{i=1}^{N_s} z_i D_i c_i\right] \qquad (16)$$

The second term on the right is zero when the composition of the electrolyte is identical at every point or when the diffusion coefficients are all the same. In this case, equation (16) reduces to Ohm's law.

$$\underline{I} = -\kappa \nabla\Phi \qquad (17)$$

where

κ = solution conductivity (1/ohm-cm) = $\left(\mathcal{F}^2 \sum_{i=1}^{N_s} z_i^2 m_i c_i\right)$

From equations (3), (9), and (15), it may be shown that

$$\nabla \cdot \underline{I} = 0 \qquad (18)$$

Equations (16) and (18) were obtained using the electroneutrality equation (eqn. 9). If equation (8) were used instead, the equations would have a more complex form.

In the earlier discussion of electroneutrality and Gauss' Law, it was observed that one of the two should be used, but not both. Thus the electrostatic potential does not, in general, satisfy Laplace's equation. To emphasize this further, equations (16) and (18) may be used to obtain the differential equation that the electrostatic potential does satisfy.

$$\left[\sum_{i=1}^{N_s} z_i^2 m_i c_i\right]\nabla^2\Phi + \nabla\left[\sum_{i=1}^{N_s} z_i^2 m_i c_i\right]\cdot\nabla\Phi + \nabla^2\left[\frac{i}{\mathfrak{F}}\sum_{i=1}^{N_s} z_i D_i c_i\right] = 0 \qquad (19)$$

Equations (1), (2), (3), (9), (10), (11), (13), and (14) form the complete set of field equations describing mass transport in electrolytic solutions. The assumptions made in obtaining them do not seriously restrict their application. In using the equations here, however, several additional assumptions have been made and these are examined below. In some cases they have been dictated by necessity; in others, they are made for the purposes of simplicity only.

It has been assumed that the solution is 'ideal' so the individual ion activity coefficients are all unity. With this assumption equation (2) reduces to

$$D_i = m_i RT \qquad (20)$$

The assumption implies that the ion diffusion coefficients are concentration independent. Also, it limits the coupling between ions to that arising from the action of the electrostatic potential. The difference between a diffusion coefficient at extreme dilution and one at one mole per liter is typically about twenty to thirty percent. By proper selection of the concentration at which a diffusion coefficient is evaluated, the variation in a particular problem can usually be made much less than this.

Neglecting ion-ion interactions is more restrictive than simply ignoring changes in the diffusion coefficients with concentration. But, there is very little published data on the thermodynamic properties of other than single-salt electrolytes, so there is no practical basis for

evaluating the necessary activity coefficients. If one wanted to study such ion-ion interactions, the practical difficulties notwithstanding, it would be preferable to use a different formulation of the flux equation (see, for example, Reference 12).

Several assumptions have been made to simplify the equations describing the solvent velocity and to decouple these equations from those describing ion transport. The first is that the solvent velocity is slowly time-varying. For an aqueous electrolyte, the rate at which an ion concentration reaches steady state is two to three orders of magnitude slower than the rate at which the solvent velocity reaches steady state following a step change in a displacement boundary condition. Since the time scale is determined by the rate of diffusion, this assumption introduces no serious error.

It is also assumed that the acceleration terms on the left-hand side of the Navier-Stokes equation are negligible with respect to the viscous terms on the right-hand side. Since the Reynolds number is less than 10^{-4} for all the problems considered here, this assumption introduces no serious error.

To decouple the equations governing the solvent motion from those governing ion transport, it is assumed that the body force in the Navier-Stokes equation is zero. The justification for this does not rest with the use of the electroneutrality equation as opposed to Gauss' law. Even when using the electroneutrality equation, equation (13) should be used to express the body force.

The electrostatic body force increases as the current density increases and as the electrolyte concentration decreases. It is negligible with respect to the viscous force when the current density is sufficiently small and the electrolyte concentration is sufficiently large. It is

difficult to establish a priori how small is 'sufficiently small' or how large is 'sufficiently large'. Equation (13) may be used after the fact, however, to estimate the magnitude of the electrostatic body force using the value of the electrostatic potential from the solution of the ion transport equations. This has been done for the problems considered in this work. The electrostatic body forces are negligible in every case.

Equation (11) may be rewritten using these assumptions.

$$-\nabla P + \mu \nabla^2 \underline{v} = 0 \tag{21}$$

The final simplification is to restrict attention to planar problems. If x, y, and z are the three orthogonal axes of a rectangular cartesian coordinate frame, and ζ is any function of the independent coordinates, this assumption may be written as

$$\frac{\partial \zeta}{\partial z} = 0 \tag{22}$$

These are the assumptions made in this study. They are typical of those usually made and are less restrictive than the assumptions invoked in most applications of the theory (see, for example, Reference 4). We have discussed them both to indicate the limitations of the theory used here and to provide a more complete view of the general theory than was presented above [12].

With the above assumptions, the field equations may be written in more compact form. Using equations (14) and (22), equation (10) becomes

$$\nabla \cdot \underline{v} = \frac{\partial v_x}{\partial x} + \frac{\partial v_y}{\partial y} = 0 \tag{23}$$

Equation (23) is satisfied identically using a stream function, Ψ, defined by

$$\underset{\sim}{v} = \text{curl}(\Psi \underset{\sim}{k}) = \frac{\partial \Psi}{\partial y}\underset{\sim}{i} - \frac{\partial \Psi}{\partial x}\underset{\sim}{j} \tag{24}$$

Using equation (21) and the stream function defined by equation (24), it follows that

$$\nabla^4 \Psi = 0 \tag{25}$$

$$\nabla^2 P = 0 \tag{26}$$

where P and $\rho\nabla^2\Psi$ satisfy the Cauchy-Riemann conditions

$$\frac{\partial P}{\partial x} = \frac{\partial}{\partial y}[\rho\nabla^2\Psi], \qquad \frac{\partial P}{\partial y} = -\frac{\partial}{\partial x}[\rho\nabla^2\Psi] \tag{27}$$

Combining equations (1) and (3) and using equations (20) and (24), the concentration of each dissolved species satisfies the equation

$$\frac{\partial C_i}{\partial t} = Z_i D_i C_i \nabla^2\phi + Z_i D_i \nabla C_i \cdot \nabla\phi + D_i \nabla^2 C_i - \nabla C_i \cdot \text{curl}(\Psi \underset{\sim}{k}) + G_i \tag{28}$$

where

$$\phi = \left(\frac{\mathcal{F}\Phi}{RT}\right) = \text{dimensionless potential} \tag{29}$$

$\left(RT/\mathcal{F}\right)$ = 25.6 millivolts at 25°C

The system of field equations is thus reduced to

equation (25), N_s equations of the form of equation (28), and the electroneutrality equation (eqn. 9).

Boundary Conditions

Consider a domain, $\mathcal{D}$, lying in the x-y plane and bounded by a curve, β. Let $\underset{\sim}{n}$ and $\underset{\sim}{t}$ be the cartesian unit normal and tangential vectors to the curve β, respectively. Following the usual convention, the unit normal is positive outward; the tangent vector is positive in the counterclockwise direction. Within $\mathcal{D}$ all the necessary functions are assumed to be defined, continuous, and have as many continuous derivatives as may be required.

It is convenient here and in later sections to use subscript notation to denote both vector components and partial differentiation. A subscript appearing alone indicates a vector component. A subscript following a comma indicates differentiation with respect to that variable. For example, if $\underset{\sim}{V}$ is a vector,

$$\underset{\sim}{V} = V_x \underset{\sim}{i} + V_y \underset{\sim}{j} = V_n \underset{\sim}{n} + V_t \underset{\sim}{t} \qquad (30\text{-a})$$

and

$$\nabla \cdot \underset{\sim}{V} = \frac{\partial V_x}{\partial x} + \frac{\partial V_y}{\partial y} = V_{x,x} + V_{y,y} = V_{n,n} + V_{t,t} \qquad (30\text{-b})$$

With this notation in mind, consider the boundary conditions for the stream function, Ψ. Within the domain, Ψ satisfies the biharmonic equation. Since the equation is fourth order, two constraints must be imposed at every boundary point. From the definition of Ψ (eqn. 24), the most natural boundary data are

$$\Psi_{,n}\Big|_\beta = -\hat{v}_t, \qquad \Psi_{,t}\Big|_\beta = \hat{v}_n \qquad (31)$$

where

$\hat{v}_n$ = velocity component normal to the curve β

$\hat{v}_t$ = velocity component tangential to the curve β

In practice, it is usually more convenient to use the value of the stream function than its tangential derivative. When $\hat{v}_n$ is known, the stream function is easily obtained by integration. If s is the coordinate measured along β,

$$\Psi(s) = \Psi(o) + \int_o^s \Psi_{,\tau}\, d\tau = \Psi(o) + \int_o^s \hat{v}_n(\tau)\, d\tau \qquad (32)$$

where the integral is taken in the counterclockwise direction. Since the fluid velocity is independent of the absolute value of Ψ, the integration constant $\Psi(o)$ may be assigned any convenient value.

In this work our primary concern is transport in a crack-like region. In this case, the boundary coincides over a portion of its length with a solid-liquid phase boundary and the fluid motion is induced by the motion of the solid boundary. The velocity of the solid boundary is independently specified and it is assumed that the fluid velocity is, at every point on the solid-liquid boundary, the same as that of the solid (the so-called zero-slip condition).

Along a line of symmetry, the tangential velocity is usually unknown; if so, it is impossible to prescribe the normal derivative of the stream function. However, the tangential velocity typically has an extreme value, so the specification of the first normal derivative may be replaced by

$$\Psi_{,nn}\Big|_\beta = \hat{v}_{t,n} = 0 \qquad (33)$$

For problems involving mass transport in a crack-like region there is generally no precise definition of the fluid velocity along that portion of the boundary corresponding to the mouth of the crack. Here it is necessary to construct approximate boundary conditions. This may be done using the lowest order polynomial that satisfies the differential equation and is consistent with the other boundary data.

The boundary specification for the ion transport equations is more involved than that for the stream function. For a solvent containing N_s dissolved species, equations (9) and (28) constitute a system of $(N_s + 1)$ equations in $(N_s + 1)$ unknowns. N_s of these are parabolic partial differential equations (first order in time and second order in space) and one is algebraic. Suppose that N_c $(N_c \leq N_s)$ species have non-zero charge numbers while $(N_s - N_c)$ have zero charge numbers. The $(N_s - N_c)$ equations are then independent; their solution reduces to the solution of $(N_s - N_c)$ separate differential equations.

The remaining equations are coupled through the electroneutrality equation. While these have a linear form, they are in general quasi-linear since the electrostatic potential is itself a function of the concentrations.

Besides the coupling of the equations, the remaining system of $(N_c + 1)$ equations is remarkable because of the character of the coupling. Since the electroneutrality equation is algebraic, the N_c concentrations are linearly dependent. This means that exactly N_c [rather than $(N_c + 1)$] conditions must be imposed at each boundary point, and these must be such that one is effectively a boundary condition on the electrostatic potential.

With the above remarks in mind, consider some of the forms which the boundary and initial conditions may assume. The initial data must be of rather simple form. The concentrations of $(N_c - 1)$ of the ions may be arbitrarily specified

as functions of the spatial coordinates. The concentration of the remaining ion is then fixed by electroneutrality. Because the differential equation for the electrostatic potential exhibits no explicit time dependence (see eqn. 19), the initial value of the potential is determined by the initial values of the ion concentrations and the boundary conditions.

The boundary conditions may take any one of a variety of forms. However, all must satisfy the constraint imposed by electroneutrality. Those easiest to use are the ones that reduce to one of the classical forms for a second order partial differential equation.

If s is the coordinate measured along β, Dirichlet boundary conditions are of the form

$$C_i \Big|_\beta = \hat{C}_i(s) \qquad i = 1,(N_s-1) \tag{34-a}$$

$$C_{N_s}\Big|_\beta = \frac{-1}{Z_{N_s}} \sum_{i=1}^{N_s-1} Z_i \hat{C}_i(s) \qquad Z_{N_s} \neq 0 \tag{34-b}$$

$$\Phi \Big|_\beta = \hat{\Phi}(s) \tag{34-c}$$

where $\hat{C}_i(s)$ and $\hat{\Phi}(s)$ are arbitrary functions of the coordinate s.

Neumann boundary conditions are of the form

$$\nabla C_i \cdot \underline{n} \Big|_\beta = C_i^*(s) \qquad i = 1,(N_s-1) \tag{35-a}$$

$$\nabla C_{N_s} \cdot \underline{n} \Big|_\beta = \frac{-1}{Z_{N_s}} \sum_{i=1}^{N_s-1} Z_i C_i^*(s) \qquad Z_{N_s} \neq 0 \tag{35-b}$$

$$\nabla\phi\cdot\underset{\sim}{n}\Big|_{\beta} = \phi^{*}(s) \qquad (35\text{-c})$$

where $C_i^{*}(s)$ and $\phi^{*}(s)$ are arbitrary functions of the coordinate s along β.

While Dirichlet and Neumann boundary conditions are easy to apply, the normal derivative of ϕ can seldom be independently specified, and it is usually necessary to use the normal flux. From equations (1), (20), and (29), the flux of the ith species is

$$\underset{\sim}{J_i} = -z_i D_i C_i \nabla\phi - D_i \nabla C_i + \underset{\sim}{v} C_i \qquad (36)$$

Equation (36) may also be written

$$\underset{\sim}{J_i} = \underset{\sim}{J_i^{c}} + \underset{\sim}{J_i^{v}} \qquad (37)$$

where

$$\underset{\sim}{J_i^{c}} = \text{chemical flux} = -z_i D_i C_i \nabla\phi - D_i \nabla C_i \qquad (38\text{-a})$$

$$\underset{\sim}{J_i^{v}} = \text{convective flux} = + \underset{\sim}{v} C_i \qquad (38\text{-b})$$

At a point on a moving boundary, the solvent velocity is equal to the velocity of the solid by the so-called zero-slip condition. There is generally no physical basis for prescribing the normal component of the total flux at such a point. The normal component of the chemical flux, however, depends on the rates of the reactions at the solid-electrolyte interface and can usually be determined. Thus, the flux specification has the form

$$\underset{\sim}{J_i^{c}}\cdot\underset{\sim}{n}\Big|_{\beta} = -\left(z_i D_i C_i \nabla\phi + D_i \nabla C_i\right)\cdot\underset{\sim}{n}\Big|_{\beta} = J_i^{*}(s), \qquad i = 1, N_s \qquad (39)$$

where the $J_i^{*}(s)$ are arbitrary functions of the coordinate s

measured along the boundary curve β.

The flux specification expressed by equation (39) is identical to a Neumann boundary condition for uncharged species. When the normal flux is zero, the flux specification looks like a homogeneous linear boundary condition in concentration.

Charge-Transfer Boundary Conditions

One of the aims of this work has been to describe the behavior of real physical systems. Among other things, this requires the use of boundary conditions consistent with the kinetics of electrochemical reactions. Boundary conditions of the type described above do not satisfy this requirement.

In the pages that follow, the relationship between mass flux and reaction current density is discussed. The relationship between the reaction current density and the field variables is then examined. Finally, the way this information is combined to construct boundary conditions is described.

To make these ideas explicit, consider as an example a simple redox reaction of the form

$$S_r \rightleftharpoons S_o + k e^- \qquad (40)$$

where

S_r = reduced substance

S_o = oxidized substance

k = electrode reaction valence = $(Z_o - Z_r) > 0$

e^- = an electron released into the solid electrode

The reaction expressed by equation (40) can take place only at an electrode-electrolyte phase boundary, since the electrons generated in the reaction must be removed from the electrolyte. By convention, the equation is written with the electrons (e^-) on the right, and the constant k is a positive integer. When the reaction goes to the right it is said to proceed in the anodic direction. When it goes to the left it is said to proceed in the cathodic direction. Since k is positive, the charge number of the oxidized species is greater than that of the reduced species, and an anodic current corresponds to a flow of positive charge from the electrode into the electrolyte.

An example of such a reaction is the oxidation of the ferrous ion to the ferric ion according to the reaction

$$Fe^{++} \rightleftharpoons Fe^{+++} + e^- \tag{41}$$

It should be emphasized that the reactions described by equations (40) and (41) differ from ordinary chemical reactions in requiring the transport of charge from one phase (the electrolyte) to another (the electrode) across a phase boundary.

For reactions more complex than those described by equations (40) and (41), it is convenient to write the reaction equation in the more compact and general form

$$\sum_{i=1}^{T_j} \gamma_{ij} M_i + k_j e^- = 0 \tag{42}$$

where

γ_{ij} = stoichiometric coefficient of ith species in jth reaction

M_i = either chemical formula of ith species or molecular weight of ith species

k_j = electrode reaction valence of jth reaction

T_j = total number of species entering into jth reaction

Note that the stoichiometric coefficients, γ_{ij}, are less than zero for the reduced species in the jth reaction and greater than zero for the oxidized species. The stoichiometric coefficients are usually assigned integer values. The electrode reaction valence satisfies the requirement

$$\sum_{i=1}^{T_j} \gamma_{ij} z_i - k_j = 0 \qquad (43)$$

When the reaction described by equation (40) procedes at an electrode-electrolyte interface, the generation of one mole of oxidized species, S_o, in the electrolyte is accompanied by the consumption of one mole of reduced species, S_r, and the passage of k moles of electrons from the electrolyte, through the electrode and into an external circuit. The overall process may be viewed as consisting of three simultaneous fluxes: a flux of oxidized species into the electrolyte, an equal flux of reduced species out of the electrolyte, and a flux, k times greater, of positive charge into the electrolyte. The charge flux is just an electrical current. Since the mass fluxes are proportional to the charge flux, it is convenient to use the reaction current to describe the reaction rate. According to the convention above, the current is positive (anodic) when the reaction procedes to the right.

Thus, when the boundary β coincides with an electrode-electrolyte phase boundary, the fluxes of the species in reaction (40) may be expressed as

$$\underline{J}_A^c \cdot \underline{n}\Big|_\beta = +\left(I/k\mathfrak{F}\right) \tag{44-a}$$

$$\underline{J}_o^c \cdot \underline{n}\Big|_\beta = -\left(I/k\mathfrak{F}\right) \tag{44-b}$$

where

I = reaction current density (amp/cm^2)

The fluxes in equations (44) are measured relative to the boundary, so the convective components do not appear in the equations.

If more than one reaction occurs, the flux of each species is the sum of the fluxes from all of the reactions. Thus, from equation (42),

$$\underline{J}_i^c \cdot \underline{n}\Big|_\beta = -\sum_{j=1}^{N_i}\left(\frac{\gamma_{ij}}{k_j \mathfrak{F}}\right) I_j \tag{45}$$

where

I_j = reaction current density of jth reaction

N_i = total number of reactions involving the ith species

Equation (45) is the desired relation between mass flux and the electrochemical reaction rates. It has the same form as equation (39). When the rates of all the reactions are constant, the boundary conditions reduce to flux boundary conditions.

To complete the boundary specification, it is necessary to express the reaction current density as a function of the other field variables. Consider, as an example, the reaction described by equation (40). The reaction current density may

be written

$$I = I_a - I_c \tag{46}$$

where

I_a = anodic current density (amp/cm^2)

I_c = cathodic current density (amp/cm^2)

In equation (46), the overall rate is expressed as the difference between the forward and backward reaction rates. These may in turn be written

$$I_a = K_a C_r \exp[\alpha k \mathfrak{F} (\Phi_m - \Phi_s)/RT] \tag{47-a}$$

$$I_c = K_c C_o \exp[-(1-\alpha) k \mathfrak{F} (\Phi_m - \Phi_s)/RT] \tag{47-b}$$

where

K_a = forward (anodic) rate constant (amp-cm/mole)

K_c = backward (cathodic) rate constant (amp-cm/mole)

C_r = concentration of reduced species (mole/cm^3)

C_o = concentration of oxidized species (mole/cm^3)

α = charge-transfer coefficient ($0 < \alpha < 1$)

Φ_m = electrostatic potential of solid metal electrode (volt)

Φ_s = electrostatic potential in the electrolyte at the phase boundary (volt)

Equations (47) are similar to those describing the forward and backward rates of a first-order, homogeneous chemical reaction. The forward rate is proportional to the concentration of the reduced species (the reactant); the

backward rate is proportional to the concentration of the oxidized species (the product). The rate constants, K_a and K_c, are intrinsically positive. Although usually written as constants, they are actually functions of temperature and pressure. The exponential terms do not appear in the equations describing the rate of a homogeneous reaction. They appear in equations (47) because the potential difference at the electrode-electrolyte interface acts as a barrier to charge transport. (For a detailed analysis of the rates of charge-transfer reactions, see Reference 5.)

A more convenient expression for the reaction rate can be obtained by rewriting equations (46) and (47). When reaction (40) is at equilibrium,

$$I = I_a - I_c = 0$$

and

$$\Delta\tilde{\Phi}^\circ = (\tilde{\Phi}_m^\circ - \tilde{\Phi}_s^\circ) = \left(\frac{RT}{kJ}\right) \ln\left(\frac{K_c C_o^\circ}{K_a C_a^\circ}\right) \qquad (48)$$

where

superscript $^\circ$ = value of parameter at equilibrium

$\Delta\tilde{\Phi}^\circ$ = equilibrium potential difference across electrode-electrolyte interface

The rate constants in equation (48) may be eliminated by introducing the standard electrode potential, E^s. The standard electrode potential is defined as the equilibrium potential difference, relative to the standard hydrogen electrode, when the activity of each species entering the reaction is one. It was assumed above that the electrolyte is an ideal solution. Invoking the same assumption here, the activity of a species is one when its concentration is

one mole per liter. Thus, from equation (48),

$$E^{\circ} = \left(\frac{RT}{kF}\right) \ln\left(\frac{K_c}{K_a}\right) \tag{49}$$

and

$$\Delta\Phi^{\circ} = E^{\circ} + \left(\frac{RT}{kF}\right) \ln\left(\frac{C_o^{\circ}}{C_r^{\circ}}\right) \tag{50}$$

Equation (50) shows how the equilibrium potential varies with concentration. The standard equilibrium potential has been tabulated for many charge-transfer reactions [13]. It may be determined directly from electrochemical experiments or by calculation from independently measured thermodynamic data.

From equation (46) and the condition for equilibrium, the anodic and cathodic current densities are equal at equilibrium. This value of the current density is called the exchange current density and may be determined from either of equations (47) and equation (48).

$$I_o = I_a^{\circ} = I_c^{\circ} = K_a C_r \exp\left[\alpha \ln\left(\frac{K_c C_o^{\circ}}{K_a C_r^{\circ}}\right)\right]$$

$$I_o = K_a^{(1-\alpha)} K_c^{\alpha} C_r^{\circ(1-\alpha)} C_o^{\circ\alpha} \tag{51}$$

where

I_o = exchange current density (amp/cm^2)

Using equations (49), (50), and (51), the reaction rate expressed by equations (46) and (47) may be written in more compact form.

$$I = I_o\left\{\left(\frac{C_r}{C_r^{\circ}}\right)\exp\left[\alpha kF\eta / RT\right] - \left(\frac{C_o}{C_o^{\circ}}\right)\exp\left[-(1-\alpha)kF\eta / RT\right]\right\} \tag{52}$$

where

$$\eta = \Phi_m - \Phi_s - \Delta\Phi_o \qquad (53)$$

Equation (52) is the form usually found in the literature. The quantity, η, defined by equation (53) is called the charge-transfer overvoltage. It indicates the degree to which the reaction departs from equilibrium. When the concentrations are fixed at their equilibrium values, the sign of the current density is the same as the sign of the charge-transfer overvoltage. Thus, the current density is anodic when the overvoltage is positive.

Two specializations of equation (52) frequently appear in the electrochemical literature and should be mentioned. When the concentrations of reacting species are everywhere equal to their equilibrium values and the charge-transfer coefficient, α, is equal to one-half, equation (52) becomes

$$I = 2I_o \sinh\left[k\mathfrak{F}\eta/RT\right] \qquad (54)$$

The other special case occurs when the overvoltage is large. When the argument of the exponential terms in equation (52) is large with respect to unity, one of the two terms is small with respect to the other. For example, when η has a large positive value, the second term can be neglected and the current density is approximately

$$I \approx I_o\left(\frac{C_R}{C_R^o}\right)\exp\left[\alpha k\mathfrak{F}\eta/RT\right] \qquad (55)$$

If, in addition, the concentration of the reduced species is close to its equilibrium value, equation (55) may be written

$$\eta \approx A + B\log(I) \qquad (56)$$

where

$$A = -\left(\frac{RT}{\alpha k \mathfrak{F}}\right)\ln(I_o) \qquad (57\text{-a})$$

$$B = +\left(\frac{RT}{\alpha k \mathfrak{F}}\right)\ln(10) \qquad (57\text{-b})$$

Equation (56) is the so-called Tafel polarization law. When η is plotted as a function of Log(I), the constants B and A correspond to the slope and zero intercept of the curve respectively. If the electrode reaction valence, k, is known, the kinetic constants α and I_o, may be determined from equations (57).

For analytic work, the exchange current density defined by equation (51) is inconvenient because its value depends on the choice of reference conditions. Since the standard electrode potential is defined with unit activities of the reacting species, it is convenient to use the same conditions to define a standard exchange current density. Thus,

$$I_o^s = K_a^{(1-\alpha)} K_c^{\alpha} = I_o\Big|_{\substack{C_R^o = 1 \\ C_O^o = 1}} \qquad (58)$$

where

I_o^s = standard exchange current density (amp-cm/mole)

The units of the standard exchange current density are chosen for later dimensional clarity. As before, it is assumed in equation (58) that the electrolyte is an ideal solution.

Taking as reference conditions unit concentrations of the oxidized and reduced species, and introducing the dimensionless potential from equation (29), equation (52) becomes

$$I = I_o^s \left\{C_R \exp[\alpha k \zeta] - C_O \exp[-(1-\alpha) k \zeta]\right\} \qquad (59)$$

where

$$\zeta = \phi_m - \phi_s - \left(\frac{\mathcal{J}E^s}{RT}\right) \tag{60}$$

By analogy with the dimensionless potential, ζ will be called the dimensionless overvoltage. Note that a zero value of the dimensionless overvoltage corresponds to zero current only in the special case when the concentrations of both the oxidized and reduced species are equal to one mole per liter.

For the example considered, the redox reaction described by equation (40), equations (44) and (59) constitute the desired boundary specification. Since the electrode is assumed to be a good conductor, ϕ_m is not a function of position but may be a function of time. The values of C_R, C_O, and ϕ_s appearing in equations (59) and (60) are those at the electrode-electrolyte interface.

Thus, when the boundary $\mathcal{B}$ to the domain $\mathcal{D}$ coincides with an electrode-electrolyte interface, and the redox reaction described by equation (40) is the only charge-transfer reaction occurring at that interface, the boundary specification is

$$-\underline{J_O^c}\cdot\underline{n}\Big|_{\mathcal{B}} = \underline{J_R^c}\cdot\underline{n}\Big|_{\mathcal{B}} = \hat{J} \tag{61-a}$$

$$\underline{J_i^c}\cdot\underline{n}\Big|_{\mathcal{B}} = 0 \qquad i \neq O,R \tag{61-b}$$

where

$$\hat{J} = \left(\frac{I_R^s}{k\mathcal{J}}\right)\left\{C_R \exp[\alpha k\zeta] - C_O \exp[-(1-\alpha)k\zeta]\right\} \tag{61-c}$$

Equations (61) are a straightforward extension of the flux boundary conditions discussed above. They are awkward to handle in practice, since they are non-linear in the dimensionless potential. But other than convenience, there is

no limitation to their use.

To generalize these results, note that equation (45) is the general relationship between mass flux and reaction current density. If, for each reaction, the current density in equation (45) can be expressed as a function of concentration and potential, the boundary specification will be complete. It should be emphasized that, while equation (59) is typical of those describing charge-transfer kinetics, equations of this form do not always provide an adequate description of reaction kinetics. An example is the reaction discussed in Appendix B.

Electroneutrality

In the original presentation of the transport equations, it was observed that Gauss' law is more accurate than the electroneutrality equation. It was asserted that the electroneutrality equation is approximately satisfied by electrolytes which are sufficiently concentrated, but no evidence was presented in support of that statement. The electroneutrality equation is, nevertheless, employed throughout this work.

At that point, we had no basis for selecting one equation over the other. Here, having examined both the field equations and boundary conditions, we are in a better position to discuss the merits of using the electroneutrality equation.

By using the electroneutrality equation, the differential equation for the electrostatic potential is simplified and reduced in order. Using equations (28) and (29) and Gauss' law (eqn. 8), the differential equation for the dimensionless potential, ϕ, is

$$\gamma \frac{\partial}{\partial t}(\nabla^2\phi) = \gamma \bar{D} \nabla^4\phi - \gamma \nabla(\nabla^2\phi)\cdot \mathrm{curl}(\Psi \underline{k}) - P\nabla^2\phi - \nabla P\cdot\nabla\phi - \nabla^2 Q \qquad (62)$$

where

$$\gamma = \epsilon RT/\mathcal{F}^2 \qquad (63\text{-a})$$

$$\bar{D} = \frac{1}{N_s}\sum_i D_i \qquad (63\text{-b})$$

$$P = \sum_i Z_i^2 D_i C_i \qquad (63\text{-c})$$

$$Q = \sum_i Z_i (D_i - \bar{D}) C_i \qquad (63\text{-d})$$

Using equations (28) and (29) and the electroneutrality equation (eqn. 9), the differential equation for the dimensionless potential is

$$P\nabla^2\phi + \nabla P\cdot\nabla\phi + \nabla^2 Q = 0 \qquad (64)$$

Equation (62) is a fourth-order, parabolic, partial differential equation. Equation (64) is second order and contains no explicit time dependence. Both equations look linear; neither is.

Rather than discuss equations (62) and (64) in their general forms, we will limit our attention to a special case for which the forms are simplified but the essential features are retained. Specifically, let

i) $D_i = \bar{D}$, all i = $1,N_s$

ii) $\frac{\partial f}{\partial t} = 0$, all f (steady state) (65)

iii) Ψ = constant (zero solvent velocity)

Using these assumptions, equations (62) and (64) become

$$\nabla\cdot(\sigma\nabla\phi) - \gamma\nabla^4\phi = 0 \tag{66}$$

$$\nabla\cdot(\sigma\nabla\phi) = 0 \tag{67}$$

where

$$\sigma = \sum_{i=1}^{N_s} z_i^2 C_i \qquad \text{(ionic strength)}$$

Using the same assumptions, equation (28) reduces to

$$z_i C_i \nabla^2\phi + z_i \nabla C_i\cdot\nabla\phi + \nabla^2 C_i + \left(G_i/\bar{D}\right) = 0 \tag{68}$$

It has already been shown that N_s equations of the form of equation (68) and the electroneutrality equation constitute a system of N_s equations in N_s unknowns. On the other hand, N_s equations of the form of equation (68) and Gauss' law comprise a system of $(N_s + 1)$ equations in $(N_s + 1)$ unknowns. The boundary specification which is complete when using the electroneutrality equation is not complete when using Gauss' law.

This result is also reflected in equations (66) and (67). Equation (66) is fourth-order in ϕ; equation (67) is second-order. To obtain a solution to equation (66), two constraints must be imposed at each boundary point.

Equation (67) requires one.

Boundary conditions for the system of equations using Gauss' law may assume various forms. As was done for the system based on the electroneutrality equation, these may be determined from a detailed analysis of the original system of equations. The same result may be developed heuristically from equations (66) and (67).

If the normal flux of each species is specified everywhere on the boundary, the normal current density is also specified (by eqn. 15). If, in addition, the ionic strength, $\Im$, is constant, flux boundary conditions are equivalent to specifying the normal derivative of ϕ everywhere on the boundary.

A boundary condition of this form is sufficient for equation (67). Another is required for equation (66). One possibility is suggested by Gauss' law; namely, specifying the charge density in the electrolyte at every point on the boundary.

For the system of equations including Gauss' law, other conditions could be imposed and it is not necessary that they be the same at every boundary point. Nevertheless, something equivalent to the condition above must be imposed in addition to those used for the system based on the electroneutrality equation.

For that portion of the boundary corresponding to an electrode-electrolyte interface, this introduces a serious problem. While the ion fluxes can be determined from the rates of the charge-transfer reactions, the first normal derivative of ϕ is proportional to the charge density on the surface of the electrode. There is published data on the rates of many electrochemical reactions, but there are virtually no data on surface charge density for solid metal electrodes. Lacking such data, we would prefer not to use Gauss' law if there is some other justification for using the electroneutrality equation.

Equations (66) and (67) differ by the appearance of a biharmonic term in equation (66) missing from equation (67). To estimate the importance of this term, consider the special case when the ionic strength, Υ, is constant throughout the electrolyte. In this case, equation (66) may be written

$$\nabla^2\left[\phi - \delta^2\nabla^2\phi\right] = 0 \tag{69}$$

where

$$\delta = \sqrt{\epsilon RT / \mathcal{F}^2 \sum_i z_i^2 c_i} \tag{70}$$

The constant δ is called the Debye length. When it is small with respect to the characteristic dimensions of the domain $\mathcal{D}$ (the electrolyte), the second term in the brackets in equation (69) is small with respect to the first. The biharmonic term in equation (66) can then be neglected, and the electroneutrality equation used to describe the charge distribution in the electrolyte.

In Figure 1, the Debye length is plotted as a function of ionic strength. It is less than 10^{-5} centimeters when the ionic strength is greater than 2×10^{-5} equivalents squared per mole liter. For a 1-1 aqueous electrolyte (e.g. an aqueous sodium chloride solution), this corresponds to a salt concentration of 10^{-5} moles per liter. The minimum dimensions of all the domains considered in this work are of the order of 10^{-3} to 10^{-2} centimeters. The ionic strengths are typically of the order of 10^{-2} to 1.0 mole per liter. Under these conditions, the electroneutrality equation does, in fact, represent a valid approximation to Gauss' law.

The use of the electroneutrality equation thus simplifies both the field equations and the boundary conditions. Because it is also an accurate approximation over a broad

range of interest, it is possible to exploit these simplifications.

Coordinate Transformations

When solving a boundary value problem, it is often convenient to choose a coordinate frame so the boundary coincides with a coordinate direction. For example, when the boundary curve $\mathcal{B}$ is a circle, it is usually convenient to transform the field equations and boundary conditions to polar coordinates so the boundary coincides with a constant value of the radial coordinate. The advantage gained in simplifying the boundary conditions is offset in part by additional complexity in the field equations.

Under the class of coordinate transformations used here the field equations are particularly well-behaved. Consider the coordinate systems (x,y) and (ξ,η). We wish to transform the field equations and boundary conditions from x-y coordinates to ξ-η coordinates in such a way that the domain $\mathcal{D}$ in the x-y coordinate frame is transformed onto the rectangle $\mathcal{R}$ in the ξ-η coordinate frame. It is assumed that such a transformation exists, so we can write

$$x = x(\xi,\eta) \tag{71-a}$$

$$y = y(\xi,\eta) \tag{71-b}$$

where the functions x and y are continuous, single-valued, and have as many continuous derivatives as may be required. In addition, it is assumed that x and y satisfy the Cauchy-Riemann conditions,

$$x_{,\xi} = y_{,\eta} \tag{72-a}$$

$$X_{,\gamma} = -y_{,\xi} \tag{72-b}$$

Under such a transformation, the field equations (eqns. 28, 9, 25, and 26) assume the following form in the ξ-γ coordinate frame:

$$H^2 C_{i,t} = Z_i D_i \nabla(C_i \nabla\phi) + D_i \nabla^2 C_i - \nabla C_i \cdot \widetilde{curl}(\psi \underline{k}) + H^2 G_i \tag{73}$$

$$\sum_{i=1}^{N_s} Z_i C_i = 0 \tag{74}$$

$$F_1 \nabla^4\psi + F_2 \nabla^2\left(\frac{\partial\psi}{\partial\xi}\right) + F_3 \nabla^2\left(\frac{\partial\psi}{\partial\gamma}\right) + F_4 \nabla^2\psi = 0 \tag{75}$$

$$\nabla^2 P = 0 \tag{76}$$

where

$\underline{l}$ = unit vector in the positive ξ-direction (77-a)

$\underline{m}$ = unit vector in the positive γ-direction (77-b)

$$\nabla = \underline{l}\frac{\partial}{\partial\xi} + \underline{m}\frac{\partial}{\partial\gamma} \tag{77-c}$$

$$\nabla^2 = \frac{\partial^2}{\partial\xi^2} + \frac{\partial^2}{\partial\gamma^2} \tag{77-d}$$

$$\nabla^4 = \frac{\partial^4}{\partial\xi^4} + 2\frac{\partial^4}{\partial\xi^2\partial\gamma^2} + \frac{\partial^4}{\partial\gamma^4} \tag{77-e}$$

$$\widetilde{curl} = \underline{l}\frac{\partial}{\partial\gamma} - \underline{m}\frac{\partial}{\partial\xi} \tag{77-f}$$

$$H^2 = x_{,\xi}^2 + x_{,\gamma}^2 \tag{77-g}$$

$$F_1 = H^2 \tag{77-h}$$

$$F_2 = -4HH_{,\xi} \tag{77-i}$$

$$F_3 = -4HH_{,\gamma} \tag{77-j}$$

$$F_4 = 6[H_{,\xi}^2 + H_{,\gamma}^2] - 2H\nabla^2 H \tag{77-k}$$

The operators in equations (77-c) through (77-f) are defined by analogy to the operators in cartesian coordinates. The function $\mathcal{H}$, defined by equation (77-g), is called the warping function and indicates the extent to which a line-element at a point in the x-y coordinate frame is stretched or compressed by the transformation at the corresponding point in the ξ-γ coordinate frame.

The electroneutrality equation (eqn. 74) is unaffected by the transformation. Equation (76) is analogous to the original equation. The conservation equation (eqn. 73) differs from the original equation only by the appearance of the warping function as a coefficient multiplier in the terms not containing spatial derivatives. Only the biharmonic equation (eqn. 75) is significantly affected by the coordinate transformation.

The transformation of boundary conditions is straightforward. Any function of the coordinates x and y may be written as a function of the coordinates ξ and γ using the transformation functions of equations (71). It should be observed, however, that, for an equation expressing a vector quantity as a function of the gradient of a scalar quantity or the curl of a vector potential, the warping function appears in the transformed equation. Thus, when transformed to the ξ-γ coordinate frame, the flux equation becomes

$$\underline{J_i} = -\frac{1}{\mathcal{H}}\left[Z_i D_i C_i \nabla\phi + D_i \nabla C_i + C_i \widetilde{\mathrm{curl}}(\psi \underline{k})\right] \qquad (78)$$

Similarly, equation (24) becomes

$$\underline{v} = \frac{1}{\mathcal{H}} \mathrm{curl}(\psi \underline{k}) \qquad (79)$$

Equations (73) through (79) may be used in any coordinate frame, (ξ,γ), for which the transformation functions satisfy the Cauchy-Riemann conditions (eqns. 72). The particular form of the transformation functions is, of course, dictated by the shape of the domain $\mathcal{D}$ in the x-y coordinate frame.

III. METHODS FOR SOLVING THE TRANSPORT EQUATIONS

In this section, some of the methods for solving the electrochemical transport equations are discussed. The numerical technique used in this work is outlined in the next section. Here, consideration is limited to the system consisting of N_s equations of the form of equation (28) and the electroneutrality equation. It is assumed that $G_i = 0$ (for all i) and that the solvent velocity, $\underline{v}$, is independently specified. For convenience, the equations are displayed below.

$$\frac{\partial C_i}{\partial t} = Z_i D_i C_i \nabla^2 \phi + Z_i D_i \nabla C_i \cdot \nabla \phi + D_i \nabla^2 C_i - \nabla C_i \cdot \underline{v} \qquad (80\text{-a})$$

$$\sum_i Z_i C_i = 0 \qquad (80\text{-b})$$

In several cases the system of equations reduces to a system of linear equations. For these cases solutions can be obtained by classical methods [12].

When the dimensionless potential is constant, equation (80-a) becomes

$$\frac{\partial C_i}{\partial t} = D_i \nabla^2 C_i - \nabla C_i \cdot \underline{v} \qquad (81\text{-a})$$

Equation (81-a) is the so-called convective-diffusion equation. Since the ion concentrations are coupled through the electroneutrality equation, the solution set contains the solutions of $(N_s - 1)$ linearly-independent differential equations.

If, in addition to the dimensionless potential, the solvent velocity is zero, equation (80-a) reduces to the equation describing transport by simple diffusion.

$$\frac{\partial C_i}{\partial t} = D_i \nabla^2 C_i \qquad (81\text{-b})$$

Once again, the solutions are coupled through the electroneutrality equation, and the solution set consists of $(N_s - 1)$ linearly-independent solutions. Equations (81) have been studied extensively. They can usually be solved by the method of separation of variables or by the use of similarity transforms. A complete discussion of solution techniques with application to specific boundary value problems is contained in References [14] and [15].

Depending on the solvent velocity, one of equations (81) can be used when the potential gradient is small. Neglecting the potential introduces an error, but this can be tested by generating solutions to the complete set of equations and determining the extent to which electroneutrality is violated. If

$$\left| \sum_{i=1}^{N_s} z_i C_i^* \right| \ll \sum_{i=1}^{N_s} z_i^2 C_i^* \qquad (82)$$

where the C_i^* are the values obtained from one of equations (81), the error is negligible.

When the electrolyte composition is everywhere the same, equations (80) reduce to Laplace's equation for the dimensionless potential.

$$\nabla^2 \phi = 0 \qquad (83)$$

As is true for the diffusion equations, methods for solving Laplace's equation are well documented. This equation has been used in a wide variety of electrochemical problems. It is accurate at short times in many time-dependent problems and at steady state in well-stirred electrolytes.

In some cases, equations (80) reduce to a system of linear equations which can be solved by classical methods. The simplest and most important is the case of the binary electrolyte [12]. When N_s is two, equations (80) can be written

$$\frac{\partial C_1}{\partial t} = Z_1 D_1 C_1 \nabla^2\phi + Z_1 D_1 \nabla C_1 \cdot \nabla\phi + D_1 \nabla^2 C_1 - \underset{\sim}{v} \cdot \nabla C_1 \qquad (84\text{-a})$$

$$\frac{\partial C_2}{\partial t} = Z_2 D_2 C_2 \nabla^2\phi + Z_2 D_2 \nabla C_2 \cdot \nabla\phi + D_2 \nabla^2 C_2 - \underset{\sim}{v} \cdot \nabla C_2 \qquad (84\text{-b})$$

$$Z_1 C_1 + Z_2 C_2 = 0 \qquad (84\text{-c})$$

Multiplying equation (84-a) by D_2, equation (84-b) by D_1, and adding

$$\frac{\partial}{\partial t}\left[D_2 C_1 + D_1 C_2\right] = D_1 D_2 \nabla^2\left[C_1 + C_2\right] - \underset{\sim}{v} \cdot \nabla\left[D_2 C_1 + D_2 C_1\right] \qquad (85)$$

Substituting for C_2 in equation (85) its value from equation (84-c) and rearranging,

$$\frac{\partial C_1}{\partial t} = \mathcal{D}_1 \nabla^2 C_1 - \underset{\sim}{v} \cdot \nabla C_1 \qquad (86)$$

where

$$\mathcal{D}_1 = \frac{(Z_1 - Z_2) D_1 D_2}{Z_1 D_1 - Z_2 D_2}$$

Equation (86) is just the convective-diffusion equation and may be solved by the technique discussed above. Note that species 2 satisfies the same differential equation (eqn. 86), and that $\mathcal{D}_2 = \mathcal{D}_1$. After solving equation (86)

for C_1, C_2 can be obtained directly from equation (84-c). The dimensionless potential can then be determined from equation (84-a). However, a simpler expression is obtained by multiplying equation (84-a) by Z_1 and equation (84-b) by Z_2. Adding the resulting equations and using equation (84-c) to eliminate C_2 yields

$$C_1\nabla^2\phi + \nabla C_1 \cdot \nabla\phi + \left[\frac{D_1 - D_2}{Z_1 D_1 - Z_2 D_2}\right]\nabla^2 C_1 = 0 \qquad (87)$$

While methods for solving Laplace's equation and the diffusion equation are well documented, there is no general procedure for solving the transport equations (eqns. 80). For problems involving dependence on one spatial variable, the method outlined in Appendix C can sometimes be used. The method is based on treating the potential ϕ as an unknown function in the solution of equations (80-a). Using these solutions and the electroneutrality equation, an integral equation is obtained for ϕ. The form of the equation varies from one problem to another but is typically nonlinear. The usefulness of the method depends on the effort required to extract a solution from the integral equation. No way has yet been found to extend the method to two or three spatial variables.

Approximate solution techniques are of two general types: approximate analytic methods and numerical methods. Perturbation methods are the most powerful of the analytic ones. These are based on the idea that a small change in one of the field variables or boundary conditions should cause only small changes in the solution. The equations for the binary electrolyte (eqns. 86 and 87) provide the most satisfactory basis for such methods.

In the simplest perturbation method, the concentrations of the two principal ions are determined from equation (86).

The concentrations of the minor species are determined from equation (28), using the electrostatic potential obtained from equation (87). The electroneutrality equation is then used to obtain an improved estimate of the potential. There are, of course, more sophisticated methods and they may be used iteratively to improve the accuracy of the approximations.

Numerical methods have received increasing attention in recent years. Much of the work has been based on some specialization of the ion transport equations. For example, the work reported in Reference [16] is based on the convective-diffusion equation. Such approximations can be extremely useful, but only that work including the effects of both diffusion and migration is considered here.

The 'MKT' analysis dev loped by T. R. Beck [10] is basically a one-dimensional, steady-state formulation of the ion transport equations using a particular set of charge-transfer boundary conditions. It is assumed that the solvent velocity is zero and that the electrolyte contains three charged species. The equations are integrated numerically using a Runge-Kutta technique, and the boundary conditions are satisfied by trial and error.

R. C. Alkire, E. A. Grens II, and C. W. Tobias [11] recently presented a more sophisticated treatment of one-dimensional transport. Developed for a study of porous electrodes, their analysis is based on a quasi-steady state formulation of the transport equations in which the solvent velocity is determined by the rate of dissolution of the metal electrode. The equations are linearized and then cast in finite difference form. The resulting system of algebraic equations is solved numerically. An iterative procedure is used to simultaneously satisfy both the field equations and boundary conditions.

There has been no report of methods for problems in two

or three spatial variables. The methods reported in References [10] and [11] could be generalized to electrolytes containing more than three charged species and, without much difficulty, to include explicit time-dependence. It is doubtful, however, that the method used in Reference [10] can be extended to problems in two or three spatial variables.

IV. COMPUTER PROGRAM DEVELOPED FOR THIS STUDY

Several specific goals were established to guide the design of the computer program. The primary goal was that the program be capable of generating time-dependent solutions to the electrochemical transport equations, using an arbitrary set of charge-transfer boundary conditions. Secondly, it was desired that the program be flexible and have a broad applicability. While the immediate aim of this study was to examine transport in crack-like regions, the program is designed to solve problems in two spatial variables rather than one. Also, the program can be easily specialized to solve Laplace's equation or the convective-diffusion equation by the input of appropriate control characters.

Basically, the program calculates three functions: the stream function, the dimensionless electrostatic potential, and the concentration of each dissolved species. In every case the approach is the same. The controlling differential equation is replaced by an equivalent difference equation at a number of preselected points. The resulting system of linear algebraic equations is then solved by Gaussian elimination. Additional subroutines are required to perform service and control functions. The most important of these are the subroutines which establish the size and shape of the physical region and those in which boundary conditions are calculated and applied.

The problem to be solved is defined by the input data under the control of the executive portion of the program. First, the initial concentrations and the transport properties of the dissolved species are specified. Up to ten species may be included in a single problem. The type of problem to be run (simple diffusion, convective diffusion, or electrochemical transport) is then determined and the

form of the boundary conditions is established. Finally, the size and shape of the physical domain are fixed.

The physical domain may be hyperbolic, elliptic, pie-shaped, or rectangular. Other shapes are possible but, as the program is now written, the transformation functions are limited to those listed. The way the domains transform to a rectangle is indicated in Figure 2. The numbered points transform to the numbered corners of the rectangle, and the lines connecting them transform to straight lines. The size of the physical domain is determined by two characteristic dimensions, the length and width. The way these are measured is also shown in Figure 2.

One finite difference grid is used for all the calculations. The grid spacing is uniform in each of the directions ξ and η. The maximum grid size which may be used is 11 by 41. As an example, the grid for a hyperbolic domain is shown in Figure 3 in both the physical coordinates and the transformed coordinates. Note that the spacings in the ξ- and η-directions are uniform but not equal.

All quantities related to the motion of the solvent are derived from the stream function. The stream function itself is calculated using a straightforward finite-difference analogue to equation (75). The resulting system of algebraic equations is solved by Gaussian elimination with back substitution to provide error control. The solvent velocity at each grid point is determined from the finite-difference analogue to equation (79).

The pressure at any point (ξ_0, η_0) in the solvent can be determined by integration of equation (21). If C is any convenient curve connecting the two points (0,0) and (ξ_0, η_0) then

$$P(\xi_0, \eta_0) = P(0,0) + \mu \int_{(0,0)}^{(\xi_0, \eta_0)} \operatorname{curl}\left(\frac{1}{R^2} \nabla^2 \psi\right) \cdot d\underline{s} \qquad (88)$$

The pressure is calculated at points along the crack centerline according to equation (88). The appropriate derivatives are replaced by their finite-difference approximations and the integration is performed numerically using the trapezoidal rule.

From equations (73) and (74), the differential equation for the dimensionless potential, ϕ, in terms of the transformed (ξ,γ) coordinates is

$$\sum_{i=1}^{N_s} Z_i^2 D_i \nabla(C_i \nabla\phi) + \sum_{i=1}^{N_s} Z_i D_i \nabla^2 C_i = 0 \qquad (89)$$

The potential is calculated using a straightforward finite-difference analogue to equation (89) at each grid point. The resulting system of algebraic equations is solved by Gaussian elimination.

Since there is no explicit time dependence in equation (89), the potential is established instantaneously. For problems in electrochemical transport, this initial value must be calculated before attempting to calculate ion concentrations at an advanced time. When the electrolyte is initially homogeneous, equation (89) reduces to Laplace's equation.

When charge-transfer boundary conditions are used, the initial estimate of the boundary conditions is generally in error. In this case it is necessary to repeat the calculation of the potential, using the previous value to obtain an improved estimate of the potential difference across the electrode-electrolyte interface. Four to six such iterations are usually sufficient to reduce the error everywhere to less than one part in ten-thousand.

At advanced times, the initial estimates of concentrations and potential all contain errors regardless of the form of the boundary conditions. Then it is necessary to

employ an iterative procedure involving all the field equations and, in some cases, the boundary conditions. This procedure is discussed more fully after first discussing the method used to advance the calculation of concentration in time.

Computation of the ion concentrations at an advanced point in time is carried out in two stages. The concentration of each species is calculated using a finite-difference analogue to equation (73). The electroneutrality equation (eqn. 74) is then used to modify these values and obtain improved concentration estimates.

Initial estimates of the ion concentrations at a new point in time are obtained using an ADI (Alternating-Direction Implicit) technique. A technique of this form was selected because, unlike forward-difference analogues to equation (73), such techniques are unconditionally stable.* There is no limit to the size of the time step beyond the practical limit required to control truncation error. In addition, ADI techniques are relatively fast as compared to other stable finite-difference approximations, e.g., backward-difference methods.

When using an ADI technique with an equation in two or three spatial variables, the problem is decomposed into two or three problems, each one of which exhibits implicit dependence on only one spatial variable. In the present case the differential equation depends on the spatial variables, ξ and γ. The finite-difference analogue to this equation consists of two parabolic difference equations. One carries an implicit dependence in the ξ-direction, the other in the

---

* Stability in this context refers to the fact that small errors due to truncation and roundoff do not propagate, but are attenuated as the calculation is carried further in time.

η-direction. In operation, the equations for the ξ-direction are solved first; then the equations for the η-direction are solved. This procedure is repeated at succeeding time steps; hence the name Alternating-Direction Implicit. At each stage the coefficient matrix for the system of algebraic equations is tri-diagonal.

A more detailed discussion of the finite-difference analogue used in the solution of equation (73) may be found in Appendix A. A comprehensive review of numerical methods for the solution of parabolic differential equations, including ADI techniques, is presented in Reference [17].

In earlier versions of the program the electroneutrality equation was used only to generate an equation and boundary conditions for the electrostatic potential. It was not used explicitly in the program. Although several different methods were tried, none were satisfactory: all resulted in systematic but uncontrolled oscillations in the electrostatic potential. While the behavior differed from one method to another, the oscillations were always accompanied by oscillations in the ion concentrations and systematic deviations from electroneutrality.

In the present program, oscillations of the ion concentrations and electrostatic potential have been brought under control by explicit use of the electroneutrality equation. The method used is redundant. The concentrations of individual species are initially treated as being independent, and each concentration is calculated using the ADI technique discussed above. This yields one concentration estimate. A second estimate is obtained using the electroneutrality equation and the first concentration estimates for all the other charged species. These estimates are then combined to yield an improved estimate.

In a typical problem, the concentration of a particular ion may be several orders of magnitude less than the total

ion concentration. For this reason it is necessary to weight the two concentration estimates rather than take a simple average. For each ion a weighting function, g_i, is computed according to the formula

$$g_i = \sum_{K=1}^{N_p} |Z_i| C^{\circ}_{ik} \Big/ \left(\sum_{l=1}^{N_p} \sum_{m=1}^{N_c} |Z_m| C^{\circ}_{ml} \right) \qquad (90)$$

where

g_i = weighting function for ith charged species

C°_{ik} = estimate of the concentration of the ith species at the kth grid point obtained using the ADI technique

N_p = total number of grid points

N_c = total number of charged species

The concentration at each point is then determined according to the formula

$$C_{ik} = (1 - g_i) C^{\circ}_{ik} + g_i C^{*}_{ik} \qquad (91)$$

where

C_{ik} = 'best' estimate of concentration of ith species at the kth grid point

$C^{*}_{ik} = -\frac{1}{Z_i} \sum_{\substack{j=1 \\ j \neq i}}^{N_c} Z_j C^{\circ}_{jk}$, estimate of the concentration of the ith species at the kth grid point based on the electroneutrality equation.

The precision of this method is quite good. The error, ϵ_{EN}, in satisfying the electroneutrality equation may be defined as

$$\epsilon_{EN} = \text{Max} \left\{ \sum_{i=1}^{N_c} Z_i C_{ik} \Big/ \sum_{i=1}^{N_c} Z_i^2 C_{ik} \right\}, \quad k = 1, N_p \qquad (92)$$

that is, the maximum value of the ratio at any grid point within the electrolyte. On a computer carrying the equivalent of eight decimal digits in single precision arithmetic, no value of ϵ_{EN} greater than 5×10^{-7} has been observed. This is the same magnitude as the roundoff error in the calculation of ϵ_{EN}.

When the concentrations, $C_i(t_o)$, and the dimensionless potential, $\phi(t_o)$ are specified at a point in time, t_o, the calculations at a new point in time, $(t_o + \Delta t)$, are carried out as follows. First, estimates of the concentrations, $C_i(t_o + \Delta t)$, are calculated using the value of the potential, $\phi(t_o)$, to approximate its value at the intermediate time, $(t_o + \frac{1}{2}\Delta t)$. These estimates, $C_i(t_o + \Delta t)$, are then used to estimate the potential, $\phi(t_o + \Delta t)$, at the new time. When necessary, as when charge-transfer boundary conditions are used, the estimates of quantities at $(t_o + \Delta t)$ are then used to revise the boundary conditions. This sequence is repeated three or four times as may be required to reduce the error to the desired level. In each such sequence, the latest estimate of the potential at the new time and the value at the previous time are used to estimate $\phi(t_o + \frac{1}{2}\Delta t)$ in the computation of the concentrations, $C_i(t_o + \Delta t)$. If more than four such iterations are required it is usually preferable to reduce the size of the time step.

In Appendix A, it is shown that the ADI method is second-order correct in both time and space when the dimensionless potential is evaluated at the intermediate point in time,

$(t_o+\frac{1}{2}\Delta t)$. Because ϕ is not specified a priori, iteration is required to retain this second-order correctness. The iterative procedure is also effective in controlling other errors of uncertain magnitude. When, for example, charge-transfer boundary conditions are used, the boundary conditions at the new time are not known at the beginning of the time step. Unless the solution technique leads to simultaneous convergence of both the field variables and the boundary conditions, the theoretical accuracy achievable using the ADI method cannot be realized.

Boundary conditions for the transport equations are imposed by straightforward application of the principles discussed in Section II. When charge-transfer boundary conditions are used, however, the procedure is somewhat involved and this case deserves some explanation.

For each charge-transfer reaction a kinetic equation, such as equation (59), must be obtained and included in the program. Storage capacity has been set aside to permit the use of up to nine such equations. The current density is calculated for each reaction and for as many boundary points as may be desired. The calculation is always based on the best estimates of the concentrations, $C_i(t_o+\Delta t)$, and potential, $\phi(t_o+\Delta t)$ at the advanced point in time available at the time of the calculation.

The potential of the metal (electrode) may be independently specified. It may be held constant or permitted to vary with time. As the program is now written, however, it is not possible to impose a constant current condition on the electrode (corresponding, for example, to a freely corroding metal).

The next step is to compute the normal flux for each species at each boundary point. The computation is performed according to equation (45) using the values of the current density just calculated.

Finally, the normal derivative of the dimensionless potential, ϕ_n, is calculated at each boundary point according to the equation

$$\phi_n = -\frac{1}{U}\left(H I_{TOT} + V_n\right) \tag{93}$$

where

ϕ_n = normal derivative of ϕ at a point on the boundary

$I_{TOT} = \underline{I} \cdot \underline{n}$

$U = \sum z_i^2 D_i C_i$

$V = \sum z_i D_i C_i$

and where the quantities I_{TOT}, U, and V are all evaluated at points on the boundary.

The current density, I_{TOT}, is taken as the sum of the partial current densities calculated earlier. The calculation is always based on the best estimates of the concentrations, $C_i(t_o + \Delta t)$ at the advanced point in time.

The estimates of the normal fluxes and the normal derivative of the dimensionless potential are used with the finite-difference analogue to the flux equation to construct the boundary conditions for each species. As mentioned above, all these estimates contain errors depending on the stage of the computation. This method of constructing boundary conditions has other drawbacks which are discussed at the close of this section.

The printed output includes coordinate data, data relevant to the solvent velocity, and transport data. The (ξ-γ) and (x-y) coordinates are calculated and printed for each grid point. The stream function and its first derivatives in the ξ- and γ-directions are also printed. The value of

the solvent velocity at each grid point is presented in two formats. In one the x- and y-components of the velocity are printed; in the other the magnitude and direction of action of the velocity vector are presented. The transport data are printed at time zero and at the end of each time step. These data include the value of the dimensionless potential and the values of the concentrations at each grid point. The partial current density for each reaction is printed for every boundary point lying on the solid-electrolyte phase boundary. Finally, the x- and y-components of the total current density are printed.

The program has been run on a Univac Corporation Model 1108 computer. The running time depends on the number of dissolved species, the mode of transport, and the number of time steps desired. For a simple diffusion problem with one dissolved species and charge-transfer boundary conditions, two to three seconds of computation time are required for each time step when using four iterations per time step. For an electrochemical transport problem with three dissolved species and constant flux boundary conditions, the computation time is about fifteen seconds per time step, again using four iterations per time step. More than half this time is required for the computation of the electrostatic potential. The total running time for a wide variety of problems is typically between five and thirty minutes.

Although the program has been successfully employed in the solution of a variety of transport problems, it has two important limitations. The method used to construct and apply boundary conditions limits the capability of the program. In particular, difficulties are encountered in problems involving either diffusion-limited partial current densities or extremely large total current densities. These limitations may be overcome by changes in the subroutine used to compute the partial current densities. That is,

rather than treating the partial current density as a constant, it might be treated as a linear function of both concentration and potential, where the linear approximation is made about the current values of the field variables.

Another limitation derives from the use of the current equation to compute $\phi_{,n}$, the normal derivative of the dimensionless potential. This results in a coupling between errors in the estimates of $\phi_{,n}$ and the concentrations. In electrochemical transport problems this introduces an instability which can be controlled only by controlling the size of the time step. While this method is successful, it is undesirable because it limits full exploitation of the ADI technique. It is felt that this limitation can be overcome by using the sum, $\sum z_i J_i / D_i$, rather than the current equation, for calculating $\phi_{,n}$.

V. RESULTS

The results presented in this section form the major part of an effort to develop a systematic and coherent view of the factors affecting solution chemistry and ion transport in crack-like regions. The results are limited to the behavior of an electrolyte in a pre-existent notch or crack on an otherwise smooth electrode surface. For the sake of clarity and simplicity, attention is focused on a single reaction and it is assumed that no homogeneous chemical reaction occurs in the electrolyte.

The reaction chosen for study is an oxide-film formation reaction. Such reactions play an important role in virtually all forms of metal corrosion. The rate of this kind of reaction cannot be adequately described by a kinetic equation of the form of equation (59). Under suitable constraints, however, behavior similar to that expressed by equation (59) may be observed (see Appendix B).

It is assumed that the oxide is formed by the reaction

$$M + 2H_2O \rightleftharpoons MO_2 + 4H^+ + 4e^- \qquad (94)$$

For consistency and completeness it is necessary to include oxide formation by direct reaction with the electrolyte. Such a reaction is represented by

$$MO^{++} + H_2O \rightleftharpoons MO_2 + 2H^+ \qquad (95)$$

This reaction does not require the transport of electrons through the oxide film. The reaction proceeds to the right or left depending only on the concentrations of the dissolved

species. The reaction rate is independent of the electrode potential.

The metal oxide is assumed to have zero electronic conductivity. All current passing through the film is conducted by the migration of ions or vacancies. As a consequence, no redox reaction can occur in the system while the oxide film is intact. Thus, equations (94) and (95) represent the complete set of possible reactions occurring at the oxide-covered metal surface. This assumption provides an accurate physical description of the oxides of titanium and aluminum.

The rate of reaction (94) can be expressed as

$$I_1 = I_{10}\left\{\exp\left[\zeta_1\right] - \exp\left[-\zeta_1\right]\right\} \tag{96}$$

where

$$\zeta_1 = \frac{\beta}{\delta}\left[\phi_m - \phi_s - \epsilon_F - \eta_s\right] \tag{97}$$

and where

I_{10} = exchange current density (amp/cm^2)

β = high field conduction coefficient (cm)

δ = oxide film thickness (cm)

ϕ_m = dimensionless potential of metal electrode

ϕ_s = dimensionless potential of electrolyte at metal-electrolyte interface

ϵ_F = Flade potential (dimensionless equilibrium potential of reaction 94)

η_s = surface overpotential

The Flade potential, ϵ_f, is taken as the equilibrium potential of reaction (94). Thus, ϵ_f is a function of the hydrogen ion concentration. It is easily shown that

$$\epsilon_f = \epsilon_f^\circ + \ln\left\{10^{+3}\left[H^+\right]\right\} \tag{98}$$

where

ϵ_f° = standard dimensionless equilibrium potential of reaction (94)

$[H^+]$ = hydrogen ion concentration (mole/cm^3)

The surface overpotential, γ_s, is determined by the rate of reaction (95). It may be determined from the equation

$$\gamma_s = \frac{1}{2}\ln\left\{\frac{I_{30}\dfrac{[MO^{++}]}{[MO_o^{++}]} + I_{20}\dfrac{[H^+]^2}{[H_o^+]^2}}{I_{20} + I_{30}}\right\} \tag{99}$$

where

I_{30} = exchange current density for anodic partial electrode reaction for reaction 95 (amp/cm^2)

I_{20} = exchange current density for cathodic partial electrode reaction for reaction 95 (amp/cm^2)

$[U]$ = concentration of species U (mole/cm^3)

The equilibrium concentrations, $[MO_o^{++}]$ and $[H_o^+]$, in equation (99) can be determined from the solubility product of the hydrated oxide or from the free energy of formation of the oxide according to reaction (95) [18].

The kinetic parameters, I_{10} and β, appearing in equations (96) and (97) have been evaluated from data reported

for titanium by H. A. Johansen and co-workers [19]. I_{1o} has been taken as 1.0×10^{-12} amps per square centimeter and β as 16×10^{-8} centimeters. The standard Flade potential, ϵ_f°, has been taken as the standard equilibrium potential for the formation of hydrated titanium dioxide by the reaction of titanium with water. The value reported by W. M. Latimer [13] is -37.1 (-0.95 volts S.H.E. at 25°C). The equilibrium concentrations in equation (99) have been evaluated from data reported by M. Pourbaix [18] for the formation of the hydrated form of titanium dioxide by the reaction of hydrogen and titanyl ions. The values are:

$$[H_o^+] = 2[MO_o^{++}] = 7.57 \times 10^{-3} \text{ moles per cubic centimeter.}$$

A detailed study of the rate of reaction (95), based on the equations developed in Appendix B, indicates that the rate is negligible with respect to the rate of reaction (94) when the solution pH is greater than minus one. For this reason and also to standardize the influence of the MO^{++} ions, the concentration of MO^{++} has been fixed at 10^{-9} moles per cubic centimeter and the rate of reaction (95) has been set equal to zero for the problems in this section. To determine γ_s, it is still necessary to evaluate the constants I_{2o} and I_{3o}. There are no data in the literature from which to evaluate these exchange current densities. The values 10^{-6} and 10^{-4} amps per square centimeter have been selected as being reasonable.

When the rate of reaction (95) is negligible with respect to the rate of reaction (94), the rate of oxide film growth may be written as

$$\dot{\delta} = \left(W I_1 / 4\rho \mathfrak{F}\right) \qquad (100)$$

where

$\dot{\delta}$ = time rate of change of the film thickness, δ (cm/sec)

W = molecular weight of the oxide (gram/mole)

ρ = mass density of the oxide (gram/cm^3)

$\mathfrak{F}$ = Faraday's constant (coul/equiv)

The parameters W and ρ have been evaluated from the chemical formula and density of titanium dioxide.

The transport properties summarized below are based on data contained in References [20], [21], and [22]. None of the references is complete; the data reported are from measurements made in binary electrolytes. The values below are based on the reported values at infinite dilution. At concentrations of 0.1 mole per liter, ionic mobilities are typically about twenty percent less than at infinite dilution.

$$D_{H^+} = 9.00 \times 10^{-5} \ (cm^2/sec)$$

$$D_{Cl^-} = 2.00 \times 10^{-5} \ (cm^2/sec)$$

$$D_{Na^+} = 1.33 \times 10^{-5} \ (cm^2/sec)$$

Reference Problem

At any point in time, the electrolyte composition in a crack-like region is determined by three factors: the crack size and shape, the boundary and initial conditions, and the transport mode. Each of these is examined below using results obtained numerically. To facilitate comparison of the results, we begin with a problem that is relatively simple,

but illustrates the general characteristics of transport in crack-like regions. It is a problem of transport by simple diffusion under constant flux boundary conditions in a hyperbolic crack.

In this problem, one ion is considered; the effects of migration and convection are ignored. The ion is the hydrogen ion and, from the values listed above, its diffusion coefficient is 9×10^{-5} centimeters squared per second. The governing differential equation is the diffusion equation, recovered from equation (73) by setting the potential, velocity, and generation rate equal to zero.

It is assumed that the electrolyte is initially homogeneous and the composition of the bulk electrolyte does not change with time. The hydrogen ion concentration at time zero and at points along the crack mouth is 10^{-7} moles per liter (pH = 7). Along the crack walls, the normal flux is constant and equal to 3.25×10^{-9} moles per square centimeter. This value is determined from the rate of reaction (94), the oxide-film formation reaction, using equation (96) with ϕ_m and ϕ_s equal to zero, a film thickness of fifty angstroms, and a hydrogen ion concentration of 10^{-7} moles per liter. The normal flux is equivalent to a current density of 314 microamps per square centimeter.

The crack is the hyperbolic crack shown in Figure 6. It is 0.20 centimeters-long and 0.02 centimeters-wide.

The results are summarized in Figures 4 and 5. In Figure 4, the hydrogen ion concentration at the crack tip is shown as a function of time. The concentration is expressed as a pH, the negative common logarithm of the hydrogen ion concentration in moles per liter. The pH falls quite rapidly. From an initial value of seven, it is less than three within one second. In ten seconds, it has a value less than one pH unit larger than its final or steady state value. The steady state is reached in approximately 700 seconds, or

about twelve minutes and the crack-tip pH is very close to one.

The change in concentration with time is accompanied by a significant change in the shape of the concentration profile. This is illustrated in Figure 5 where the concentration at points on the crack centerline is shown at three different times. In order to display all three curves on a single graph, the data are presented in terms of the dimensionless parameter $\tilde{C}$, defined as

$$\tilde{C}_i = \left(\frac{C_i(x) - C_i^\circ}{C_i(0) - C_i^\circ} \right) \tag{101}$$

where

$C_i(x)$ = concentration evaluated at the distance x from the crack tip

$C_i(0)$ = concentration evaluated at the crack tip

C_i° = concentration at the mouth of the crack (equal to the concentration in the bulk electrolyte)

The lower curve is a typical short-time concentration profile. The concentration gradient is large in the region near the crack tip, approaches zero in the central region, and increases again near the mouth of the crack. The central curve, corresponding to a later point in time, behaves similarly, but the change in the concentration gradient is not as extreme as in the lower curve. The upper curve corresponds to the steady state. The gradient is small at the crack tip and increases continuously as the distance from the crack tip increases.

The shape of the concentration profile is strongly influenced by the crack-like geometry. At short times the influence of the ends is small except in the regions near the

tip and the mouth of the crack. The flux in the central region is primarily in the transverse direction. The small gradient in the central region of the lower curve in Figure 5 is almost entirely due to an increase in the crack width with increasing distance from the crack tip, rather than significant transport in the longitudinal direction. As the steady state is approached, the flux in the longitudinal direction becomes much greater than that in the transverse direction except in the region near the crack tip. There, both components remain of the same order of magnitude.

Crack Shape

The effects of changes in the crack shape are shown in the next series of problems. Except for the crack shapes, the problems are identical to the reference problem. One species, the hydrogen ion, is considered. Transport is by simple diffusion. The ion flux normal to the electrode-electrolyte interface is constant and equivalent to a current density of 314 microamps per square centimeter. The bulk-solution pH is seven.

The crack profiles are shown in Figure 6. They are rectangular, hyperbolic, and pie-shaped. All are nominally 0.2 centimeters long by 0.02 centimeters wide. The pie-shaped crack is one percent shorter than the others because of the coordinate transformation used. The area of metal-electrolyte interface is virtually the same for all of the cracks; the maximum difference between any two is less than five percent. The crack volumes vary by a factor of two.

The influence of shape on the behavior with time is illustrated in Figure 7. The crack-tip pH is shown as a function of time for each of the three crack shapes. For the pie-shaped crack the approach to steady state is initially somewhat faster, for the rectangular crack the approach is

initially slower, than for the hyperbolic crack. However, the times to reach the steady state are virtually the same, about 700 seconds or twelve minutes. The steady-state crack-tip pH is approximately one for all three shapes. The differences are more apparent when the values are expressed in terms of concentration rather than pH. For the pie-shaped crack, the steady-state crack-tip concentration is 0.137 moles per liter. For the hyperbolic crack, the value is 0.099 moles per liter. For the rectangular crack it is 0.079 moles per liter.

The crack shape influences the form of the concentration profile as shown in Figure 8. The steady-state concentration along the crack centerline is plotted as a function of distance from the crack tip for each of the three crack shapes. The ordinate in Figure 8 is $\tilde{C}$ as defined by equation (101). Thus, only differences in the shapes of the concentration profiles are shown in the figure.

For the pie-shaped crack, the concentration profile is very nearly linear, with a slight deviation from linearity in the region close to the crack tip.* The concentration profile is parabolic for the rectangular crack. The profile for the hyperbolic crack lies between the other two.

The influence of time on the shape of the concentration profile is discussed above for the case of the hyperbolic crack. The behavior is summarized in Figure 5 where the concentration on the crack centerline is shown at three different times. Similar curves are presented for the pie-shaped crack in Figure 9 and for the rectangular crack in Figure 10.

---

* The deviation from linearity near the crack tip is caused by 'chopping off' the tip of the wedge in making the coordinate transformation. It may be shown that the profile is linear over the entire crack length only when the crack tip coincides with the point of intersection of the extensions of the two straight sides. (see pages 95 and 96)

The times are the same as those in Figure 5. As in Figure 5, the data are presented in terms of the dimensionless parameter $\tilde{C}$ in order to display the curves in a single graph.

Comparison of Figures 5, 9, and 10 reveals that the behavior with time is similar for all three crack shapes. At short times there is negligible transport in the longitudinal direction over most of the crack length. The concentration gradient is large in the region near the crack tip, decreases to a small value in the central region, and increases somewhat near the mouth of the crack. At intermediate times the behavior is similar, but the change in the gradient over the length of the crack is less extreme than at the shorter times. At large times the concentration profiles approach steady state curves characteristic of the particular crack shape.

It is stated above that the concentration gradient in the central region of the crack at short times is primarily due to an increase in the crack width with increasing distance from the crack tip. This is apparent from the lower curves (elapsed time equal to 0.164 seconds) in Figures 9 and 10. In the central region of the bottom curve in Figure 9, the concentration decreases linearly with increasing distance from the crack tip. For this crack, the width also increases linearly. In the central region of the bottom curve in Figure 10, on the other hand, the concentration remains constant. Since this crack is rectangular, its width is also constant.

Two-Dimensional Effects

The problems discussed in this section have been solved using a two-dimensional formulation of the transport equations. For problems involving transport in crack-like regions, however, one might expect transport in the transverse

direction to play a relatively minor role. This expectation is based on simple dimensional considerations. For a more quantitative view, data from the previous set of problems may be used. The rectangular crack is particularly convenient for this purpose because of its simple geometry.

The transverse concentration gradient varies from zero along the crack centerline to a finite value at the crack wall (the metal-electrolyte phase boundary). At the wall, the transverse gradient is proportional to the normal flux and, because of the boundary conditions, remains constant with time. The longitudinal gradient varies with both time and position. The ratio of the two gradients provides a simple and direct measure of their relative magnitudes.

In Figure 11 the gradient ratio is shown as a function of time for three points adjacent to the crack wall. This ratio is defined as the magnitude of the longitudinal concentration gradient divided by the transverse concentration gradient. The points are located at distances from the crack tip equal to one-eighth, one-fourth, and one-half times the overall crack length.

At short times, transport in the transverse direction is much greater than in the longitudinal direction, and the gradient ratios are small at all three points. As time increases, transport in the longitudinal direction becomes increasingly important. At the end of one minute, the gradient ratios are all of the order of one, and the gradients in the longitudinal and transverse directions are approximately equal. As time increases further, the ratio at each point approaches a steady state value which is a function of distance from the crack tip. Because the crack width and normal flux are both constants, the steady state value at each point is proportional to the total wall area lying between that point and a point on the crack centerline at the crack tip. The steady state values at one-eighth, one-fourth, and

one-half are, therefore, 3.5, 6.0, and 11.0, respectively. Only for points close to the crack tip are the transverse and longitudinal concentration gradients of the same order of magnitude.

Two-dimensional transport effects may also be viewed from another perspective. Since there is a concentration gradient in the transverse direction, the concentration varies from point to point on a section perpendicular to the crack axis. As a measure of this variation, consider the parameter $\hat{C}(X_o)$ defined as

$$\hat{C}(X_o) = \left| \frac{C_w(X_o) - C_c(X_o)}{C_w(X_o) - C^o} \right| \qquad (102)$$

where

$C_w(X_o)$ = concentration at a point adjacent to the crack wall and located at a distance X_o from the crack tip

$C_c(X_o)$ = concentration at a point on the crack centerline and located at a distance X_o from the crack tip

C^o = concentration in the bulk electrolyte

When $\hat{C}(X_o)$ is one, the concentration at the given transverse section is highly non-uniform. When $\hat{C}(X_o)$ is zero, the concentration is uniform across the section. Because of the assumed symmetry about the crack centerline, the numerator in equation (102) is equal to the difference between the maximum and minimum concentrations on the given transverse section.

The functions $\hat{C}(X_o)$ for three transverse sections are shown as functions of time in Figure 12. The sections are located at distances of one-eighth, one-fourth, and one-half

times the overall crack length. The curves for the sections at one-eighth and one-fourth are indistinguishable and are shown as a single curve. The curve for one-half lies slightly above the other curve.

Initially, the concentration changes more rapidly at points along the wall than at points away from it. There is a substantial variation in the concentration across the width of the crack and the function $\hat{C}(X_o)$ is close to one. As time increases, the concentration becomes more uniform and the variation across the width of the crack decreases. After one minute, the variation is about one percent. As steady state is approached the variation becomes quite small. It is less than one percent at all three sections.

These results indicate that two-dimensional transport effects are significant only at short times or at points near the ends of a crack. The results for hyperbolic and pie-shaped cracks are similar. In the case of the gradient ratio, however, they do not admit as simple a geometric interpretation as is the case for the rectangular geometry.

Crack Length

The effect of crack length is illustrated by the next series of problems. The cracks have hyperbolic profiles and are 0.02 centimeters wide. The influence of crack width is considered elsewhere.

Consideration is limited to hydrogen ion transport by simple diffusion with a constant normal flux at the crack wall. The flux is determined from the rate of the film formation reaction (eqn. 94) with the potential difference at the metal-electrolyte interface equal to zero and the hydrogen ion concentration equal to 10^{-7} moles per liter (pH = 7.0). The oxide film thickness is fixed at fifty angstroms. This corresponds to a normal current density of 314

microamps per square centimeter. The hydrogen ion concentration in the bulk electrolyte is 10^{-7} moles per liter.

At this point, it is convenient to introduce the notion of a crack aspect ratio. The aspect ratio will be defined as the ratio of crack length to crack width where the crack width is measured at the mouth of the crack. In this problem set, the cracks have aspect ratios ranging from 1.25 to 40. The profiles of three are shown in Figure 13. In the upper portion of the figure, the cracks are drawn to the same scale in the length and width directions. In the lower portion, they are drawn with the scale in the width direction ten times the scale in the length direction. The cracks have aspect ratios of 1.25, 10, and 40. The crack with the aspect ratio of ten is the one used as a reference problem. The profiles range from what should probably be called a 'dimple' to a truly crack-like geometry.

The results are summarized in Figures 14, 15, and 16. In Figure 14, the crack-tip pH is plotted as a function of time for each of the geometries shown in Figure 13. Both the time to reach steady state and the steady state concentration increase with increasing crack length. Even for the shortest crack (the 'dimple'), the steady state pH is less than three.

In Figure 15, the steady-state crack-tip pH is shown as a function of crack length. Note that the scale on the abscissa is logarithmic rather than linear. The curve exhibits a slight negative curvature for small values of crack length but approaches linearity as the crack length increases. The curvature at small values of the crack length is a result both of the function plotted and the method used to define the crack domain. As the crack length approaches zero, the pH at the crack tip assymptotically approaches the bulk solution pH. In this case that value is seven. The method used to define the crack domain and its effect on these results is discussed below.

For values of the crack aspect ratio much greater than one, the curve becomes linear. In this range a doubling of the crack length reduces the crack-tip pH by 0.6. In the next section, it is shown that the slope of this curve is independent of the normal flux.

The steady-state concentration profiles for the cracks in Figure 13 are shown in Figure 16. The data have been normalized by plotting on the ordinate the function $\tilde{C}$, defined by equation (101). A curve has been drawn through the points for the 0.200-centimeter-long crack. No attempt has been made to draw curves for the other two geometries, since this would obscure the data themselves. It may be seen that all the data very nearly fall on a single curve.

The data for the 0.025-centimeter-long crack fall slightly below those for the other two geometries. Like the curvature exhibited at small crack lengths in Figure 15, this is due to the method used to define the crack domain. When transforming a crack onto a rectangle in the computer program, the crack is bounded on the solution side, not by a straight line, but by an ellipse. As a result, the crack length measured along the crack centerline from the tip to the bounding ellipse is greater than the length measured to the metal surface. For the longer cracks the difference between the two is negligible; but for the 0.025-centimeter-long crack the difference is about ten percent.

Boundary Conditions

In the problems considered thus far, the flux normal to the crack wall (metal-electrolyte phase boundary) has been treated as constant. In the next series of problems, the effects of other boundary conditions are examined. The cracks are 0.200-centimeters long by 0.020-centimeters wide and hyperbolic in profile. Consideration is limited to

hydrogen ion transport by simple diffusion.

The concentration dependence of the normal flux is examined first. The flux is determined from the rate of the film formation reaction (eqn. 94) with the potential difference across the metal-electrolyte interface equal to zero, and the oxide film thickness equal to fifty angstroms. The current density is calculated from equation (96) using the hydrogen ion concentration at points adjacent to the crack wall. Thus, the normal flux varies both with time and position along the crack wall. The hydrogen ion concentration in the bulk electrolyte is 10^{-7} moles per liter.

The results are summarized in Figures 17, 18, and 19. In Figure 17, the crack-tip pH is shown as a function of time. The results of the reference problem are included for comparison. The curve for this problem lies everywhere above the one for the reference problem. As these results show, including the concentration dependence of the normal flux in the boundary conditions reduces the flux and increases the steady state pH. In particular, when the pH at the metal-electrolyte interface is 2.5, the normal flux is about one and one-half orders of magnitude less than when the pH is seven. The magnitude of this effect may vary from one reaction to another, but the direction is always the same. An increase in the concentration of a product species always decreases the reaction rate.

The variation of the steady state concentration along the crack centerline is shown in Figure 18. The results obtained for the reference problem are also shown for comparison. The data have been normalized by plotting as the ordinate the function $\tilde{C}$ defined by equation (101). The concentration profile for this problem is very nearly the same as that for the reference problem. The former, however, lies everywhere above the latter.

Because the flux normal to the crack wall decreases as

the hydrogen ion concentration increases, it is greater at the mouth of the crack than at the crack tip. This is shown in Figure 19 where the normal flux is plotted as a function of distance from the crack tip at steady state. For convenience, the flux is expressed as a current density. The flux at the mouth of the crack is more than eight times greater than at the crack tip.

When the longitudinal concentration profile is compared with one obtained for a constant value of the normal flux, as in Figure 18, it may be seen that the effect of the variation in the normal flux is to reduce the magnitude of the longitudinal concentration gradient near the crack tip, and to increase it near the mouth of the crack. The concentration profile for product species obtained using charge-transfer boundary conditions is always found to lie above that obtained using constant flux boundary conditions.

The same boundary conditions at the crack wall have been used to investigate the effect of changes in the concentration of the bulk electrolyte. The concentration dependence of the normal flux is considered but the oxide-film thickness is fixed at fifty angstroms. The potential difference at the interface is set equal to zero.

The results are summarized in Figure 20. Here the pH at the crack tip is shown as a function of the pH in the bulk electrolyte. There are two distinct regions in the figure. In the first, the pH in the bulk electrolyte is small and the crack-tip pH is approximately equal to the pH in the bulk electrolyte. In this region, the concentration difference between the tip and the mouth of the crack is much less than the concentration at the mouth of the crack. The variation in the pH along the length of the crack is negligible and the normal flux is essentially constant everywhere along the crack wall.

In the second region, where the pH in the bulk electro-

lyte is large, the pH at the crack tip is virtually independent of the pH in the bulk electrolyte. In this region, the difference between the concentrations at the tip and the mouth of the crack is much greater than the concentration at the mouth of the crack. Thus, the hydrogen ion concentration in the bulk electrolyte may be treated as being zero, and the variation in the normal flux along the crack wall is virtually the same as that shown in Figure 19.

In the final problem of this set, the effects of both film growth and concentration are considered. The normal flux is determined from the rate of the oxide-film formation reaction (eqn. 94) with the potential difference across the metal-electrolyte interface equal to zero. The hydrogen ion concentration in the rate equation (eqn. 96) is taken as the concentration in the electrolyte at points adjacent to the crack wall. The initial film thickness is taken as fifty angstroms at every point on the boundary. The film thickness at each boundary point is then obtained by numerical integration of equation (100).

The results are summarized in Figures 21 and 22. In the upper portion of Figure 21, the crack-tip pH is shown as a function of time. For comparison, a curve showing the response in the absence of film growth (corresponding to the upper curve in Figure 17) is also shown. In the lower portion of the figure, the film thickness at the crack tip is shown as a function of time.

At very short times, there is no sensible change in the oxide-film thickness and the pH versus time curve coincides with that obtained using a constant film thickness. With increasing time, the thickness of the oxide film increases, decreasing the hydrogen ion flux into the crack. The concentration at the crack tip then becomes less (the pH greater) than in the comparable problem with no film growth. Continued film growth results in the most striking feature

of the pH-versus-time curve. At about one hundred seconds the curve exhibits a minimum after which the pH rises continuously.

This calculation was terminated after an elapsed time of about three thousand seconds or fifty minutes (calculated time, not computer running time) so no detailed information was obtained on the behavior at large times. It should be observed, however, that the concentration in the crack cannot attain a steady state value unless the rate of oxide film growth becomes zero. Thus, the pH will continue to rise toward the bulk electrolyte value (in this case seven) unless some other reaction intervenes or the potential difference across the metal-electrolyte interface is reduced to its equilibrium value.

For the first problem in this set, the oxide-film thickness was fixed at fifty angstroms. Under this constraint, the normal flux was found to exhibit considerable variation along the length of the crack. It is shown in Figure 19, for example, that the normal flux near the mouth of the crack is about eight times greater than at the crack tip. When the influence of oxide film growth is considered, however, it is found that the normal flux at the crack wall is very nearly constant. In Figure 22, the normal flux, expressed as a current density, is shown as a function of distance from the crack tip. The variation in the film thickness along the length of the crack is also shown. The difference in the normal flux between the tip and the mouth of the crack is less than ten percent. The greater thickness of the film near the mouth of the crack tends to compensate for the lower ion concentration in this region.

Convective Transport

Thus far, our attention has been restricted to problems involving transport by simple diffusion. The effects of convection and migration have been ignored. We now wish to consider these other modes of transport. The effects of convective transport are considered in the next series of problems. Transport by migration is considered in the following problem set.

When a structural member containing a crack is loaded, the crack opens and the volume of the crack increases. The crack volume likewise increases as a crack grows or lengthens. In either case, some of the electrolyte is drawn into the crack from the bulk solution in the same way liquid is drawn into a suction pump. Our interest here is in the effect of such flow on the composition of the electrolyte in the crack.

To be more explicit, consider the pie-shaped crack shown at the top of Figure 23. If the crack deforms in such a way as to remain pie-shaped, the straight sides must remain straight. In this case, it is convenient to identify two modes of crack deformation. For the mode identified as 'crack growth' in Figure 23, the sides of the crack are displaced vertically with no change in the crack angle. The ratio of the vertical displacement of a point on the crack wall to the horizontal displacement of the crack tip is a constant for all points on the crack wall. For the mode identified as 'crack opening' in Figure 23, the crack angle increases with no change in the displacement of the crack tip. In this case, the displacement of a point on the crack wall is proportional to its distance from the crack tip. Any crack deformation, satisfying the requirement that the pie-shaped crack remain pie-shaped, can be expressed as a linear combination of these two deformation modes.

A closed-form solution for the solvent velocity in a pie-shaped crack has been obtained using the Stokes-flow approximation to the Navier-Stokes equations. When the crack angle, 2α, is small, the solution may be expressed approximately as

$$v_r = -\frac{3}{4}\left[r\left(\frac{\dot{\alpha}}{\alpha}\right) + 2\dot{a}\right]\left[1 - \left(\frac{\theta}{\alpha}\right)^2\right] \qquad (103\text{-a})$$

$$v_\theta = \frac{\alpha}{2}\left[r\left(\frac{\dot{\alpha}}{\alpha}\right) + \dot{a}\right]\left[3\left(\frac{\theta}{\alpha}\right) - \left(\frac{\theta}{\alpha}\right)^3\right] \qquad (103\text{-b})$$

where

v_r = velocity component in the radial (longitudinal) direction (cm/sec)

v_θ = velocity component in the tangential (transverse) direction (cm/sec)

α = crack half angle (radian)

a = crack length (cm)

$\dot{\alpha}$ = time rate of change of crack half angle (radian/sec)

$\dot{a}$ = time rate of change of crack length (cm/sec)

r, θ = coordinate of a point (cm, radian)

The stream lines corresponding to the velocities in equations (103) are shown in the central portion of Figure 23 for the two modes of crack deformation. In the lower portion of the figure, the magnitudes of the centerline velocities are shown as functions of the distance from the crack tip.

For both deformation modes, the solvent flow is toward the crack tip. At a given distance from the crack tip, the velocity in the radial direction is a maximum on the crack

centerline. For the 'crack opening' mode, the magnitude of the solvent velocity increases linearly as the distance from the crack tip increases. For the 'crack growth' mode, the solvent velocity is independent of the distance from the crack tip.

The results obtained for the pie-shaped crack provide a good approximation to solvent motion in a crack-like region. For the numerical work, however, a different geometry has been used. This geometry is somewhat less restrictive and of more direct physical significance. The configuration adopted is shown in Figure 24. It consists of a double edge-notched tensile specimen 2.40 centimeters wide. The side notches are 0.20-centimeter-long by 0.02-centimeter-wide hyperbolic notches. The deformation of the crack walls is determined from A. A. Griffith's [23] analysis for a specimen containing deep hyperbolic notches. The rate of crack deformation is found to be directly proportional to the specimen loading rate.

In this series of problems consideration is limited to transport of the hydrogen ion and the normal flux is constant at every point along the crack wall. The flux is determined from the rate of the film formation reaction (eqn. 94) with the potential difference at the metal-electrolyte interface equal to zero and the hydrogen ion concentration equal to 10^{-7} moles per liter. The oxide-film thickness is fixed at fifty angstroms. Under these conditions the current density normal to the crack wall is 314 microamps per square centimeter. The hydrogen ion concentration in the bulk electrolyte is taken as 10^{-7} moles per liter.

The solvent velocity is calculated using a prescribed specimen loading rate and the initial specimen geometry. The crack dimensions are assumed to remain constant with time. In reality, while the length of the crack is not

affected by the loading, the crack width increases with time. The effect of changes in the crack width, ignored in this set of problems, is examined below.

In Figure 25, the magnitude of the solvent velocity along the crack centerline is shown as a function of distance from the crack tip. The nominal net-section strain rate is 10^{-6} centimeters per centimeter per second. The velocity is for all intents and purposes a linear function of distance from the crack tip. The velocity is zero at the crack tip and a maximum at the mouth of the crack. At the mouth of the crack, the centerline velocity is 3.34×10^{-5} centimeters per second. Since the rate of deformation of each point along the crack wall is a linear function of the nominal strain rate, the velocity at any other strain rate may be determined by simple proportioning from this curve.

With the nominal net-section strain rate equal to 10^{-6} centimeters per centimeter per second, the difference between the results obtained with convective transport and those obtained in the reference problem is barely perceptible. With the strain rate increased to 10^{-4} centimeters per centimeter per second, a difference is readily apparent. The results obtained at the latter strain rate are summarized in Figures 26 and 27.

In Figure 26, the crack-tip pH is shown as a function of time. The solid curve corresponds to the results for the convective-diffusion problem at a nominal strain rate of 10^{-4} centimeters per centimeter per second (maximum solvent velocity of 3.34×10^{-3} centimeters per second). A broken curve, illustrating the behavior observed for the reference problem, is included for comparison. The results for the two problems are virtually identical for times less than seventy seconds, about one-tenth of the time required to reach steady state. For times greater than

seventy seconds, the crack-tip pH for the convective transport problem is somewhat greater than that for the reference problem. At steady state, the ion concentration at the crack tip for the convective transport problem is about twenty-five percent less than that for the reference problem.

The steady state concentration along the crack centerline is shown as a function of distance from the crack tip in Figure 27. The results of the convective transport problem and the reference problem are both shown in the figure. The data for the reference problem have been normalized in the same way as in previous figures. The function plotted as the ordinate is $\bar{C}$ defined by equation (101). The data for the convective transport problem have been normalized in the same way except that the value C(0) in the denominator in equation (101) has been taken as the value obtained in the reference problem. In other words, in normalizing the data both sets have been divided by the same number.

The effect of the solvent motion is to reduce the magnitude of the concentration gradient and thereby to reduce the concentration at every point within the crack. The influence on the concentration gradient is the greatest at the mouth of the crack where the solvent velocity is a maximum. The influence decreases as the distance from the crack tip decreases and the solvent velocity decreases.

Crack Width

As mentioned above, the effect of changes in the crack geometry with time was ignored in generating the results summarized in Figures 26 and 27. A substantial change in the crack dimensions may occur, however, in times of the order of the time required to reach steady state, particularly at the higher strain rates. For example, when the nominal net-section strain rate is constant and equal to

10^{-4} centimeters per centimeter per second and when the specimen configuration is that shown in Figure 24, the crack width increases from an initial value of 0.02 centimeters to 0.26 centimeters in 700 seconds. Thus, in the time required to reach steady state the crack width would have increased by a factor of thirteen.

The significance of such a change may be judged from the results of a set of problems run for hyperbolic cracks of various widths. The cracks are all 0.20 centimeters long. Transport is by simple diffusion. The boundary conditions are identical to those used in the reference problem and in the convective-diffusion problem.

The results are summarized in Figure 28. The steady state concentration at the crack tip is expressed in moles per liter and plotted as a function of crack width. For comparison with the convective-diffusion problem discussed above, the steady state concentration for the crack 0.20-centimeters long by 0.02-centimeters wide loaded at a rate of 10^{-4} centimeters per centimeter per second is shown in the figure. The times required for such a crack to attain the same width as the widths of the cracks included in this problem set are also shown.

The steady state concentration at the crack tip is reduced by a factor of about one-half each time the crack width is doubled. By comparison, had the crack width in the convective-diffusion problem been allowed to increase rather than being fixed at 0.02 centimeters, it would have doubled in about sixty seconds or less than one-tenth of the time required to reach steady state.

These results indicate that geometry exerts a much stronger influence on composition than does solvent motion. This conclusion is strengthened by the results mentioned above for a loading rate of 10^{-6} centimeters per centimeter per second. At this loading rate, the effect of convection

was barely perceptible. The difference between the concentration calculated for this problem and that obtained for the reference problem was everywhere less than half of one percent. Nevertheless, for times of the order of the time to reach steady state, the width of this crack should have more than doubled, reducing the concentration by more than one half.

Migration

In the problems discussed thus far, transport by migration has been ignored. The results are, therefore, strictly valid only when the electrostatic potential is everywhere diminishingly small. One indication of the range of applicability of these results is provided by the next problem. A broader view is provided by the analytic results presented in the next section.

The problem considered here is one of electrochemical transport in a rectangular crack 0.20-centimeters long by 0.02-centimeters wide. The choice of the rectangular crack shape is based on the results presented above on the effect of crack shape and to facilitate a later comparison with an analytic solution to a similar problem.

The electrolyte consists of three ions: the sodium ion (Na^+), the chloride ion (Cl^-), and the hydrogen ion (H^+). The bulk electrolyte is a 0.6-mole per liter sodium-chloride solution with a pH of seven. The initial composition of the electrolyte is the same.

At the crack wall, the normal fluxes of both the sodium ion and the chloride ion are zero. The hydrogen ion flux is constant and has the same value as in the reference problem. That is, the value is determined from the rate of reaction (94) with the potential difference across the metal-electrolyte interface equal to zero, the pH equal to seven, and the

oxide-film thickness equal to fifty angstroms. Therefore, the normal current density is 314 microamps per square centimeter.

The behavior with time is summarized in Figure 29. Two curves are shown. The first shows the variation in the crack-tip pH with time. Perhaps the most striking aspect of this curve is its similarity to the curves obtained in earlier problems. It exhibits no new or unusual features.

The second curve in Figure 29 illustrates the behavior of the electrostatic potential, measured at the crack tip, with time. Since the electrostatic potential is zero at the mouth of the crack, the potential at the crack tip is numerically equal to the potential drop along the length of the crack. Note that this potential drop is always positive. That is, it is always of a sense to carry some portion of the total current.

At short times, the gradient of the hydrogen ion concentration is small, and nearly all of the current is carried by the migration of ions in the electrostatic field. The electrostatic potential remains close to its initial value of about nine millivolts. As the hydrogen ion concentration reaches a value of about one percent of its steady state value, the potential begins to decrease rapidly. As the hydrogen ion concentration increases further, an increasing fraction of the total current is carried by hydrogen ion diffusion and the electrostatic potential continues to drop. At steady state, a substantial fraction of the total current is carried by diffusion and the electrostatic potential stabilizes at about 1.5 millivolts. This is approximately one-fifth of the initial value.

Two unusual features of the potential versus time curve should be mentioned. At short times, the computed value of the potential rises before it starts to fall again, introducing a 'bump' in the curve. This 'bump' is an artifact

caused by truncation error in calculating the boundary conditions. It does not represent the true behavior of the system, so the solid curve is not drawn through this data. At steady state, the calculated values are erratic. Variations in the computed values as large as eight percent may be observed. This behavior also derives from the method used to construct boundary conditions. As indicated in Section IV, it is planned to modify the routines used in the computation of the boundary conditions. The planned modification should eliminate both of these defects.

The influence of migration on the behavior of the hydrogen ion may be judged by comparing the pH-versus-time curve in Figure 29 with the upper curve in Figure 7. That curve was obtained using the same crack geometry and boundary conditions as the present problem, but with transport by simple diffusion only. The two curves are virtually identical. There is a difference between the two, but the difference is extremely small when the concentrations are expressed in terms of pH.

The effect of migration is shown more clearly in Figure 30. Here the steady-state hydrogen ion concentration along the crack centerline is shown as a function of distance from the crack tip. In addition to the results for this problem, the results obtained for transport by simple diffusion are reproduced from Figure 10. The effect of migration is to reduce the hydrogen ion concentration everywhere within the crack. However, the reduction is quite small. In the present case, transport by both migration and diffusion, the concentration is about three percent less than in the case of transport by diffusion only.

The influence of the potential gradient on the salt ions is summarized in Figures 31 and 32. In Figure 31, the changes in the concentrations of all three ions are shown as functions of time. In every case, the quantity plotted on

the ordinate is the difference between the concentration at the crack tip and the initial concentration in the electrolyte. Alternately, since the initial concentration of each ion is the same as its concentration in the bulk electrolyte, the ordinate may be viewed as the total concentration difference over the length of the crack.

The curves have several interesting features. Perhaps the most obvious is the way changes in the ion concentrations are coupled by the requirement of electroneutrality. The increase in the hydrogen ion concentration is accompanied by an increase in the concentration of the negative salt ion (Cl^-) and a decrease in the concentration of the positive salt ion (Na^+). In addition, the hydrogen ion reaches a stable steady-state value in less time than does the positive salt ion. The ions do not respond with a single time dependence. This is, perhaps, not surprising. The diffusion coefficients of the three ions are unequal, that of the hydrogen ion being the greatest and that of the positive salt ion the least. However, this behavior is in contrast to that of the binary electrolyte where the system responds with a single time-dependence.

The difference in the transport properties of the two positive ions is also reflected in the behavior of the negative salt ion. At first, the concentration of the negative ion increases with time. Then, a point is reached after which the concentration of the hydrogen ion remains essentially unchanged, while the concentration of the positive salt ion continues to decrease under the influence of the electrostatic potential. The concentration of the negative ion then passes through a maximum and subsequently decreases. Finally, the concentration of the negative salt ion approaches a steady state value from above.

The steady-state concentration profiles are shown in Figure 32. There are three curves, one for each ion.

Plotted on the ordinate is the difference between the concentration at a point on the crack centerline and the concentration in the bulk electrolyte. The abscissa is distance from the crack tip. The concentration profiles are all very nearly parabolic. As required by electroneutrality, the sum of the ordinates is everywhere equal to zero.

The spatial variation of the electrostatic potential is illustrated in Figure 33. The initial and steady state values along the crack centerline are shown as functions of distance from the crack tip. The shapes of the curves are nearly the same. The initial profile is parabolic and the final profile is very nearly parabolic as well. However, the magnitude of the potential at steady state is much less, five times smaller, than it is immediately following immersion of the specimen.

In Figure 34, the current density measured along the crack centerline is shown as a function of distance from the crack tip. Since the normal flux at the crack wall is constant, this curve is invariant with time. The curve is linear over most of the crack length. Near the mouth of the crack, however, there is a moderate deviation from linearity caused by two-dimensional transport effects.

At elapsed times which are small with respect to the time required to reach steady state, essentially all of the current is carried by the migration of ions in the electrostatic field. On the other hand, at times of the order of the time to reach steady state, a substantial portion of the current may be carried by ion diffusion. There is no unique method for determining the fraction of the total current carried by diffusion as opposed to the fraction carried by migration. But, we can obtain a measure of this fraction in a way that is reasonable and makes some physical sense.

One way to estimate the fraction of the total current carried by diffusion is simply to partition the total flux

of each ion into a diffusion flux and a migration flux, and consider the ratio of the current carried by the diffusion fluxes to the total current. Thus we might define

$$P_1 = \left|\underline{I}_D\right| \Big/ \left|\underline{I}_D + \underline{I}_M\right| \tag{104}$$

where

$$I_D = -\mathfrak{F}\nabla\left(\sum_i z_i D_i C_i\right) \tag{105-a}$$

$$I_M = -\mathfrak{F}\left(\sum_i z_i^2 D_i C_i \nabla\phi\right) \tag{105-b}$$

The partitioning of the current might also be reasonably approached from another point of view. At steady state, the total flux of both salt ions must everywhere be equal to zero. This follows from the boundary conditions and conservation of mass. Thus, the current must all be carried by hydrogen ions, and we might consider the fraction of the total current carried by hydrogen ion diffusion, namely

$$P_2 = \left|\hat{\underline{I}}_D\right| \Big/ \left|\underline{I}_D + \underline{I}_M\right| \tag{106}$$

where

$$\hat{\underline{I}}_D = -\mathfrak{F} z_H D_H \nabla C_H \tag{107}$$

These two measures of the fraction of the total current carried by diffusion, P_1 and P_2, are shown in Figure 34. The fractions have been evaluated from the steady state data shown in Figures 32 and 33, and are plotted as functions of distance from the crack tip. The value of P_1 is everywhere less than P_2, but both measures indicate that a greater

fraction of the total current is carried by diffusion as the distance from the crack tip increases. Also, both measures indicate that a greater portion of the total current is carried by diffusion than is carried by migration.

VI. DISCUSSION

The results presented in the last section covered a broad range of geometric and kinetic variables. The effect of each was examined separately and in some detail. In this section a more general perspective is adopted. First, based on the numerical results of the last section, the characteristics of transport in crack-like regions are summarized. Consideration is then centered on the extent, if any, to which this characterization is of more general validity.

Like other computer programs, the program developed in this study is capable of providing detailed answers to particular questions. It is ill-suited to and inefficiently employed in a parametric analysis of a wide range of a large number of variables. Therefore, it will be convenient in this discussion to draw upon the one-dimensional steady-state transport analysis developed in Appendix C. While its formulation constrains the application of this analysis, it has the important advantage that many useful results may be expressed in a simple, closed form.

From the results of the previous section, the following general observations can be made:

1) Time - The initial rate of change of the crack-tip pH is quite large. For times greater than or equal to the diffusion time,* however, the time rate of change of the pH is small regardless of the form of the boundary conditions. Referring to Figure 4, for example, with a constant normal flux at the crack wall sufficient to produce a steady-state crack-tip pH equal to one, the

---

* The diffusion time is defined here as (a^2/D) where a is the crack length and D is the diffusion coefficient of the dissolved species of interest.

crack-tip pH is less than five in one millisecond and less than two in ten seconds. These times should be compared to the diffusion time of 444 seconds or the time to reach steady state of 700 seconds.

Under more complex boundary conditions, the steady state may not be attained in times of the order of the diffusion time. Shown in Figure 21, for example, are results obtained using charge-transfer boundary conditions with oxide film growth. Even here, the time-rate-of-change of the pH is small for times of the order of the diffusion time and larger. At the end of one hour, for example, the pH differs by less than one unit from the value at one minute.

While this observation has been expressed in terms of the pH, it applies equally to the common logarithm of the concentration of any dissolved species. It is asserted, not that changes in concentration with time are insignificant, but that the order of magnitude of the concentration is slowly time-varying over most of the observable time domain.

2) Two-Dimensional Transport Effects - The influence of transport in the transverse direction as compared to the longitudinal direction may be judged from the variation in the electrolyte composition across the width of the crack. If a variation of less than one percent is regarded as negligible, the effects of transport in the transverse direction are negligible at times greater than the diffusion time for all cracks having an aspect ratio greater than three. At large times and in regions near the ends of a crack, composition variations due to transport in the transverse direction may be observed, but these are small as compared with the variations along the length of the crack.

3) Crack Geometry, Shape - The shape of a crack has a modest but definite effect on the behavior of the electrolyte contained within it. The shape affects both the magnitude of the crack tip concentration and the shape of the longitudinal concentration profile. For example, under identical constant flux boundary conditions, the steady-state concentration difference between the tip and the mouth of a pie-shaped crack is nearly twice as great as for a rectangular crack having the same length and width. For the same boundary conditions, the steady-state longitudinal concentration profile is approximately linear for the pie-shaped crack and parabolic for the rectangular crack. The results for a hyperbolic crack lie between those for the other two crack shapes.

4) Crack Geometry, Length and Width - The geometric parameters having the greatest effect on electrolyte composition are the length and the width of the crack. The results for hyperbolic cracks with constant flux boundary conditions may be cited as an example. To a good first approximation, the steady-state concentration difference between the tip and the mouth of the crack is found to be proportional to the square of the crack length and the reciprocal of the crack width (see eqn. 111).

5) Boundary Specification Along the Crack Wall - The form of the boundary conditions along the crack wall (metal-electrolyte interface) may have a significant influence on the concentration of an ion as measured by its average or maximum value. It has little effect, however, on the shape of the concentration profile. This is illustrated, for example, by the results shown in Figures 18 and 19.

6) Composition of the Bulk Electrolyte - The electrolyte composition in the bulk solution may bear no direct relation to that within a crack-like region. This is illustrated by the results shown in Figure 20.

7) Transport by Convection - The solvent motion associated with crack opening or 'yawning' has a negligible influence as compared to the effects of crack geometry and transport by simple diffusion.

8) Transport by Migration - Transport by migration in an electrostatic field appears to have little influence on the concentration of the product species. The principal effect of migration is to alter the concentrations of the salt ions in accordance with the requirement of electroneutrality.

The first two observations are perhaps not surprising since they are consistent with simple dimensional arguments. The remainder are based solely on numerical results, those presented in the last section and many others not shown explicitly. They point to the conclusion that the factors which exert a primary influence on the concentration of the ith species in a crack-like region are: $\bar{J}_i$, the mean value of the normal flux of the ith species; a, the crack length; and b, the crack half-width. Other factors, such as crack shape or transport mode, appear to exert a secondary influence.

While the above observations represent an accurate summary of the numerical results, the data upon which they are based is limited. The last observation in particular is based on the results of a single problem. There remains the question, therefore, of whether these observations are generally applicable to transport in crack-like regions.

To answer this question requires further information.

Rather than generate additional numerical results, it is more convenient to exploit the observation that composition variations in the transverse crack direction are small with respect to variations in the longitudinal direction. This suggests that a crack-like region may be treated with reasonable accuracy as a one-dimensional continuum. The reduction of the problem to dependence on one spatial variable results in a simplified set of governing differential equations as shown in Appendix C. The advantage of this approach is that closed-form solutions may be obtained for a number of cases important to our discussion.

Simple Diffusion - Dominant Effects

Suppose we begin by looking at transport by diffusion only. Consider a single species, S_i, in a rectangular crack with a constant flux, J_i^n, normal to the crack wall. From equations (C-3a, -8 and -9) in Appendix C, the steady state concentration is

$$(C_i - C_i^\circ) = \left(\frac{J_i^n}{D_i}\right)\left[\frac{1}{2a}(a^2 - x^2) + (a - x)\right] \qquad (108)$$

where

C_i = concentration of ith dissolved species (mole/cm^3)

C_i° = concentration of ith species in the bulk electrolyte (mole/cm^3)

J_i^n = normal flux of ith species at the crack wall (positive inward) (mole/cm^2-sec)

D_i = diffusion coefficient of ith species (cm^2/sec)

a = crack length (cm)

b = crack half-width (cm)

x = distance from the crack tip (cm); $[o \leq x \leq a]$

A similar result may be obtained for transport by diffusion within a pie-shaped crack. From equations (C-3b, -8 and -9) in Appendix C with a constant normal flux, J_i^n, the steady-state concentration of the ith species is

$$(C_i - C_i^\circ) = \left(\frac{J_i^n}{D_i}\right)\left[\sqrt{1 + (a/b)^2}\,(a - x) + \epsilon a\sqrt{1 + (a/b)^2} - 1\right)\ln\left(\frac{x}{\epsilon a}\right] \tag{109}$$

where

ϵ = a number between zero and one, typically small

x = distance from the point of intersection of the extensions of the straight sides of the crack (cm) $[\epsilon a \leq x \leq a]$

It should be noted that the normal flux, J_i^n, appearing in equations (108) and (109) is taken as positive for a mass flux INTO the crack. Also, in obtaining equation (109), the crack tip is located a distance ϵa from the point of intersection of the extensions of the straight sides of the crack. Thus, in general, the width of the crack at the crack tip is non-zero and the crack profile is similar to that of the pie-shaped crack shown in Figure 6.

From equation (108), the steady-state concentration profile for a rectangular crack is parabolic. From equation (109), the steady-state concentration profile in a pie-shaped crack is very nearly linear. The deviation from linearity is significant only for values of x close to ϵa when the second term in the brackets on the right-hand side of equation (109) is no longer negligible. When ϵ, in equation (109), is zero, the width of the pie-shaped crack is zero at

the crack tip, and equation (109) reduces to

$$(C_i - C_i^\circ) = \left(\frac{J_i^n}{D_i}\right)\sqrt{1 + (a/b)^2}\,(a - x) \qquad (109\text{-a})$$

The steady state concentration is a linear function of distance from the crack tip.

The steady-state concentration difference between the tip and the mouth of the crack is obtained by setting x equal to zero in equation (108) or (109-a). For a rectangular crack,

$$\Delta C_i = (C_i - C_i^\circ)\Big|_{x=0} = \frac{J_i^n}{D_i}\left[\frac{a^2}{2b} + a\right] \qquad (110\text{-a})$$

For a pie-shaped crack,

$$\Delta C_i = (C_i - C_i^\circ)\Big|_{x=0} = \frac{J_i^n a}{D_i}\sqrt{1 + (a/b)^2} \qquad (110\text{-b})$$

When the aspect ratio, (a/b), is much greater than one, the relations expressed by equations (110) may be expressed approximately by

$$\Delta C_i = \alpha\left[\frac{J_i^n a^2}{2 D_i}\right] \qquad (111)$$

where

α = a shape factor, and

$\alpha = 1$, for a rectangular region

$\alpha = 2$, for a pie-shaped region

Equation (111) is entirely consistent with the results obtained numerically for transport by simple diffusion with constant flux boundary conditions. The steady-state concentration difference between the tip and the mouth of a crack is directly proportional to the normal flux and to the square of the crack length. It is inversely proportional to the diffusion coefficient and the width at the mouth of the crack. The constant α, viewed as a shape factor, will have a value between one and two for all crack geometries likely to be found in nature.

Boundary Conditions

While equation (111) adequately summarizes the results obtained for simple diffusion with constant flux boundary conditions, it does not explain the behavior observed with charge-transfer boundary conditions. (The important feature of such a boundary specification is that the reaction rate, or reaction current density, changes with changes in the concentrations of the dissolved species. For the reaction used in the numerical calculations, the hydrogen ion was the only dissolved species affecting the reaction rate and its normal flux was directly proportional to the reaction current density.) Since the hydrogen ion concentration was a function of distance from the crack tip, one would expect its normal flux to likewise be a function of distance and this was in fact observed. With the normal flux varying from point to point along the crack wall, one would further expect the shape of the concentration profile to differ from that of a similar curve obtained using constant flux boundary conditions. This was also observed, but the difference was small (see Figure 18).

At this point our concern is not with the validity of the numerical results. The question is, do those results

reflect the particular kinetic formulation used in that work, or does the form of the boundary conditions generally have a small effect on the shape of the concentration profile? Here, as above, the one-dimensional transport analysis developed in Appendix C is useful in framing an answer. Consider a single dissolved species, S_i, contained in a rectangular crack and assume that transport is by simple diffusion. From equations (C-8 and -9) in Appendix C, the steady state concentration is

$$(C_i - C_i^o) = \frac{1}{D_i}\left\{ J_i^t(a-x) + \frac{1}{b}\int_x^a \left[\int_o^\xi J_i^w(\xi)\, d\xi \right] d\xi \right\} \qquad (112)$$

where

J_i^t = normal flux of the ith species at the crack tip (mole/cm^2-sec)

$J_i^w(x)$ = normal flux of the ith species along the crack wall at a distance, x, from the crack tip (mole/cm^2-sec)

ξ, ζ = dummy variables

Note that both fluxes are positive when they correspond to flows INTO the crack. Also, when the metal-electrolyte interface is everywhere homogeneous, J_i^t is equal to $J_i^w(0)$.

The normal flux, J_i^w, may be treated two different ways. It may be viewed either as an explicit function of the distance x or as a function of concentration (an implicit function of x). Neither approach is completely satisfactory. When the flux is treated as a function of concentration, it is highly desirable (although, perhaps, not absolutely necessary) that the functional form used be consistent with some charge-transfer kinetic relation. Normally then, the

first step is to specify a charge-transfer reaction and kinetic equation. Once this is done, the functional relation between normal flux and concentration may be determined and the result used with equation (112) to determine the concentration. Unfortunately, it is usually not possible to obtain a closed-form solution to the resulting integral equation, so our first objective, that of obtaining a simple but completely general result, cannot be achieved in this manner. Nevertheless, a closed-form solution can be obtained for one important case and this is to be examined below. First, it will be useful to consider the other alternatives.

When the flux is treated as a function of distance, evaluation of the integral on the right-hand side of equation (112) is straightforward and yields an explicit expression for the concentration. Such a formulation has the advantage of simplicity, but explains neither how nor why the flux actually varies under a given set of boundary conditions. However, it does provide a means for establishing bounds on the effect of differences in the form of the flux specification. Specifically, by treating the normal flux as a function of distance, it is possible to establish absolute upper and lower bounds on the shape of the concentration profile.

To establish bounds of this type it is not necessary to specify the form of $J_i^w(x)$. It will be assumed, however, that J_i^w is expressible as an explicit function of x and is everywhere of the same sign as J_i^t. Following notation introduced above, the shape of the concentration profile may be conveniently characterized by the parameter $\tilde{C}$ defined by equation (101). Therefore, replacing $C_i(x)$ in equation (101) by its value in equation (112), the shape of the concentration profile is given by

$$\tilde{C}_i = \left[\frac{C_i(x) - C_i^\circ}{C_i(o) - C_i^\circ}\right] = \left[\frac{J_i^t(a - x) + I(x)}{J_i^t a + I^*}\right] \qquad (113)$$

where

$$I(x) = \frac{1}{b}\int_{x}^{a}\left[\int_{0}^{\xi} J_i^w(\xi)\,d\xi\right]d\xi \qquad (114\text{-a})$$

$$I^* = I(0) \qquad (114\text{-b})$$

Several features of equation (113) should be emphasized. First, it may be seen that I(x) is a monotonic function of x and is bounded by

$$\left|\left[1-\left(\frac{x}{a}\right)\right]I^*\right| \leq \left|I(x)\right| \leq \left|I^*\right| \qquad (114\text{-c})$$

Also, since J_i^w is everywhere of the same sign as J_i^t, I(x) is monotonically increasing or decreasing according as J_i^t is negative or positive. From this it follows that $\tilde{C}_i$ is characteristically positive regardless of the sign of the flux, that is, without regard to whether the normal flux is into or out of the crack.

The bounds we seek are simply the upper and lower limits of the right-hand side of equation (113). For example, the lower bound is approached as the integral I^* becomes small. That is,

$$L_l = \lim_{I^*\to 0}(\tilde{C}_i) = 1 - \left(\frac{x}{a}\right) \qquad (115)$$

The lower limit is approached, therefore, when the flux at the crack tip is much greater than the flux at any point along the crack wall. This behavior may be observed physically when the composition of the metal at the crack tip is significantly different from the composition along the crack wall.

When the integral I^* becomes large, or the flux J_i^t becomes small, a different behavior is observed. The limit as

J_i^t becomes small is

$$L_1 = \lim_{J_i^t \to 0}(\vec{C}_i) = I(x)/I^* \qquad (116\text{-a})$$

The desired upper bound corresponds to the upper bound of L_1 defined by equation (116-a). From the inequality (114-c) it follows that

$$L_u = \mathrm{Max}(L_1) = 1 \qquad (116\text{-b})$$

The upper limit is approached when the flux near the mouth of the crack is much greater than the flux at the crack tip or other points along the crack wall. This behavior may be observed physically when the concentration in the crack approaches its equilibrium value.

Therefore, when the normal flux is everywhere of the same sign, the shape of the concentration profile lies between the limits

$$1 - \left(\frac{x}{a}\right) \leq \left[\frac{C_i(x) - C_i^e}{C_i(o) - C_i^e}\right] \leq 1 \qquad (117)$$

In addition, the graph of the function $C_i(x)$ is a continuous curve and has a slope which is everywhere of the same sign.

Similar limits may be obtained for cracks having other than a rectangular shape. Such limits provide no detailed view of the conditions existing in cracks, but they serve to emphasize that the concentration of a dissolved species is of the same order of magnitude nearly everywhere within a crack. In addition, these limits and the general form of charge-transfer kinetic equations strongly suggest that the normal flux is likewise, nearly everywhere, of the same order of magnitude.

An indication of how the concentration actually varies within the limits described by equation (117) can be obtained

from the solution of equation (112) using a simple relation between concentration and flux. First, however, it should be noted that, for any charge-transfer reaction, the functional relation between normal flux and concentration is always expressible in the general form

$$J_i^n = \alpha_i - \beta_i C_i^p \tag{118}$$

The coefficients α_i and β_i may be functions of the potential difference across the metal-electrolyte interface and the concentrations of other dissolved species. The constant p is typically a positive integer but can be any positive number. The general solution of equations (112) and (118) is beyond the scope of the present work. Here it is assumed that α_i and β_i are functions only of the potential difference across the metal-electrolyte interface. Further, in order to display a closed-form solution, the constant p is taken as one. For our purposes then, equation (118) may be written

$$J_i^n = \beta_i(C_i^{eq} - C_i) \tag{119}$$

where

$$C_i^{eq} = \alpha_i/\beta_i$$

Equation (119) represents a substantial simplification of equation (118). Still, it provides an adequate description of a broad class of charge-transfer reactions. In this class, for example, are many dissolution-precipitation reactions. Before continuing, it may be useful to examine a specific reaction in order to show the relationship between equation (119) and the usual kinetic description of charge-transfer reactions. This will also provide a basis for evaluating the parameters β_i and C_i^{eq}. A metal-ion dissolu-

tion reaction serves as a good example. Such a reaction may be written

$$M \rightleftharpoons M^{z^+} + z^+ e^- \tag{120}$$

Equation (120) may be viewed as a specialization of equation (40). For this reaction, the reduced species (M) is insoluble and the charge-transfer valence is the same as the charge (z^+) on the oxidized species (M^{z+}, the metal ion). Letting the subscript i represent the metal ion and following the notation of Section II, the normal flux is

$$J_i^n = \frac{I_o^s}{z_i \mathcal{F}} \left\{ \exp[\alpha z_i \zeta] - \frac{C_i}{C_i^s} \exp[-(1-\alpha) z_i \zeta] \right\} \tag{121}$$

where

$$\zeta = \phi_m - \phi_s - \epsilon_s \tag{121-a}$$

and

I_o^s = standard exchange current density (amp/cm^2)

α = charge-transfer coefficient

C_i^s = standard equilibrium concentration (mole/cm^3)

ϕ_m = dimensionless potential of the metal

ϕ_s = dimensionless potential of the electrolyte at the metal-electrolyte interface

ϵ_s = dimensionless standard electrode potential

By convention, the standard conditions are taken with C_i^s equal to one mole per liter.

By direct comparison of equation (119) and (121),

$$C_i^{eq} = C_i^{\circ} \exp[z_i \xi] \tag{122-a}$$

$$\beta_i = \left(\frac{I_o^{\circ}}{z_i C_i^{\circ} \mathfrak{F}}\right)\left(\frac{C_i^{eq}}{C_i^{\circ}}\right)^{-(1-\alpha)} \tag{122-b}$$

The equilibrium concentration, C_i^{eq}, is a function of the dimensionless overpotential. It increases as the applied potential increases. The slope, β_i, depends on both the exchange current density and the equilibrium concentration. It increases as the exchange current density increases and decreases as the equilibrium concentration increases. From a comparison of equations (122-a) and (122-b), it is clear that the slope, β_i, can be written as an explicit function of the dimensionless overpotential. In many respects such a form is preferable. However, the equation is written the way it is to emphasize the relationship between the slope and the equilibrium concentration.

When J_i^n in equation (119) is used to express J_i^t and J_i^w in equation (112), it may be shown that the concentration is

$$(C_i - C_i^{\circ}) = (C_i^{eq} - C_i^{\circ})\left[1 - \frac{\cosh(\lambda\xi) + \gamma\sinh(\lambda\xi)}{\cosh(\lambda) + \gamma\sinh(\lambda)}\right] \tag{123}$$

where

$$\lambda = \sqrt{\beta_i a^2 + b D_i} \tag{124-a}$$

$$\gamma = \left(b\lambda a\right) \tag{124-b}$$

$$\xi = \left(x/a\right) \tag{124-c}$$

A simpler form may be used when the crack aspect ratio is large.

$$(C_i - C_i^\circ) = (C_i^{eq} - C_i^\circ)\left[1 - \frac{\cosh(\lambda\xi)}{\cosh(\lambda)}\right] \qquad (125)$$

For reasons of simplicity, equation (125) will be used through the remainder of this discussion.

To compare this result with those obtained earlier, it is again convenient to use the function $\tilde{C}_i$ defined by equation (101). From equations (101) and (125),

$$\tilde{C}_i = \left[\frac{\cosh(\lambda) - \cosh(\lambda\xi)}{\cosh(\lambda) - 1}\right] \qquad (126)$$

The behavior described by equation (126) is summarized in Figure 35. The function $\tilde{C}_i$ is shown for several values of the parameter λ. When λ is less than one, the deviation from the parabolic profile characteristic of constant flux boundary conditions is small. An increase of λ by one-and-one-half orders of magnitude results in a concentration profile which is virtually flat over ninety percent of the crack length. Only in a region close to the mouth of the crack does the concentration differ significantly from the value at the crack tip.

The normal flux can be determined from equations (119) and (125). After introducing $\tilde{J}_i$, a non-dimensionalized flux, for later notational convenience, the result is

$$\tilde{J}_i = \frac{J_i^n}{\beta_i(C_i^{eq} - C_i^\circ)} = \frac{\cosh(\lambda\xi)}{\cosh(\lambda)} \qquad (127)$$

The behavior of the normal flux is summarized in Figure 36. The dimensionless flux, $\tilde{J}_i$, is shown as a function of ξ

for the same values of λ as those used in Figure 35. When λ is less than one-third, the normal flux is essentially constant over the entire crack length. Increasing λ by two orders of magnitude reduces the normal flux to a value close to zero over most of the crack length. Only in the region near the mouth of the crack is the flux appreciable. Comparison of Figures 35 and 36 shows that the change in the shape of the concentration profile from parabolic to flat is associated with a change in the distribution of the normal flux along the length of the crack.

The change from a parabolic to a flat concentration profile occurs over a relatively narrow range of λ values. The reason for the change is shown in Figure 37. The lower curve is a graph of the concentration ratio, Q_i, as a function of λ where Q_i is defined as the ratio of the concentration difference between the tip and the mouth of the crack to the concentration difference at equilibrium. That is,

$$Q_i = \left[\frac{C_i(n) - C_i^o}{C_i^n - C_i^o}\right] = \left[\frac{\cosh(\lambda) - 1}{\cosh(\lambda)}\right] \qquad (128)$$

For small values of λ, the concentration ratio, Q_i, increases as the square of λ. As λ approaches one, Q_i begins to deviate from the curve for small λ values. For values of λ greater than 10, Q_i is independent of λ and equal to one. Therefore, the change from a parabolic to a flat concentration profile occurs when the concentration in the crack approaches its equilibrium value.

The practical significance of these results depends on the range of λ values likely to be encountered physically. An estimate of this range can be constructed from estimates of the parameters in equation (124-a). However, a more convenient form may be obtained by replacing β_i in equation (124-a) by its value in equation (122-b) and setting the

charge-transfer coefficient equal to one-half. That is,

$$\lambda^2 = \frac{I_o^s a^2}{b \mathfrak{F} z_i D_i \sqrt{C_i^s C_i^{eq}}} \qquad (129)$$

Values of the exchange current density, I_o^s, are typically of the order of 10^{-9} to 10^{-3} amps per square centimeter. Ion diffusion coefficients are about 10^{-5} centimeters squared per second at room temperature. The equilibrium concentration may vary over a wide range depending on the value of the overpotential, ζ, but the range, 10^{-9} to 10^{-1} moles per cubic centimeter, appears reasonable. The crack dimensions may also vary over a wide range. However, a crack length of one centimeter and a crack aspect ratio of one hundred are typical. Faraday's constant is about 10^{+5} coulombs per equivalent. Ion valences are all of the order of magnitude of one. By convention, the standard equilibrium concentration is 10^{-3} moles per cubic centimeter. Using these values in equation (129), the range of λ values is found to be 10^{-13} to 10^{+5}.

A very small or very large value of λ characterizes a reaction which is displaced far from equilibrium. Very small values correspond to large positive overpotentials and thus, to large positive values of the normal flux, J_i^n. Very large values correspond to large negative overpotentials and thus, to large negative values of J_i^n. For reactions close to equilibrium, the value of λ is typically in the range, 10^{-2} to 10.

The limits, λ equal to zero and λ equal to infinity, correspond respectively to positive and negative values of the normal flux. However, it should be cautioned that the sign of the flux does not necessarily determine the shape of the concentration profile. The sign of the flux is determined by the sign of $(C_i^{eq} - C_i^o)$. That is, the flux is

positive or negative according as the equilibrium concentration is greater than or less than the concentration in the bulk electrolyte. On the other hand, the shape of the concentration profile depends only on the value of λ. That value is in turn a function of C_i^{eq}, but it is independent of the concentration in the bulk electrolyte.

Taken together, the above results indicate that treating the normal flux as a constant is an accurate approximation for a wide range of λ values. More precisely, when λ is less than or equal to one, the error introduced by using a parabolic approximation to $\tilde{C}_i$ is everywhere less than one percent. In terms of the kinetic parameters of equation (121), the error in $\tilde{C}_i$ is less than one percent when

$$\exp\left[(1-\alpha)z_i\zeta\right] \geq \left(\frac{I_0^s a^2}{z_i D_i C_i^s 3b}\right) \tag{130}$$

Of the results thus far, two are particularly striking. The first is the bounds given by equation (117). The second is the close conformity of the actual concentration profile to the parabolic approximation over a wide range of λ values. These results suggest that a satisfactory approximation to the concentration in a crack-like region may be obtained from an equation of the form of equation (118) or (119), and the average concentration calculated from equation (108). For example, assuming that the crack aspect ratio is large and treating J_i^n as a constant, the average concentration, C_i^*, calculated from equation (108) is

$$C_i^* = C_i^s + \frac{J_i^n a^2}{3bD_i} \tag{131-a}$$

Replacing C_i in equation (119) by C_i^*,

$$J_i^n = \beta_i(C_i^{eq} - C_i^*) \tag{131-b}$$

Equations (131) constitute a system of two equations in two unknowns. Letting J_i^* be the value of J_i^n, which satisfies equations (121), the solution of this system of equations is

$$C_i^* = C_i^\circ + \frac{\lambda^2(C_i^{eq} - C_i^\circ)}{3 + \lambda^2} \qquad (132\text{-a})$$

$$J_i^* = \frac{\beta_i(C_i^{eq} - C_i^\circ)}{1 + \lambda^2/3} \qquad (132\text{-b})$$

The procedure is essentially the same when the flux is given by an equation of the form of equation (128). However, the system of equations will usually be larger and may be non-linear.

The agreement between equation (132-a) and the average concentration from equation (125) is excellent. Equation (132-a) is assymptotically correct for both small and large λ values. The maximum error is about twelve percent at a λ value of about four.

In contrast, equation (132-b) is correct only for small values of λ. Letting $\bar{J}_i$ be the average value of the normal flux calculated from equations (119) and (125), the ratio, $(\bar{J}_i/J_i^*)$, is

$$\left(\frac{\bar{J}_i}{J^*_i}\right) = \frac{1}{\lambda}\left[1 + \frac{\lambda^2}{3}\right]\tanh(\lambda) \qquad (133)$$

This flux ratio is shown as a function of λ by the upper curve in Figure 37. For λ values less than one the ratio is essentially one. For larger λ values, the ratio increases with increasing λ, so J_i^* underestimates the true average value by increasingly greater amounts. This occurs because the true value of the flux always remains different from zero in a small region near the mouth of the crack. As a

result, the true value of the average flux approaches zero more slowly with increasing λ than does J_i^*.

Whether the discrepancy between J_i^* and $\bar{J}_i$ is significant is a moot question. Because of the shape of the concentration profile for large values of λ, the average flux, $\bar{J}_i$, provides a less accurate measure of the reaction rate in the crack interior than does J_i^*. On the other hand, J_i^* provides a poor estimate of the total mass flux entering or leaving through the mouth of the crack.

This analysis is consistent with the numerical results and places them in a broader perspective. It shows that the concentration profile is nearly parabolic over a wide range of conditions. Significant deviations from the parabolic shape do occur for values of λ greater than one, but for values greater than thirty, the concentration profile is virtually flat. Only for λ in the range between one and thirty does the shape of the concentration profile differ significantly from one of the two limits, so the parameter λ may be used as a quick and simple indicator of the shape of the concentration profile. Finally, it has been shown that accurate estimates of the concentration and the flux in the interior of a crack-like region may be obtained from the assumption that the normal flux is uniform. The accuracies of these estimates are virtually independent of the actual shape of the concentration profile.

The numerical results, the bounds summarized by equation (117), and the one-dimensional analysis presented above, form a coherent and fairly complete description of the interaction between normal flux and concentration in a crack-like region. The results of the numerical calculations and those of the one-dimensional analysis provide specific examples of how the normal flux actually varies from point to point along the crack wall depending on the reaction kinetics, the applied potential, and the composition of the bulk electrolyte.

These results indicate that the shape of the concentration profile is very nearly parabolic over a wide range of conditions. In addition, the results of the one-dimensional analysis in general, and equation (127) in particular, emphasize that when the metal-electrolyte interface is homogeneous, the normal flux is everywhere of the same sign. Finally, the results most important to an understanding of transport in crack-like regions are the bounds summarized by equation (117). These bounds, together with the fact that the concentration is a smooth, continuous function of distance, indicate why the form of the boundary conditions does not have a strong influence on the shape of the concentration profile. They also provide a theoretical basis for the use of approximations such as equations (132) to estimate the composition within a crack-like region.

Convective Transport

The numerical work indicated that transport by diffusion plays a dominant role in determining the concentration in a crack-like region. Transport by convection and migration appeared to have little effect on the results, either at short times or long times. If this is generally true, the complexity of many electrochemical transport problems may be substantially reduced. If not, it may still be possible to generate useful results using a diffusion analysis. In this case, however, it will first be necessary to determine the range over which the effects of migration and convection are negligible and to estimate bounds on the errors introduced when they are not.

The results of the last section indicate that convection plays a minor role in the case of a hyperbolic crack subjected to the opening mode of crack deformation. That convective transport is almost always unimportant may be shown

from the one-dimensional transport analysis in Appendix C. Consider first the opening mode of crack deformation and, for simplicity, assume that the crack is rectangular. If the crack walls move outward with a uniform velocity, v_ω, the rectangular region remains rectangular, and the average longitudinal velocity, $\bar{v}$, is

$$\bar{v} = -\left(\frac{v_\omega a}{b}\right)\xi \tag{134}$$

where

$$b = b_o + v_\omega t \tag{135}$$

and

b_o = value of the crack width, b, at time zero (cm)

t = time (sec)

ξ = dimensionless distance from the crack tip (x/a)

Note that the average longitudinal velocity, $\bar{v}$, is a linear function of distance from the crack tip. The same result is obtained for the opening mode of deformation regardless of the crack shape.

From equations (C-2 and -4) in Appendix C, the differential equation describing convective transport in a rectangular crack is

$$\frac{\partial C_i}{\partial \tau} + v^* \frac{\partial C_i}{\partial \xi} - \frac{\partial^2 C_i}{\partial \xi^2} - \left(\frac{J_i^n a^2}{D_i b}\right) = 0 \tag{136}$$

where

$$\tau = D_i t \tag{137-a}$$

$$v^* = \bar{v} a / D_i \tag{137-b}$$

As the coefficient v^* approaches zero, the convective term approaches zero, and equation (136) approaches the differential equation governing transport by simple diffusion. When v^* is greater than zero, omission of the convective term introduces an error. For example, when v^* is one-tenth, the error introduced by neglecting the convective term is about two percent; when v^* is one, the error is about fifteen percent. By comparison, the maximum value of v^* in the convective-diffusion problems of the last section was about seven. For that value of v^*, the deviation of the solution from the solution for simple diffusion was about twenty-five percent.

At short times, the concentration at the crack tip is influenced only by conditions existing in a region close to the tip. But, by equation (134), the velocity there is zero. Therefore, equation (136) reduces to the equation describing transport by simple diffusion and, at short times, the solvent motion has no effect on the concentration at the crack tip. This was observed in the results presented in the last section.

At large times, motion of the solvent affects the concentration everywhere within the crack. But, from the definition of v^* and equations (134) and (135), it may be shown that

$$|v^*| < \frac{a^2 (p - p_0)}{12 \mu b} \tag{138}$$

In particular, for times of the order of the time to reach the steady state,

$$t \geqq a^2 / D_i \tag{139-a}$$

and

$$|v^*| \leq \left(\frac{b - b_o}{b}\right) < 1 \qquad (139\text{-b})$$

Thus, for times of the order of the time to reach the steady state, the error introduced by neglecting the convective term is less than twenty percent. The error may be greater than this at shorter times, but it is certainly less at larger times.

For technical alloys, the crack deformation rates which can be sustained for extended periods of time are limited by metal fracture. Thus, for problems of practical interest, the crack deformation rates will be small and the errors will be less than that corresponding to the absolute upper bound in equation (139-b). In this connection, it should be emphasized that a v^* value of seven was obtained in the numerical calculations only by ignoring changes with time in the crack dimensions.

For the mode of crack deformation we have called the crack growth mode, the longitudinal solvent velocity is constant along the length of the crack and the velocity profile is approximately parabolic at every cross-section. As a result, the velocity relative to the crack tip is zero, and, according to the one-dimensional transport analysis, the governing differential equation reduces to that for transport by simple diffusion. Thus, when the boundary conditions are expressed as functions of distance from the crack tip (a moving coordinate), the analysis of problems involving the growth mode of crack deformation is identical to that for transport by simple diffusion in a stationary crack.

The above results show that the convective term may be omitted in almost all problems involving transport in a crack-like region. For the opening mode of crack deformation,

the error introduced by neglecting the convective term does not exceed twenty percent for times greater than (a^2/D_i). For the growth mode of crack deformation, no error is introduced by neglecting convective transport relative to the crack tip, since this contribution is in fact zero.

Migration

The results of only one electrochemical transport problem were presented in the last section. Those results were consistent with the view that diffusion is the dominant mode of ion transport. However, none of the data presented indicates the range over which this observation may be valid. It is not clear, for example, that the diffusion equation even constitutes a useful approximation outside the range of very small current densities.

To evaluate the importance of transport by migration and to understand the role of the electrostatic potential in electrochemical transport requires a more detailed analysis. Once again, the one-dimensional transport analysis provides a suitable framework. It has been possible to obtain a general solution to a class of problems which includes the problem solved numerically as a special case. A detailed discussion of this solution is contained in Appendix D. Because the solution is expressible in closed-form and is not too complicated, it is ideally suited to our present purposes.

It is assumed that the crack is rectangular and the system is at steady state. Transport is by diffusion and migration. The electrolyte contains three dissolved species with the charge numbers

$$z_1 = -z_2 = z_3 = +1 \qquad (140)$$

Species one and two will be called the salt ions and species three will be called the product ion. By analogy with the problem solved numerically, the species one, two, and three may be associated with the ions Na^+, Cl^-, and H^+ respectively. The subscript notation is adopted here both for convenience and to emphasize that the results are in no way restricted to a particular electrolyte.

The boundary conditions are similar to those used in the problem solved numerically. No restriction is imposed on the normal flux of species three. The normal flux of species one and two is taken as zero at every point along the metal-electrolyte interface. In the notation introduced above,

$$J_i^t = J_i^\omega = 0, \quad i = 1,2 \tag{141}$$

From equations (D-6, -10, -11, and -12) in Appendix D, the steady state solution is

$$C_1 = C_1^\circ / U(x) \tag{142}$$

$$C_2 = (C_1^\circ + C_3^\circ) U(x) \tag{143}$$

$$C_3 = (C_1^\circ + C_3^\circ) U(x) - C_1^\circ / U(x) \tag{144}$$

$$\phi = \ln[U(x)] \tag{145}$$

where

$$U(x) = 1 + \frac{1}{2} \int_x^a J_3^\omega(\xi) d\xi \tag{146}$$

$$g(x) = D_3 (C_1^\circ + C_3^\circ) \left[J_3^t + \frac{1}{b} \int_0^x J_3^\omega(\xi) d\xi \right] \tag{147}$$

The correctness of this solution may be verified by direct substitution of equations (142 - 147) into the flux equation and the electroneutrality equation (eqns. C-4 and -5 in Appendix C). Note that the dimensionless potential, ϕ, has been set equal to zero at the mouth of the crack (x = a). This has been done for convenience and consistency with the numerical work, since the absolute value of the potential has no effect on the results.

Several features of the solution deserve special emphasis. The concentration of species one, the positive salt ion, is inversely proportional to the function u(x); the concentration of species two, the negative salt ion, is directly proportional to u(x). This suggests that the solution may be unbounded as u(x) approaches either zero or infinity. It may also be seen that the diffusion coefficients of the salt ions do not appear in the equations. In fact, the steady state solution never includes the diffusion coefficient of a species whose flux is zero.

When the normal flux of species three is constant everywhere along the metal-electrolyte interface,

$$J_3^t = J_3^\omega = J_3^n, \text{ a constant} \tag{148}$$

and equations (146) and (147) may be written

$$U(x) = 1 + \frac{J_3^n}{2D_3(C_1^\circ + C_3^\circ)}\left[(a-x) + \frac{1}{2L}(a^2 - x^2)\right] \tag{149}$$

$$g(x) = \frac{J_3^n}{D_3(C_1^\circ + C_3^\circ)}\left[1 + \left(\frac{x}{L}\right)\right] \tag{150}$$

When the normal flux of species three is constant, the current density normal to the metal-electrolyte interface, I_n, is also constant and may be written as

$$I_n = \mathfrak{F} J_3^n \tag{151-a}$$

The current density in the longitudinal direction, I_ℓ, is

$$I_\ell = \mathfrak{F} J_3^n \left[1 + \left(\frac{x}{b}\right)\right] \tag{151-b}$$

I_ℓ is a linear function of distance from the crack tip. When the crack aspect ratio is large, the current density at the mouth of the crack may be one or more orders of magnitude greater than I_n.

From equations (145) and (149), the steady state value of the potential difference between the tip and the mouth of the crack, $\Delta\phi_{ss}$, is

$$\Delta\phi_{ss} = \ln\left\{1 + \frac{J_3^n a^2}{4\mathfrak{F} L_3 (C_1^\circ + C_3^\circ)}\left[1 + \left(\frac{2b}{a}\right)\right]\right\} \tag{152}$$

For comparison, the initial value of the potential difference, $\Delta\phi_\circ$, is

$$\Delta\phi_\circ = \frac{J_3^n a^2 \left[1 + \left(\frac{2b}{a}\right)\right]}{4\mathfrak{F}\left[C_1^\circ (D_1 + L_1) + C_3^\circ (D_3 + L_3)\right]} \tag{153}$$

where, in writing equation (153) it is assumed that the initial composition of the electrolyte is everywhere constant and equal to the composition of the bulk electrolyte.

For simplicity and clarity, we will focus attention on the special case when J_3^n is constant. Also, for the example to be presented, the transport properties, crack dimensions, and boundary conditions will be the same as those used in the electrochemical transport problem solved numerically. The

normal current density, I_n, will be treated as the independent variable. This specialization permits a direct comparison with the numerical problem and provides a feel for magnitudes not conveyed when results are presented in dimensionless form.

Thus, the parameters of the solution will have the following values unless otherwise stated.

$$\begin{aligned} a &= 0.200 \text{ cm} \\ b &= 0.020 \text{ cm} \\ C_1^o &= 0.6 \times 10^{-3} \text{ mole/cm}^3 \\ C_3^o &= 1.0 \times 10^{-10} \text{ mole/cm}^3 \\ D_1 &= 1.33 \times 10^{-5} \text{ cm}^2/\text{sec} \\ D_2 &= 2.00 \times 10^{-5} \text{ cm}^2/\text{sec} \\ D_3 &= 9.00 \times 10^{-5} \text{ cm}^2/\text{sec} \end{aligned} \qquad (154)$$

For the numerical problem, the normal current density, I_n, was 314 microamps per square centimeter (J_3^n was 3.25×10^{-9} moles per square centimeter per second). When I_n is assigned this value and the other parameters are evaluated as shown above, the agreement between this solution and the numerical solution is excellent. When the appropriate quantities are plotted in Figures 30, 32, 33, and 34, the points are coincident with those shown for the numerical results, with one exception. The current density versus distance curve does not show the deviation from linearity exhibited by the numerical results.

The behavior of this system over a broad range of current densities is summarized in Figures 38, 39, and 40. In Figure 38, the crack-tip pH (defined here as the negative common logarithm of C_3, evaluated at x equal to zero) is

shown as a function of the normal current density. The concentration of species three is calculated from equations (144) and (149) using the values of the parameters given in equations (154). The point on the curve corresponding to the results of the numerical problem is shown by a solid circle. The pH which would exist in the absence of a potential gradient (transport by simple diffusion) is shown by a broken line.

As the current density increases, the concentration increases and the crack-tip pH decreases. When the current density is small, the potential gradient is small and the pH is essentially the same as would be calculated ignoring the effects of migration. Here, the two curves are coincident. As the concentration approaches the value of the salt concentration in the bulk electrolyte (pH $\approx$ 0), the potential gradient begins to affect the solution and the curves separate. At high current densities, the curves become parallel. At any given current density, the diffusion curve indicates a pH value 0.301 less than the true value. Thus, the effect of migration at high current densities is to reduce the product ion concentration to a value one-half as large as that predicted by diffusion alone.

In Figure 39, the crack tip concentrations of all three ions are shown as functions of the normal current density. The concentrations are calculated from equations (142), (143), (144), and (149) using the values of the parameters in equations (154). The solid points indicate the results of the numerical problem.

When the current density is small, the concentration of the product ion is small compared to that of the positive salt ion. In this range, the concentrations of the salt ions are insensitive to the applied current or the presence of the product ion. The product ion behaves as though it carried no charge. As the current density increases, the

concentration of the product ion increases. When it reaches a value close to that of the salt in the bulk electrolyte, there are sensible changes in the concentrations of the salt ions. The electrolyte within the crack becomes enriched in the negative salt ion and depleted in the positive salt ion. This trend continues with further increases in the current density. At very large currents, the crack becomes severely depleted in the positive salt ion. In this range, the behavior is, for all intents and purposes, the same as in a binary electrolyte.

The behavior of the electrostatic potential is illustrated in Figure 40. The potential difference between the tip and the mouth of the crack is shown as a function of the applied current density. Two values are shown. The upper curve is the initial value of the potential difference. It was constructed using equation (153) and the data in equations (154). The lower curve is the steady state value. It was obtained from equation (152), again using the data in equations (154). The solid points indicate the results of the numerical problem.

When the normal current density is small, both values of the potential are proportional to the applied current, but the steady state value is about one-fifth of the initial value. As the current density increases, the initial value remains proportional to the current. In contrast, the steady state value is proportional to the current only within a limited range. Beyond this range, the slope of the potential-current curve decreases with increasing current. At very large current densities the ratio of the steady state potential to the initial potential approaches zero. By comparison with Figure 39, it may be seen that the current density corresponding to the upper limit of the proportional behavior is the same as that required to raise the product ion concentration to the level of the salt concen-

tration in the bulk electrolyte.

The example above illustrates most of the important features of electrochemical transport. It shows the entire range of behavior of the product ion, from simple diffusion at low current densities to behavior as one of the ions in a binary electrolyte at high current densities. It shows the effects of the electroneutrality requirement by the changes in the concentrations of the salt ions with changes in the applied current. Most importantly, it shows how the electrostatic potential changes with changes in the applied current. Being a specific example, however, it illustrates these effects in relation to a specific set of boundary conditions. It does not indicate the range over which the effects may be observed, nor does it provide a truly satisfactory basis for understanding them. For this, it is necessary to return to the solution as expressed by equations (142 through 145) and equation (149).

Consider first the behavior of the product ion when the normal current density is positive. Over most of the range of positive current densities, the product ion behaves in one of two ways. Depending on the composition of the bulk electrolyte, it may behave at low current densities as an uncharged species, obeying the differential equation for transport by ordinary diffusion. At sufficiently large current densities, it always behaves as one species in a binary electrolyte. (This may be shown to hold quite generally, without regard for the number or charges of the other charged species, as long as each of these species has a zero normal flux.) The transition from one behavior to the other typically occurs over a relatively narrow range of current densities.

All of this is readily apparent when equation (144) is

written in the form*

$$\Delta C_3 = C_3(o) - C_3^\infty = \delta C_3 \left[1 - \tfrac{1}{2} f(\delta C_3)\right] \qquad (155)$$

where

$$\delta C_3 = \frac{J_2^n a^2}{2 D D_3} \left[1 + \frac{3 b^2}{a^2}\right] \qquad (156\text{-a})$$

and

$$f(\delta C_3) = \frac{\delta C_3 + 2 C_3^\infty}{\delta C_3 + 2 (C_1^\infty + C_3^\infty)} \qquad (156\text{-b})$$

Comparison of equations (156-a) and (110-a) shows that δC_3 is just the concentration difference between the tip and the mouth of the crack that exists when the product species carries no charge. When $f(\delta C_3)$ is zero, the product ion behaves as an uncharged species. When it is large, the product ion behaves as an ion in a binary electrolyte.

From equation (156-b), the function $f(\delta C_3)$ is bounded by the limits

$$0 < \frac{C_3^\infty}{C_1^\infty + C_3^\infty} < f(\delta C_3) < 1 \qquad (157)$$

From these bounds and equation (155), it is clear that the

---

* For notational convenience, equation (144) has been evaluated at x equal to zero, the crack tip. For a general value of x, it is necessary only to replace the right-hand side of equation (156-a) by the right-hand side of equation (108).

actual concentration difference between the tip and the mouth of the crack is never less than one-half, nor greater than one, times the concentration difference corresponding to transport by diffusion only. It is also apparent that the product ion can actually behave as an uncharged species only when its concentration in the bulk electrolyte is small with respect to the concentration of the positive salt ion.

The transition from one mode of behavior to the other occurs within a relatively narrow range. Suppose, for example, that C_3^o is much less than C_1^o. In this case, the error introduced by assuming that transport is by diffusion is less than ten percent when δC_3 is less than $(\frac{4}{9}C_1^o)$. On the other hand, treating the electrolyte as a binary introduces less than ten-percent error when δC_3 is greater than $(16C_1^o)$. So, the electrolyte must actually be treated as a ternary system only over a range of about two orders of magnitude.

The behavior of the salt ions follows that of the product ion. When $f(\delta C_3)$ is small with respect to one, their concentrations are essentially the same as those in the bulk electrolyte. When $f(\delta C_3)$ is very close to one, the concentration of the positive salt ion is near zero, while the concentration of the negative salt ion is approximately equal to that of the product ion. Clearly, then, the value of the function $f(\delta C_3)$ completely characterizes the behavior of the system when the current density is positive.

When the current density is negative, the behavior is different in one important respect. Since negative concentrations are not physically allowable, there is a lower limit to the allowable values of the normal current density. In the terminology of equations (155) and (156), δC_3 is bounded from below. The value of this bound is obtained by setting $C_3(0)$ equal to zero in equation (155). Thus

$$\delta C_3 \geq -2(C_1^\circ + C_3^\circ)\left[1 - \sqrt{1 - \left(\frac{C_3^\circ}{C_1^\circ + C_3^\circ}\right)}\right] \qquad (158)$$

From equations (156-b) and (158), it follows that for negative values of the normal current density

$$0 \leq \left[1 - \sqrt{1 - \left(\frac{C_3^\circ}{C_1^\circ + C_3^\circ}\right)}\right] \leq f(\delta C_3) \leq \left(\frac{C_3^\circ}{C_1^\circ + C_3^\circ}\right) \leq 1 \qquad (159)$$

Comparison of equations (157) and (159) shows that the function $f(\delta C_3)$ is always non-negative and is bounded by the limits zero and one. It provides the same characterization of the system and is amenable to the same interpretation at negative currents as at positive current densities.

The normal current density corresponding to the limiting value of δC_3 in equation (158) is called the limiting diffusion current density or, simply, the diffusion current density. It may be determined from equations (151-a), (156-a), and (158). The values of the concentrations and the electrostatic potential at the crack tip may be obtained from equations (142 through 145) and equation (149), again, using the limiting value of δC_3 from equation (158). The results are

$$I_n = \frac{4bzFD_3(C_1^\circ + C_3^\circ)}{a^2 + 2ab}\left[1 - \sqrt{1 - \left(\frac{C_3^\circ}{C_1^\circ + C_3^\circ}\right)}\right] \qquad (160\text{-a})$$

$$C_1(0) = \sqrt{C_1^\circ(C_1^\circ + C_3^\circ)} \qquad (160\text{-b})$$

$$C_2(0) = \sqrt{C_1^\circ(C_1^\circ + C_3^\circ)} \qquad (160\text{-c})$$

$$C_3(0) = 0 \qquad (160\text{-d})$$

$$\phi(0) = \frac{1}{2} \ln\left[\frac{C_1^o}{C_1^o + C_3^o}\right] \qquad (160\text{-e})$$

The value of the diffusion current density in equation (160-a) is consistent with simple dimensional arguments. It increases as the crack length decreases and as the ion concentration in the bulk electrolyte increases. The concentrations of the salt ions are equal and approach zero as the salt concentration in the bulk electrolyte approaches zero. The value of the electrostatic potential, which is equal to the potential difference between the tip and the mouth of the crack, approaches zero as the concentration of the product ion in the bulk electrolyte approaches zero. This is not surprising since the diffusion current density approaches zero at the same time. As the concentration of the positive salt ion approaches zero, the electrostatic potential at the crack tip approaches minus infinity. The diffusion current density then approaches a value twice as large as the one corresponding to transport by simple diffusion.

It should be emphasized that the potential difference between the tip and the mouth of the crack is unbounded only in the case of a binary electrolyte. The presence in the bulk electrolyte of a third ion, having the same charge as the product ion, eliminates the singularity at the crack tip. However, this ion must be present in relatively large concentrations to have a practical effect. For example, when the concentration of the positive salt ion, C_1^o, in equation (106-e) is equal to that of the product ion, C_3^o, the potential difference corresponding to the limiting diffusion current density is nine millivolts. When C_1^o is equal to $10^{-2}C_3^o$, the potential difference is 59 millivolts. When C_1^o is equal to $10^{-4}C_3^o$, the potential difference is 118 millivolts. These values should be compared to eighteen millivolts, the value

of the potential difference when the normal current density is of the same magnitude, but of the opposite sign as the diffusion current density in the binary system.

From the definition of conductivity following equation (17), it is clear that small changes in composition produce small changes in conductivity. The large potential changes illustrated above suggest, therefore, that the steady state potential does not satisfy Ohm's law at current densities close to the diffusion current density.

The same conclusion, over a broad range of current densities, is suggested by the results shown in Figure 40. The steady-state potential difference was obtained from the solution of the governing differential equations, assuming that the time rates-of-change of the ion concentrations were small with respect to the other terms in the equations. The initial value was obtained from the same set of equations, assuming this time that the electrolyte was homogeneous. As indicated above, this is equivalent to the requirement that the current and potential satisfy Ohm's law. While both assumptions are valid in their stated time domains, the Ohm's law statement does not appear to be valid at steady state.

Since Ohm's law is often used in the solution of electrochemical transport problems, it is worth considering whether its use is ever justified. First, however, it will be convenient to rewrite equations (152) and (153) in terms of the parameter δC_3 defined by equation (156-a). From equations (152) and (156-a), the steady-state potential difference between the tip and the mouth of the crack is

$$\Delta\phi_{ss} = \ln\left[1 + \frac{\delta C_3}{2(C_1^0 + C_3^0)}\right] \qquad (161)$$

Similarly, from equations (153) and (156-a), the initial value is

$$\Delta\phi_o = \frac{D_3 \delta C_3}{C_1^o(D_1 + D_2) + C_3^o(D_2 + D_3)} \qquad (162)$$

The ratio of the two values provides a simple measure of the agreement between Ohm's law and the actual steady state potential. For simplicity, we will consider only the case when C_3^o is small with respect to C_1^o. In this case, the bulk electrolyte is for all intents and purposes a binary salt solution.

When the current density is small, the logarithm in equation (161) may be approximated by its second term, and the ratio of the potential differences is

$$\frac{\Delta\phi_{ss}}{\Delta\phi_o} = \frac{D_1 + D_2}{2D_3} \qquad (163)$$

The ratio is one when the diffusion coefficient of the product ion is equal to the arithmetic average of the diffusion coefficients of the salt ions. So, Ohm's law may yield a satisfactory approximation to the steady state potential when the diffusion coefficients are all about the same. Although this condition was not satisfied in the example problem, it often is satisfied for problems not involving either the hydrogen or the hydroxyl ions.

At high current densities, the approximation based on Ohm's law is never correct. It consistently overestimates the true steady state potential by a significant margin. This follows directly from equations (161) and (162). The steady state potential increases as the logarithm of the concentration δC_3; Ohm's law indicates that it should increase linearly.

While Ohm's law may yield incorrect estimates of the electrostatic potential, the major objection to its use is

philosophical rather than practical. Its use carries the implication that migration is the primary mode of current transport and that compositional differences between the crack and the bulk electrolyte are negligible. In fact, one-half or more of the total current is transported by diffusion, and, as has been shown, the compositional differences this requires are often substantial.

When the ion with the non-zero flux has a negative charge, it is only necessary to replace u in equation (145) by (1/u) and assign the opposite signs to the charge numbers in equation (140). This changes the sign of the relation between the normal flux and the current density but has no other effect. Therefore, the results presented here apply to any 1-1-1 electrolyte for which the normal fluxes of two species are zero. They may be conveniently summarized as follows.

1) When it is assumed that transport is by simple diffusion, the resulting estimate of the product ion concentration is never in error by more than a factor of two.

2) An estimate of the error in the above approximation may be obtained from the ratio, R_c, of the calculated concentration to the total salt concentration in the bulk electrolyte. When the ratio is less than one-half, the error is less than ten percent. When the ratio is greater than twenty, the error is between 1.9 and 2.0. In the latter case, the electrolyte essentially behaves as a binary system, so the binary approximation will often be more useful in this range than the simple diffusion analysis.

3) The concentrations of the salt ions follow that of the product ion. The crack is depleted in the salt ion carrying the same charge as the product ion, and concen-

trated in the salt ion carrying the opposite charge.

4) The potential is described by Ohm's law at times small with respect to the diffusion time (a^2/D_i). The steady state potential may be approximated using equation (161) with δC_3 replaced by its approximate value from the diffusion analysis. If the concentration estimate is corrected as indicated above, the expression for the potential is exact.

These results are consistent with those obtained numerically. They indicate that the diffusion equation provides a good estimate of the concentration of a product species. When the requirements of electroneutrality are considered, satisfactory approximations to the salt ion concentrations may also be obtained.

Recapitulation

When the separate observations and findings of the last two sections are viewed as a whole, they form a coherent and fairly complete picture of corrosion and transport in crack-like regions. They indicate that the average concentration of an ion which enters into a surface reaction is, to a good first approximation, given by

$$\bar{C}_i = C_i^s + \left(\frac{\bar{J}_i^n a^2}{2D_i}\right) \qquad (164)$$

Thus, the factors which have a primary influence on the composition within a crack-like region are the average values of the normal ion fluxes, the crack aspect ratio, and the crack length. Other factors, such as the shape of the crack, the exact form of the boundary conditions, and the transport mode, can and do affect the composition. In general, however,

these factors are of lesser importance.

Operationally, the results suggest that first order approximations to the ion concentrations may be obtained using a method similar to that described by equations (132). The accuracy of the resulting estimates may then be determined by comparing them with the ionic strength of the bulk electrolyte. For most problems it will be found that the electrolyte can be treated either as an ordinary solution or as a binary electrolyte. That is, either the dissolved species may be treated as having zero charge and the gradient of the electrostatic potential ignored, or they may be treated as charged species moving in the electrostatic field created by the transport of the two principal ions.

Clearly, situations will arise for which neither of these approximations is satisfactory. In such cases, it will be necessary to use the more sophisticated solution techniques developed in this work. When two-dimensional transport effects are known or thought to be important the numerical method is particularly well-suited. When the boundary conditions are simple and the time-rate-of-change of the electrolyte composition is small, the steady state form of the one-dimensional transport analysis is preferred. For problems involving time-dependence or complex boundary specifications, the numerical technique is the best of the existing methods. However, a numerical method based on the one-dimensional transport analysis would be simpler and more efficient in the long run.

VII. CONCLUDING REMARKS

The work presented here was originally aimed at developing an analytic framework for the study of stress corrosion cracking. As the work progressed, it became clear that it would be necessary first to determine what factors most strongly affect corrosion and transport processes in cracks. Only then would it be reasonable to undertake the modeling of such a complex process as crack growth. While the results do not go beyond that first stage, they do provide a basis for a discussion of some general aspects of stress corrosion cracking.

One of the longstanding rules of thumb in stress corrosion cracking is 'metals that corrode don't stress corrode'. Like other such rules, it is not necessarily true, but it points out that, by and large, alloys susceptible to cracking in a particular environment do not actively corrode in that environment. They typically have corrosion potentials in the passive region, a range of potentials within which a metal-oxide is stable in contact with water.* When there is an adequate oxygen supply, the oxide usually forms by reaction of the metal with dissolved oxygen. When the oxygen supply is limited, as is probable in a crack or crevice, the oxide forms either by hydrolysis of metal ions or by direct reaction of the metal with water. Regardless of the reaction path, the formation of a metal-oxide in the absence of free oxygen is accompanied by the release of hydrogen ions.

If the electrolyte within a crack is depleted in oxygen, the pH should be in the acid range. Evidence presented in two recent papers, one by B. F. Brown, C. T. Fujii, and E. P. Dahlberg [3] and the other by J. A. Smith, M. H. Peterson,

---

* See the footnote at the bottom of page 134.

and B. F. Brown [24], indicates that this is, in fact, the case. Their data show that for cracks in a variety of materials the pH is in the range between about 1.5 and 3.5. In general, the data indicate that the greater the oxide stability, the lower the measured pH.

These pH measurements may be used with the results of the last section to obtain some general estimates of the conditions in stress corrosion cracks. For example, equation (164) can be used to estimate the normal current density at the metal-electrolyte interface due to oxide film growth. Consider a crack 1-millimeter long by 0.01-millimeter wide and suppose that the bulk electrolyte is a neutral, 0.6-mole per liter, sodium-chloride solution. Using 9×10^{-5} centimeters squared per second as the value of the hydrogen ion diffusion coefficient, the average value of the normal current density is in the range 3×10^{-7} to 3×10^{-5} amperes per square centimeter.

If the rate of film growth changes significantly from point to point along the crack wall, the average normal current density is not a good indicator of the local reaction rate. If, as appears likely, the rate at the crack tip is much greater than at points more distant, the current density in that region will be about two orders of magnitude greater than the average calculated above. Whatever the case, the current density at the mouth of the crack is in the range 3×10^{-5} to 3×10^{-3} amperes per square centimeter.

There is little published data regarding the concentrations of ions other than the hydrogen ion. Measurements reported in Reference 3 indicate the presence of metal ions but provide no estimates of their concentrations. From the reported pH values and the solubility products of the various metal hydroxides, however, it appears that the metal ion concentrations are small and that the hydrogen ion is the

principal product ion.*

As shown in the last section, the importance of migration may be estimated from the ratio of the product ion concentration in the crack to the ionic strength of the bulk electrolyte. From the measurements reported in Reference 3, the minimum pH was about 1.5, corresponding to a hydrogen ion concentration of about 0.03 moles per liter. The ionic strength of the electrolyte (0.6-mole per liter, sodium-chloride solution) was about 1.2 moles per liter. The ratio of the two is forty. Thus, the effects of migration and the gradient of the electrostatic potential should be negligible over most of the crack length. It is interesting to note that in T. R. Beck's original 'MKT' analysis [10], the same result was obtained. A large potential gradient in the region close to the crack tip was later generated by introducing a diffusion-limited chloride ion flux.

The results presented in the last two sections are based on a planar analysis and are strictly valid only when transport in the specimen thickness direction is negligible. In most experimental work no attempt is made to control transport in this direction. A planar analysis should nevertheless yield results consistent with experiment when the specimen thickness is large with respect to the crack length. When the thickness is small, the analysis will fail.

In practice, a planar analysis should be approximately correct for points closer to the crack tip than about one-half the specimen width. At points more distant, composition variations in the specimen thickness direction will be much greater than those in the crack length direction. Corrosion

---

* The system examined in Reference 24 is an exception to this rule. The metal (AISI 4340 steel) may crack at active corrosion potentials. Although the crack is acidified by what appears to be a hydrolysis reaction, the hydrolyzed species is soluble.

processes on the crack faces will then be little different from those on the sides of the specimen. Therefore, finite-width specimens should behave as if the crack length were constant whenever the crack length is greater than about one-half the specimen width.

This view is consistent with the outstanding success obtained in correlating susceptibility to cracking and crack growth rates with applied stress intensity. For pre-cracked specimens of a fixed alloy composition, tested under constant conditions in a given electrolyte, there appears to be a critical stress intensity, K_{ISCC}, below which cracks do not propagate. This critical value is independent of the crack length or the specimen configuration [25]. In the last section it was shown that convective transport is significant only at very high loading rates. In the usual range of loading rates, the major effect of the applied stress on ion transport is its effect on the crack aspect ratio. For a pre-cracked specimen such as that shown in Figure 24, the crack aspect ratio depends on its value under no load and the stress intensity. By using a fatigue crack as a starter notch, the crack aspect ratio at zero load is effectively standardized, and the aspect ratio becomes a function of the stress intensity only. Therefore, if the crack length to specimen width ratio is in the range where the 'effective' crack length remains constant, the effect of the stress field on ion transport is determined by the applied stress intensity and the variables describing the crack geometry do not behave as independent variables.

These remarks are not meant to imply that the stress field has no influence other than its influence on ion transport. The applied stress intensity has a strong influence on fracture surface morphology and may affect the kinetics of charge-transfer reactions. The fact that the stress intensity influences all these factors is one of the more serious

obstacles to determination of the underlying mechanisms of cracking.

The need for accurate kinetic data has been stressed throughout this work. Qualitative observations and order of magnitude estimates such as those presented above provide some insight into the stress corrosion process. But these are really not adequate for understanding or controlling stress corrosion cracking and, if history is a useful guide, they are just as likely to be wrong as right.

Consider some of the interpretations made of the observed low values of the crack pH. This observation has been viewed as providing support for at least three different mechanisms for crack growth. While it would be unfair and misleading to imply that these proposals are based on no other experimental data, a low pH is a critical factor in each of them.

T. P. Hoar [26] has argued that a low pH inside the crack is consistent with a metal-dissolution mechanism. Under such circumstances, the rate of oxide-film formation should be suppressed and consequently the rate of metal dissolution highly favored near the crack tip. Others argue that a low pH should accelerate the rate of hydrogen ion discharge on the bare metal surface at the crack tip, and that fracture must then be the consequence of hydrogen embrittlement (see Reference 27). Still others find support for a film rupture mechanism. Here it is argued that the low pH confirms the hypothesis that oxide film growth is the primary reaction occurring in cracks. If this is the case, rupture of the film under applied stress may then cause the crack to propagate a short distance into the metal until it again comes to rest and the process repeats itself.

Obviously a low pH value neither confirms nor refutes any of these theories. Together with other data, the measurements reported in Reference 3 do imply that hydrogen

ions are generated either by the hydrolysis of metal ions or by oxide film growth. Whether this reaction is even critical to crack propagation remains to be determined. For many systems, a low crack pH is expected simply from the exposure of clean and highly reactive metal surface to an oxygen depleted electrolyte. When this is the case, a low pH could be the consequence of crack growth and not the underlying cause of it.

Regardless of the actual mechanism of crack growth, it is clear that all require a fine balance between the rates of several different reactions. For example, if crack propagation is due to hydrogen embrittlement in a near neutral electrolyte, there must first be a source of hydrogen ions. The rate of generation of these ions must be approximately equal to their rate of discharge on the metal surface. The rate of hydrogen absorption must be fast with respect to the rate of formation of molecular hydrogen and its rate of transport away from the crack tip. Finally, the rate of metal dissolution must be slow with respect to the rate of hydrogen absorption.

Because there is qualitative agreement between the experimental data and several different failure mechanisms, it is not possible to determine the actual mechanism in a given system by a single simple experiment. In order to subject any of the mechanistic theories of stress corrosion to a critical test, at least three elements will be required. First, the mechanism must be cast in a quantitative form. This will probably require independent evaluation of qualitative relationships which have not yet been quantified. In the case of hydrogen embrittlement, for example, the relationship between K_{IC}, the critical stress intensity for rapid fracture, and the concentration of occluded hydrogen is required. Next, accurate and independently measured electrochemical kinetic data must be obtained. Using this data,

the analytic techniques presented here may be used to characterize the environment and to determine whether the actual reaction rates are consistent with the mechanism postulated. Finally, the quantitative predictions generated in this way must be subjected to rigorous experimental verification.

Conclusions

1) A method has been developed for the numerical solution of the electrochemical transport equations based on dilute solution theory and subject to an arbitrary set of charge-transfer boundary conditions. It has been applied to problems involving dependence on time and two spatial variables.

2) The factors of primary importance in determining the electrolyte composition within a crack-like region are the average values of the species fluxes normal to the solid-liquid interface, the crack length, and the crack aspect ratio. Other factors, such as the crack shape, the form of the boundary conditions, and the transport mode can affect the composition. However, these factors are of lesser importance.

3) When the crack aspect ratio is greater than three and the elapsed time is greater than the diffusion time (a^2/D), the effects of transport in the transverse crack direction are negligible.

4) The average concentration of an ion within a crack-like region is given to a good first approximation by equation (164).

$$\bar{C}_i = C_i^\circ + \left(\frac{\bar{J}_i a^2}{2bD_i}\right)$$

The accuracy of this approximation may be determined from the ratio of the calculated value to the ionic strength of the bulk electrolyte.

5) As shown by equation (164), the electrolyte composition within a crack may differ substantially from that in

the bulk solution.

6) An accurate representation of reaction kinetics is required to determine the detailed behavior of an electrolyte within a crack-like region.

7) Many individual results have been presented which cannot be conveniently summarized but have direct application to pitting corrosion, crevice corrosion, and stress corrosion cracking.

Recommendations and Future Work

1) For application to stress corrosion cracking, pitting corrosion and crevice corrosion, a method should be developed for the numerical solution of the one-dimensional formulation of the transport equations presented in Appendix C. This should permit improved resolution in regions with large gradients and result in at least an order of magnitude reduction in core storage requirements and computation time.

2) The methods and results developed in this study should be applied to the study of stress corrosion cracking. Particular emphasis should be placed on the identification of allowable reactions in the system under investigation and on a determination of the kinetics of these reactions.

3) The many individual results presented here provide tools for the study of such corrosion phenomena as pitting, crevice corrosion, and intergranular corrosion. Application of these results to such corrosion processes should be undertaken.

REFERENCES

1) A. P. Bond and E. A. Lizlovs, "Anodic Polarization of Austenitic Stainless Steels in Chloride Media," Journal of the Electrochemical Society, 115 (11), 1130-1135, (Nov. 1968).

2) N. D. Greene, W. D. France, Jr., and B. E. Wilde, "Electrode Mounting for Potentiostatic Anodic Polarization Studies," Corrosion, 21 (9), 275-276, (Sept. 1965).

3) B. F. Brown, C. T. Fujii, and E. P. Dahlberg, "Methods for Studying Solution Chemistry Within Stress Corrosion Cracks," Journal of the Electrochemical Society, 116 (2), 218-219, (Feb. 1969).

4) J. Newman, "Engineering Design of Electrochemical Systems," Industrial and Engineering Chemistry, 60 (4), 12-27, (Apr. 1968).

5) K. J. Vetter, Electrochemical Kinetics: Theoretical and Experimental Aspects, Academic Press Inc., New York, (1967).

6) J. G. Hines, "On the Propagation of Stress-Corrosion Cracks in Metals," Corrosion Science, 1 (1), 21-48, (Aug. 1961).

7) D. A. Vermilyea and C. S. Tedman, Jr., "A Simple Crevice Corrosion Theory," Journal of the Electrochemical Society, 117 (4), 437-440, (Apr. 1970).

8) W. D. France, Jr. and N. D. Greene, Jr., "Passivation of Crevices During Anodic Protection," Corrosion, 24 (8), 247-251, (Aug. 1968).

9) T. R. Beck, "Stress Corrosion Cracking of Titanium Alloys II: An Electrochemical Mechanism," Journal of the Electrochemical Society, 115 (9), 890-896, (Sept. 1968).

10) T. R. Beck and E. A. Grens II, "An Electrochemical Mass Transport-Kinetic Model for Stress Corrosion Cracking of Titanium," Journal of the Electrochemical Society, 116 (2), 177-184, (Feb. 1969).

11) R. C. Alkire, E. A. Grens II, and C. W. Tobias, "A Theory for Porous Electrodes Undergoing Structural Changes by Anodic Dissolution," Journal of the Electrochemical Society, 116 (10), 1328-1333, (Oct. 1969).

12) J. Newman, "Transport Processes in Electrolytic Solutions," Advances in Electrochemistry and Electrochemical Engineering, Vol. 5, C. W. Tobias, Editor, Interscience Publishers, New York, (1967), 87-135.

13) W. M. Latimer, The Oxidation States of the Elements and Their Potentials in Aqueous Solutions, 2nd Ed., Prentice-Hall Inc., New York, (1952).

14) H. S. Carslaw and J. C. Jaeger, Conduction of Heat in Solids, 2nd Ed., Oxford University Press, London, (1959).

15) J. Crank, The Mathematics of Diffusion, Oxford University Press, London, (1956).

16) K. B. Prater and A. J. Bard, "Rotating Ring - Disk Electrodes I: Fundamentals of the Digital Simulation Approach. Disk and Ring Transients and Collection Efficiencies," Journal of the Electrochemical Society, 117 (2), 207-213, (Feb. 1970).

17) J. Douglas, Jr., "A Survey of Numerical Methods for Parabolic Differential Equations," Advances in Computers, Vol. 2, A. D. Booth and R. E. Meagher, Editors, Academic Press Inc., New York, (1961), 1-54.

18) M. Pourbaix, Atlas of Electrochemical Equilibria, Pergamon Press Inc., New York, (1966).

19) H. A. Johansen, G. B. Adams, Jr., and P. Van Rysselberghe, "Anodic Oxidation of Aluminum, Chromium, Hafnium, Niobium, Tantalum, Titanium, Vanadium, and Zirconium at Very Low Current Densities," Journal of the Electrochemical Society, 104 (6), 339-346, (June 1957).

20) G. Milazzo, Electrochemistry: Theoretical Principles and Practical Applications, Elsevier Publishing Co., New York, (1963).

21) R. Parsons, Handbook of Electrochemical Constants, Butterworth Publications Ltd., London, (1959).

22) Handbook of Chemistry and Physics, 51st Ed., R. C. Weast, Editor, Chemical Rubber Co., Cleveland, (1970).

23) A. A. Griffith, "Stresses in a Plate Bounded by a Hyperbolic Cylinder," Reports and Memoranda No. 1152 (M.55.), Aeronautical Research Committee, H. M. Stationery Office, London, (Jan. 1928).

24) J. A. Smith, M. H. Peterson, and B. F. Brown, "Electrochemical Conditions at the Tip of an Advancing Stress Corrosion Crack in AISI 4340 Steel," Corrosion, 26 (12), 539-542, (Dec. 1970).

25) C. D. Beachem and B. F. Brown, "A Comparison of Three Precracked Specimens for Evaluating the Susceptibility of High-Strength Steel to Stress Corrosion Cracking," Stress Corrosion Testing, ASTM STP-425, American Society for Testing and Materials, Philadelphia, (1967). 31-40.

26) T. P. Hoar, "Stress-Corrosion Cracking," Corrosion, 19 (10), 331t-338t, (Oct. 1963).

27) P. R. Rhodes, "Mechanism of Chloride Stress Corrosion Cracking of Austenitic Stainless Steels," Corrosion, 25 (11), 462-472, (Nov. 1969).

APPENDIX A

Finite-Difference Analogue for the Ion Conservation Equation

A key element in the numerical solution of the electrochemical transport equations is the method used to solve the ion conservation equation, equation (73) on page 38. In the notation of equations (77), the equation may be written

$$\mathcal{H}^2 \frac{\partial C_i}{\partial t} = z_i D_i \nabla(C_i \nabla\phi) + D_i \nabla^2 C_i - \nabla C_i \cdot \widetilde{\mathrm{curl}}(\psi \underline{k}) + \mathcal{H}^2 G_i \qquad \text{(A-1)}$$

In the computer program developed for this study, equation (A-1) is solved using an Alternating-Direction Implicit (ADI) technique. The term ADI describes a general concept or approach rather than a particular algorithm. It may be applied to any algorithm using a computational sequence in which the equations are first made implicit in one coordinate direction and then in another. Such methods have the advantages of unconditional stability and computational speed. This appendix is included to show how this concept has been applied to the solution of equation (A-1).

Let

$$f(j,k,l) = f(j\Delta\xi, k\Delta\eta, l\Delta t) \qquad \text{(A-2)}$$

where f is any function of the coordinates ξ, η and t. Then by analogy with differential operators, we may define the following difference operators

$$\Delta_\xi f(j,k,\ell) = \frac{1}{2\Delta\xi}\left[f(j+1,k,\ell) - f(j-1,k,\ell)\right] \qquad \text{(A-3)}$$

$$\Delta_\gamma f(j,k,\ell) = \frac{1}{2\Delta\gamma}\left[f(j,k+1,\ell) - f(j,k-1,\ell)\right] \qquad \text{(A-4)}$$

$$\Delta^2_\xi f(j,k,\ell) = \frac{1}{\Delta\xi^2}\left[f(j+1,k,\ell) - 2f(j,k,\ell) + f(j-1,k,\ell)\right] \qquad \text{(A-5)}$$

$$\Delta^2_\gamma f(j,k,\ell) = \frac{1}{\Delta\gamma^2}\left[f(j,k+1,\ell) - 2f(j,k,\ell) + f(j,k-1,\ell)\right] \qquad \text{(A-6)}$$

$$\Delta_t f(j,k,\ell) = \frac{1}{\Delta t}\left[f(j,k,\ell) - f(j,k,\ell-1)\right] \qquad \text{(A-7)}$$

The central-difference operators defined by equations (A-3 through A-6) are second-order correct. That is, the error introduced by using the difference operator to approximate the analogous differential operator is proportional to $\Delta\xi^2$ (or $\Delta\gamma^2$). The backward-difference operator defined by equation (A-7) is first-order correct.

The finite-difference analogue to equation (A-1) is written as two equations. In the first, derivatives of concentration in the ξ-direction are approximated at $(\ell+\frac{1}{2})\Delta t$, while those in the γ-direction are approximated at $\ell\Delta t$. In the second, the sequence is reversed and the calculation is advanced another half time-step. Derivatives of concentration in the γ-direction are approximated at $(\ell+1)\Delta t$ and derivatives in the ξ-direction are approximated at $(\ell+\frac{1}{2})\Delta t$. There are several ways to treat the products of the derivatives of C_i and Φ. In the present version of the program, these are approximated at $(\ell+\frac{1}{2})\Delta t$.

The difference equations are

$$H^2(j,k)\Delta_{\frac{1}{2}t}C(j,k,\ell+\tfrac{1}{2}) = D\Delta_\xi^2 C(j,k,\ell+\tfrac{1}{2}) + D\Delta_\eta^2 C(j,k,\ell) \qquad \text{(A-8)}$$

$$- \Delta_\xi C(j,k,\ell+\tfrac{1}{2})\Delta_\eta \Psi(j,k) + \Delta_\eta C(j,k,\ell)\Delta_\xi \Psi(j,k)$$

$$+ Q(j,k,\ell+\tfrac{1}{2}) + H^2(j,k) G(j,k,\ell+\tfrac{1}{2})$$

$$H^2(j,k)\Delta_{\frac{1}{2}t}C(j,k,\ell+1) = D\Delta_\xi^2 C(j,k,\ell+\tfrac{1}{2}) + D\Delta_\eta^2 C(j,k,\ell+1) \qquad \text{(A-9)}$$

$$- \Delta_\xi C(j,k,\ell+\tfrac{1}{2})\Delta_\eta \Psi(j,k) + \Delta_\eta C(j,k,\ell+1)\Delta_\xi \Psi(j,k)$$

$$+ Q(j,k,\ell+\tfrac{1}{2}) + H^2(j,k) G(j,k,\ell+\tfrac{1}{2})$$

where

$$\left(\frac{2}{\Sigma D}\right) q(j,k,\ell+\tfrac{1}{2}) = C(j,k,\ell)\left[\Delta_\xi^2 \Phi(j,k,\ell) + \Delta_\eta^2 \Phi(j,k,\ell)\right] \qquad \text{(A-10)}$$

$$+ C(j,k,\ell+1)\left[\Delta_\xi^2 \Phi(j,k,\ell+1) + \Delta_\eta^2 \Phi(j,k,\ell+1)\right]$$

$$+ \Delta_\xi C(j,k,\ell)\Delta_\xi \Phi(j,k,\ell) + \Delta_\eta C(j,k,\ell)\Delta_\eta \Phi(j,k,\ell)$$

$$+ \Delta_\xi C(j,k,\ell+1)\Phi(j,k,\ell+1) + \Delta_\eta C(j,k,\ell+1)\Delta_\eta \Phi(j,k,\ell+1)$$

$$G(j,k,\ell+\tfrac{1}{2}) = \tfrac{1}{2}[G(j,k,\ell) + G(j,k,\ell+1)] \qquad \text{(A-11)}$$

Note that in writing equations (A-8 through A-11) the species subscript i has been omitted and the stream function has been written as a time invariant quantity. This was done for simplicity. Values of the functions q and G at the advanced time are obtained by iteration as explained in the text.

The net effect of alternately applying equations (A-8) and (A-9) can be seen from the sum of the two equations.

$$\frac{H^2(j,k)}{\Delta t}[C(j,k,\ell+1) - C(j,k,\ell)] = D\Delta_\xi^2 C(j,k,\ell+\tfrac{1}{2}) + \tfrac{1}{2}D[\Delta_\eta^2 C(j,k,\ell) + \Delta_\eta^2 C(j,k,\ell+1)]$$

$$- \Delta_\xi C(j,k,\ell+\tfrac{1}{2})\Delta_\eta \Psi(j,k) \qquad \text{(A-12)}$$

$$+ \tfrac{1}{2}[\Delta_\eta C(j,k,\ell) + \Delta_\eta C(j,k,\ell+1)]\Delta_\xi \Psi(j,k)$$

$$+ q(j,k,\ell+\tfrac{1}{2}) + H^2(j,k)G(j,k,\ell+\tfrac{1}{2})$$

The term on the left-hand side is just the central difference approximation for the partial time derivative of C at time $(\ell+\frac{1}{2})\Delta t$. It is analogous to equations (A-3) and (A-4) and may be shown to be second-order correct. Therefore, equation (A-12) is second-order correct in both time and space when q and G are correctly evaluated at time $(\ell+\frac{1}{2})\Delta t$. When the functions q and G are evaluated at time $\ell\Delta t$, the equation remains second-order correct in space but is reduced to first-order correctness in time.

APPENDIX B

Reaction Kinetics

Before the techniques developed here can be applied in the study of a particular system, one must first decide what reactions are relevant to the behavior of that system, and then obtain quantitative expressions for the rates of those reactions. For example, having determined that a redox reaction of the form of equation (40) is important, one must decide whether an equation of the form of equation (59) is suitable for expressing its reaction kinetics. If so, the parameters I_o^s and α must be evaluated. If not, another expression must be found and its parameters evaluated. The same thing applies to the other reactions in the system.

For the work presented here, it was decided to select a simple system of reactions which would exhibit a fairly wide range of behavior without being excessively complicated. It was also desired that the system of reactions be one for which some, if not all, of the kinetic constants could be evaluated from published data.

A system of reactions modeled after the oxide-film formation reactions in the titanium-water system met these requirements. A key factor in this choice was that the oxides of titanium have an extremely low electronic conductivity. Virtually all of the current passing through the film must be transported by ions or vacancies rather than by electrons. In the limit of zero electronic conductivity, no redox reaction can occur on an oxide-covered metal surface, since the electrons generated cannot pass through the film. In this case, the only allowable reactions are oxide film growth by ion or vacancy migration through the film, and ion-exchange reactions at the oxide-electrolyte interface. By further limiting the ion-exchange reactions to a single

dissolution-precipitation reaction, a relatively simple system of reactions is obtained which nevertheless retains some physical relevance.

The reactions considered, therefore, may be written

$$M + 2H_2O \rightleftharpoons MO_2 + 4H^+ + 4e^- \qquad \text{(B-1)}$$

$$MO_2 + 2H^+ \rightleftharpoons MO^{2+} + H_2O \qquad \text{(B-2)}$$

Reaction (B-1) may be viewed as an overall reaction consisting of three steps.

$$M(\text{metal}) \rightleftharpoons M^{4+}(\text{oxide}) + 4e^- \qquad [I_1] \qquad \text{(B-3a)}$$

migration of ions or vacancies through oxide film $\qquad [I_1] \qquad$ (B-3b)

$$2[H_2O \rightleftharpoons O^{2-}(\text{oxide}) + 2H^+(\text{elect})] \qquad [2I_2] \qquad \text{(B-3c)}$$

Steps (B-3a) and (B-3c) are charge-transfer reactions. Step (B-3b) is a transport requirement imposed by the finite thickness of the oxide film. The current density corresponding to each step is shown in brackets for later reference. If no other reaction occurs, stoichiometry of the oxide requires that the current density I_2 be one-half I_1.

Reaction (B-2) may be viewed as consisting of two partial reactions.

$$MO^{2+}(\text{oxide}) \rightleftharpoons MO^{2+}(\text{elect}) \qquad [I_3] \qquad \text{(B-4a)}$$

$$O^{2-}(\text{oxide}) + 2H^{+}(\text{elect}) \rightleftharpoons H_2O \qquad [-I_2] \qquad \text{(B-4b)}$$

Reactions (B-4) are both charge-transfer reactions occurring at the oxide-electrolyte interface. Reactions (B-4b) and (B-3c) are identical but are written in the opposite directions. Again the current density corresponding to each reaction is shown in brackets. When reaction (B-2) is the only reaction, stoichiometry of the oxide requires that I_2 equal minus I_3.

The overall system of two reactions consists of three partial reactions. The requirement of stoichiometry may be written as

$$I_1 - I_2 - I_3 = 0 \qquad \text{(B-5)}$$

To obtain a complete description of the reaction kinetics it is necessary to express the current densities, I_1, I_2, and I_3, as functions of concentration and potential. Following Vetter [5] it is assumed that reaction (B-3a) is near equilibrium and transient transport effects in the oxide film are ignored. The current density I_1 may then be expressed using the high field conduction equation. The current densities are

$$I_1 = I_1^{\circ}\left\{\exp\left[\frac{\beta}{\delta}(\phi_m - \phi_s - \epsilon_F - \gamma_s)\right] - \exp\left[-\frac{\beta}{\delta}(\phi_m - \phi_s - \epsilon_F - \gamma_s)\right]\right\} \qquad \text{(B-6)}$$

$$I_2 = I_2^{\circ}\left\{\exp[2\alpha\gamma_s] - \left(\frac{[H^{+}]_s}{[H^{+}]_o}\right)^{2}\exp[-2(1-\alpha)\gamma_s]\right\} \qquad \text{(B-7)}$$

$$I_3 = I_3^{\circ}\left\{\exp[2\alpha\gamma_s] - \frac{[MO^{2+}]}{[MO^{2+}]_o}\exp[-2(1-\alpha)\gamma_s]\right\} \qquad \text{(B-8)}$$

Equations (B-5 through B-8) provide the complete kinetic description of reactions (B-1) and (B-2). Because the solution of these equations for γ_s is lengthy and involved and a parametric analysis of the equations indicated that I_3 is small over a wide range of pH and potential, it was decided to treat reaction (B-2) as being close to equilibrium. Equation (99) in the text is the result of this assumption. A simple algorithm for obtaining γ_s from this system of equations has since been developed, so a simplifying assumption of the kind used here need not be invoked in future work.

Once γ_s has been determined, the ion fluxes and oxide-film growth-rate may be expressed as

$$\underline{J(H^+)} \cdot \underline{n} = -I_2/\mathfrak{F} \qquad \text{(B-9a)}$$

$$\underline{J(MO^{2+})} \cdot \underline{n} = -I_3/2\mathfrak{F} \qquad \text{(B-9b)}$$

$$\dot{\delta} = W(I_1 - 2I_3)/4\rho\mathfrak{F} \qquad \text{(B-9c)}$$

APPENDIX C

Electrochemical Transport in a Crack-Like Region

When the aspect ratio of a notch or crack is large, the effects of transport in the transverse direction can be neglected and the region treated as a one-dimensional continuum. The equations describing transport in such a region are developed in this appendix and the solutions for two important cases are presented. A solution technique based on developing an integral equation for the electrostatic potential is also discussed. An example of the use of this technique is presented in Appendix D.

Consider a region in the x-y plane bounded by the x-axis and the line $y = f(x)$ as shown in Figure 41. The region corresponds to one-half the section of a crack produced by a cutting-plane perpendicular to both the crack plane and the crack front. The x-axis coincides with the crack centerline; the line $y = f(x)$ coincides with one crack face. The region is assumed to be symmetric about the crack centerline so the second crack face corresponds to the line $y = -f(x)$. For the control volume shown in Figure 41, the equation of mass conservation may be written

$$J_i\Big|_{\substack{x\\ t+\epsilon\Delta t}} g(x)\Delta t - J_i\Big|_{\substack{x+\Delta x\\ t+\epsilon\Delta t}} g(x+\Delta x)\Delta t + J_i^n\Big|_{\substack{x+\eta\Delta x\\ t+\xi\Delta t}} \Delta S\Delta t = \left[C_i\Big|_{\substack{x+\xi\Delta x\\ t+\Delta t}} - C_i\Big|_{\substack{x+\xi\Delta x\\ t}}\right]\Delta x\,\frac{1}{2}\left[g(x) + g(x+\Delta x)\right] \qquad (C\text{-}1)$$

Taking the limit of equation (C-1) as Δx and Δt approach zero, the differential form of the mass conservation equation is

$$\frac{\partial}{\partial x}(J_i y) - J_i^n \frac{ds}{dx} + y \frac{\partial C_i}{\partial t} = 0 \qquad \text{(C-2)}$$

where

$$\frac{ds}{dx} = \sqrt{1 + \left(\frac{dy}{dx}\right)^2} \qquad \text{(C-2a)}$$

When the mouth of the crack is located at x equal to a, and b is the crack half-width measured at the crack mouth,

$$y = b, \qquad \frac{dy}{dx} = 0 \qquad \text{(C-3a)}$$

for a rectangular crack and

$$y = \left(\frac{b}{a}\right)x, \qquad \frac{ds}{dx} = \sqrt{1 + \left(\frac{b}{a}\right)^2} \qquad \text{(C-3b)}$$

for a pie-shaped crack. Note that the fluxes J_i and J_i^n in equation (C-2) are flux densities and not total fluxes. Also, the quantities appearing in the equation correspond to average values across the crack width.

To complete the description, the flux equation and the electroneutrality equation are required.

$$J_i = -z_i D_i C_i \frac{\partial \phi}{\partial x} - D_i \frac{\partial C_i}{\partial x} + v C_i \qquad \text{(C-4)}$$

$$\sum_i z_i C_i = 0 \qquad \text{(C-5)}$$

When the average solvent velocity, v, has been determined, equations (C-2, -4, and -5) represent the complete system of equations describing mass transport in a crack-like region.

When the line $y = f(x)$ is the generator of a surface of revolution about the x-axis rather than a sheet, the enclosed region is pit-like rather than crack-like. Using the same procedure as that used to obtain equation (C-2), the conservation equation for such a region is

$$\frac{\partial}{\partial x}(J_i y^2) - 2 J_i^n y \frac{ds}{dx} + y^2 \frac{\partial c_i}{\partial t} = 0 \qquad \text{(C-6)}$$

When equation (C-6) is used instead of equation (C-2), the results are modified in detail but not in principle. Therefore, it will not be considered further.

At steady state, integration of the conservation equation is straightforward. Since the boundary conditions typically require specifying the flux at the crack tip and the concentration at the crack mouth, it is convenient to express the result as

$$J_i = \frac{1}{y}\left[y(\rho)\bar{J}_i(\rho) + \int_\rho^x J_i^n(\xi)\, y'(\xi)\, d\xi\right] \qquad \text{(C-7)}$$

where the crack tip is located at x equal to p and the prime denotes differentiation with respect to the argument of a function.

As indicated in the text, there are two important limits to the behavior of an electrolyte. The first is when the total normal current density is small. The ions then behave as uncharged species obeying the equation of transport by simple diffusion. The second is when the current density is large. The concentrations of the two principal ions closely approximate those of the ions in a binary electrolyte. The potential gradient is determined by the need to satisfy both the boundary conditions of the principal ions and the electroneutrality equation. The concentrations of the minor

ionic species are strongly affected by the potential gradient but they themselves have virtually no effect on it.

Consider the case of steady-state transport by simple diffusion. From equations (C-4) and (C-7) with ϕ' and υ equal to zero

$$C_i' = -J_i/D_i$$

or

$$C_i = C_i^\circ + \int_x^a f_i(\xi)\, d\xi \qquad \text{(C-8)}$$

where

$$f_i(x) = J_i/D_i = \frac{1}{D_i y}\left[y(p)\, J_i(p) + \int_p^x J_i^n(\xi)\, s'(\xi)\, d\xi\right] \qquad \text{(C-9)}$$

The solution is almost as simple for the case of steady-state transport in a binary electrolyte. From equations (C-4) and (C-7) with υ equal to zero

$$z_1 C_1 \phi' + C_1' = -f_1(x) \qquad \text{(C-10a)}$$

$$z_2 C_2 \phi' + C_2' = -f_2(x) \qquad \text{(C-10b)}$$

where f_1 and f_2 are defined according to equation (C-9). Adding equations (C-10) and using the electroneutrality equation to eliminate both the electrostatic potential and C_2, it follows that

$$C_1' = -\left(\frac{z_2}{z_2 - z_1}\right)\left[f_1(x) + f_2(x)\right]$$

or

$$C_1 = C_1^\circ + \left(\frac{z_2}{z_2 - z_1}\right)\int_x^a \left[f_1(\xi) + f_2(\xi)\right] d\xi \qquad \text{(C-11)}$$

The concentration C_2 may be obtained from equation (C-11) by simply interchanging the subscripts one and two.

When the normal flux of one of the two species, say species two, is everywhere zero, it follows from equation (C-9) that f_2 is also zero. Since the ith diffusion coefficient enters the result only through f_i, it is clear that the solution does not depend on the diffusion coefficient of a species with zero flux. Comparing equations (C-8) and (C-11) with f_2 equal to zero, it may be seen that

$$\frac{\left[C_1 - C_1^\circ\right]_{BIN}}{\left[C_1 - C_1^\circ\right]_{DIL}} = \left(\frac{z_2}{z_2 - z_1}\right) \qquad \text{(C-12)}$$

For the problem presented in the text this ratio was one-half. It will typically lie between one-quarter and three-quarters.

The electrostatic potential may be obtained from equations (C-10a) and (C-11). However, we will use a different method in order to show how an integral representation may be used to solve certain electrochemical transport problems.

Consider a steady state system for which the solvent velocity is zero. From equations (C-4, -7, and -9), the differential equation governing ion transport may be written in the form

$$\left[C_i \exp(z_i\phi)\right]' = -f_i \exp(z_i\phi) \qquad \text{(C-13)}$$

Integrating,

$$c_i = \left\{ c_i^\circ + \int_x^a f_i(\xi) \exp[z_i \phi(\xi)]\, d\xi \right\} \exp[-z_i \phi(x)] \qquad \text{(C-14)}$$

where, for convenience, $\phi(a)$ has been set equal to zero. Note that, as before, the kernel f_i contains all the information regarding the normal flux and the crack shape. When the potential, ϕ, is everywhere zero, equation (C-8) is recovered. When ϕ is known or otherwise specified, as for a minor ionic species in a near-binary electrolyte, equation (C-14) expresses the solution and no additional information is required.

In general, the electrostatic potential is not known and the electroneutrality equation must be used. Thus, from equations (C-5) and (C-14),

$$\sum_i z_i \left\{ c_i^\circ + \int_x^a f_i(\xi) \exp[z_i \phi(\xi)]\, d\xi \right\} \exp[-z_i \phi(x)] = 0 \qquad \text{(C-15)}$$

Every steady-state one-dimensional electrochemical transport problem is reducible to the problem of finding a value of ϕ that satisfies equation (C-15). In practice, there are two ways to do this. The first is direct numerical solution of the integral equation. The second is, through repeated differentiation, to derive an equivalent differential equation. It may be possible to solve this equation analytically. Otherwise, it can be solved numerically.

The derivation of an equivalent differential equation is straightforward but laborious. For example, in the case of a binary electrolyte, equation (C-15) may be written

$$z_1 c_1^\circ + z_2 c_2^\circ U^{(z_1 - z_2)} + z_1 \int_x^a f_1(\xi) U(\xi)^{z_1} d\xi + z_2 U^{(z_1 - z_2)} \int_x^a f_2(\xi) U(\xi)^{z_2} d\xi = 0 \qquad \text{(C-16)}$$

where

$$U(x) = \exp[\phi(x)] \tag{C-17}$$

Differentiating once and rearranging,

$$-\left[z_1 f_1 + z_2 f_2\right] \frac{U^{(z_2+1)}}{U'} + z_2(z_1 - z_2)C_2^\circ + z_2(z_1 - z_2)\int_x^a f_2(\xi)\,U(\xi)^{z_2}\,d\xi = 0 \tag{C-18}$$

Differentiating again and rearranging yields the desired differential equation.

$$\left[(z_1 f_1 + z_2 f_2)\frac{U}{U'}\right]' + z_1 z_2 (f_1 - f_2) = 0 \tag{C-19}$$

Integration of equation (C-19) is straightforward. After evaluating the constants of integration using equations (C-17) and (C-18), it follows that

$$\phi = \ln U = -\int_x^a \frac{\left[z_1 f_1(\xi) + z_2 f_2(\xi)\right] d\xi}{-z_1 z_2 \left[C_2^\circ + C_2^\circ \int_\zeta^a \left[f_1(\eta) + f_2(\eta)\right] d\eta\right]} \tag{C-20}$$

The correctness of this result may be verified by comparison with the result obtained directly from equations (C-10a) and (C-11). The labor involved does not justify using equation (C-15) for a binary system. For more complex electrolytes, however, there is no other straightforward method for solving the steady-state transport equations, and a method based on the solution of equation (C-15) is necessary whether it is recognizable as such or not.

APPENDIX D

Electrochemical Transport in a 1-1-1 Ternary Electrolyte

Determination of the implicit function ϕ defined by equation (C-15) in Appendix C is the key step in solving one-dimensional steady-state electrochemical transport problems. Since the equation is non-linear, it usually is impossible to obtain a solution in closed-form and approximate methods must be used. In several cases, however, closed-form solutions can be displayed and one of these is presented in this appendix.

Consider a 1-1-1 ternary electrolyte for which the normal flux of one species is everywhere zero. In the terminology of Appendix C

$$\bar{z}_1 = -\bar{z}_2 = \bar{z}_3 = +1 \qquad \text{(D-1a)}$$

and

$$f_1(x) = 0 \qquad \text{(D-1b)}$$

With these values, equation (C-15) can be written in the form

$$C_1^\circ - C_2^\circ U^2 - U^2 \int_x^a \frac{f_2(\xi)}{U(\xi)}\, d\xi + C_3^\circ + \int_x^a f_3(\xi)\, U(\xi)\, d\xi = 0 \qquad \text{(D-2)}$$

where $u(x)$ is defined according to equation (C-17). Differentiating once and rearranging

$$[f_2 - f_3]\frac{1}{U'} - 2C_3^\circ - 2\int_x^a \frac{f_2(\xi)}{U(\xi)}\, d\xi = 0 \qquad \text{(D-3)}$$

Differentiating and rearranging again, the desired differential equation is obtained.

$$\left[(f_2 - f_3)\frac{U}{U'}\right]' + \left[f_2 + f_3\right] = 0 \qquad \text{(D-4)}$$

By the definition of u(x) and equation (D-3),

$$U(a) = \exp[\phi(a)] = 1 \qquad \text{(D-5a)}$$

$$U'(a) = 2C_2^\circ / (f_2(a) - f_3(a)) \qquad \text{(D-5b)}$$

Therefore, integrating equation (D-4) twice and using equations (D-5), it follows that

$$\phi = \ln U = \int_x^a \frac{[f_2(\xi) - f_3(\xi)]\,d\xi}{\left\{2C_2^\circ + \int_\xi^a [f_2(\eta) + f_3(\eta)]\,d\eta\right\}} \qquad \text{(D-6)}$$

The ion concentrations may be determined from equation (D-6) and equation (C-14). For example, for species two

$$C_2 = \left\{C_2^\circ + \int_x^a f_2(\xi)\exp[-\phi(\xi)]\,d\xi\right\}\exp[\phi(x)] \qquad \text{(D-7)}$$

To carry out the integration, it is convenient to define a new variable. Note that equation (D-6) may be written in the form

$$\phi = \int_x^a \frac{[f_2(\xi) + f_3(\xi) - 2f_3(\xi)]\,d\xi}{\left\{2C_2^\circ + \int_\xi^a [f_2(\eta) + f_3(\eta)]\,d\eta\right\}}$$

or

$$\Phi = \ln\left\{1 + \frac{1}{2C_2^\circ}\int_x^a [f_2(\xi) + f_3(\xi)]\,d\xi\right\} - \Psi(x) \qquad \text{(D-8)}$$

where

$$\Psi(x) = \int_x^a \frac{f_2(\xi)\,d\xi}{\left\{C_2^\circ + \frac{1}{2}\int_\xi^a [f_2(\gamma) + f_3(\gamma)]\,d\gamma\right\}} \qquad \text{(D-9)}$$

Using equations (D-8) and (D-9), equation (D-7) becomes

$$C_2 = C_2^\circ\left\{1 - \int_x^a \exp[\Psi(\xi)]\,\frac{d\Psi}{d\xi}\,d\xi\right\}\exp[-\Psi]\exp[\Phi+\Psi]$$

or

$$C_2 = C_2^\circ\left\{1 + \frac{1}{2C_2^\circ}\int_x^a [f_2(\xi) + f_3(\xi)]\,d\xi\right\} \qquad \text{(D-10)}$$

Since $f_1(x)$ was assumed to be zero,

$$C_1 = C_1^\circ \exp[-\Phi(x)] \qquad \text{(D-11)}$$

and by electroneutrality

$$C_3 = C_2 - C_1 \qquad \text{(D-12)}$$

Equations (D-6, -10, -11, and -12) express the general solution for a 1-1-1 ternary electrolyte for which one of the positively charged species has zero normal flux. Note that for a 1-1-1 ternary containing two negatively charged ions

and one positively charged ion and for which one of the negative ions has zero normal flux, the same solution is obtained except that Φ is the negative of the value given by equation (D-6). Also, the signs of the charge numbers must then be taken opposite to those shown in equation (D-1a).

FIGURES

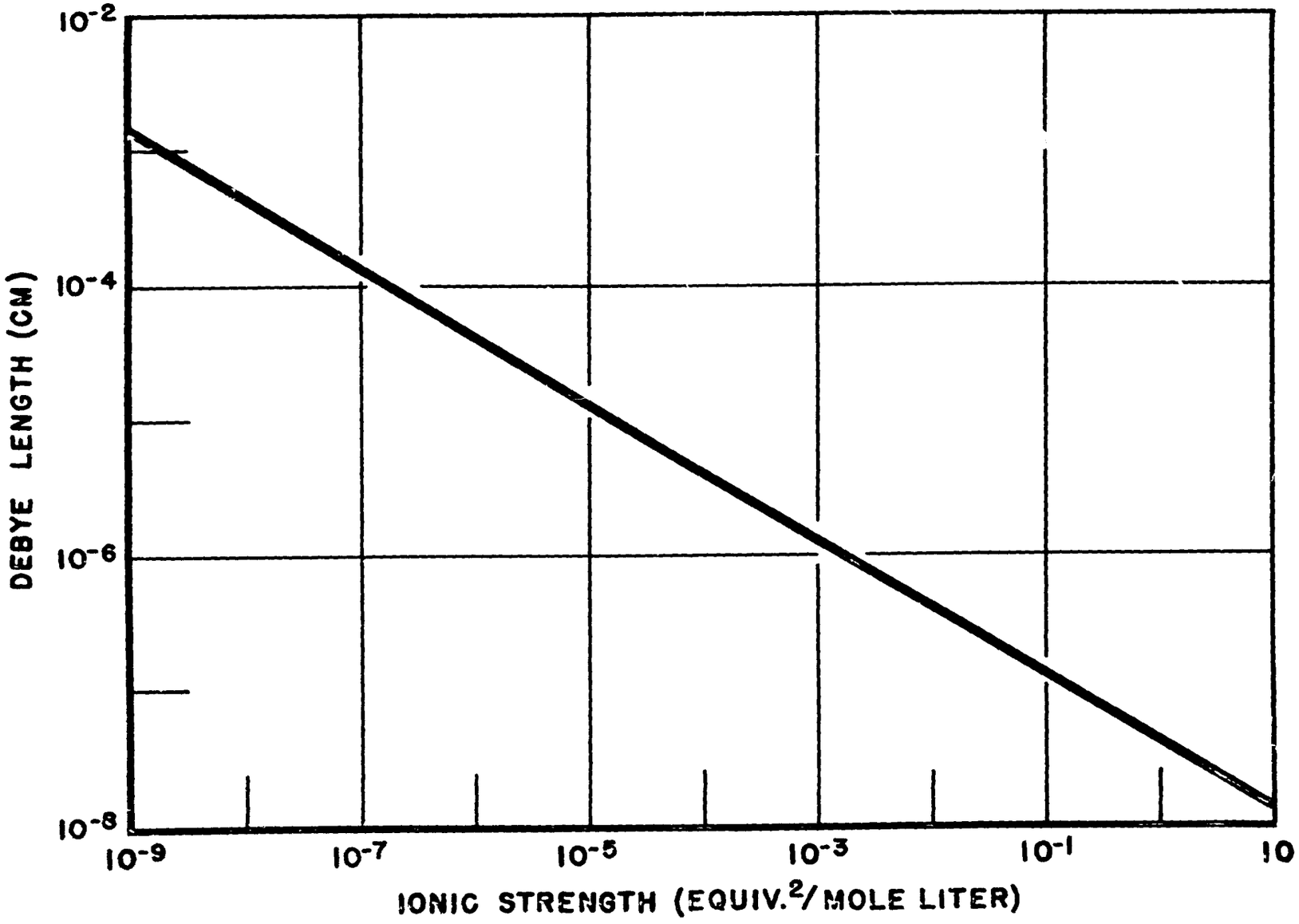

Fig. 1 The dependence of the Debye length on ionic strength for an aqueous electrolyte.

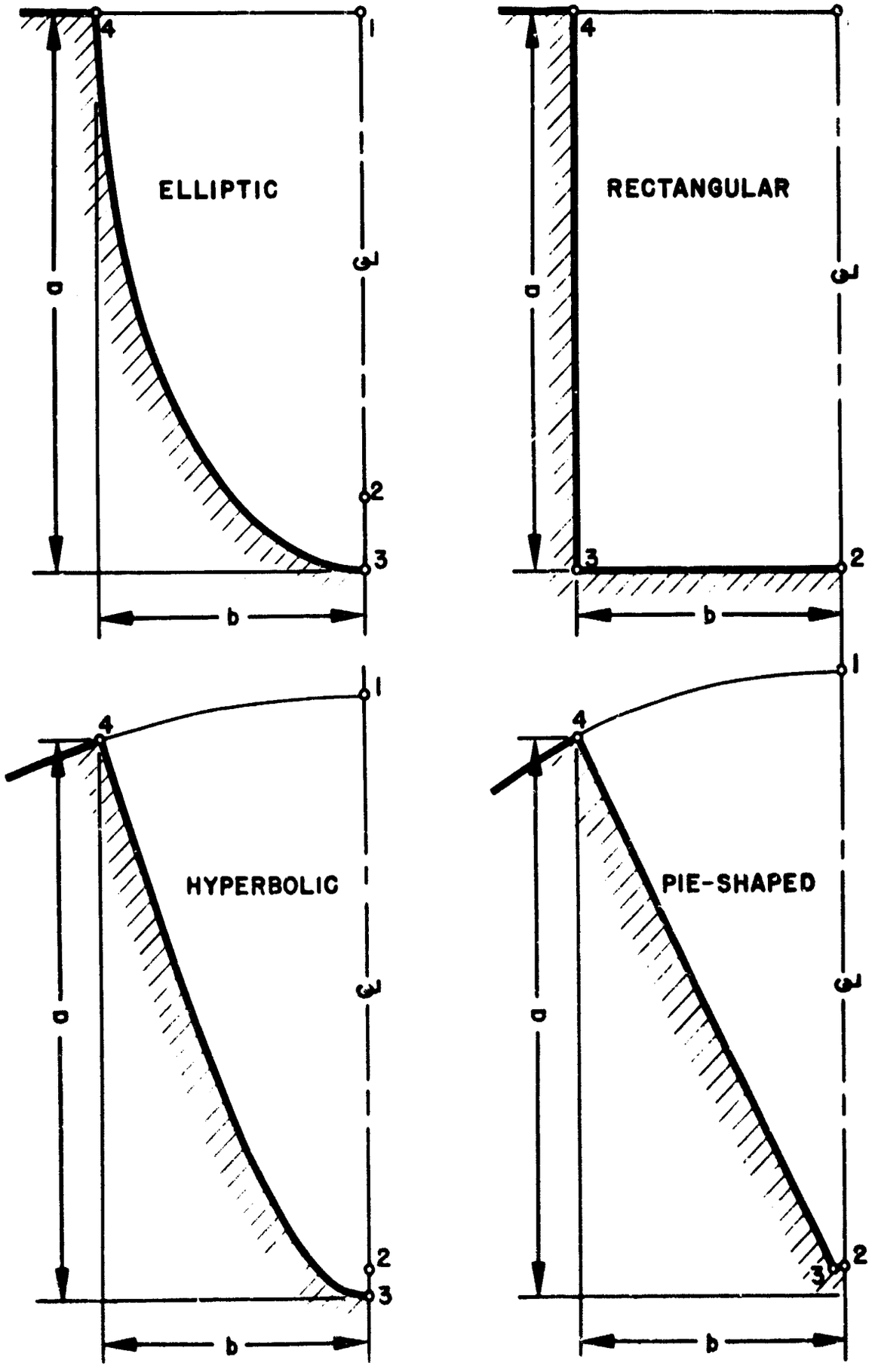

Fig. 2 Cocrdinate transformations from the physical (x-y) plane onto the descriptive (ζ-η) plane.

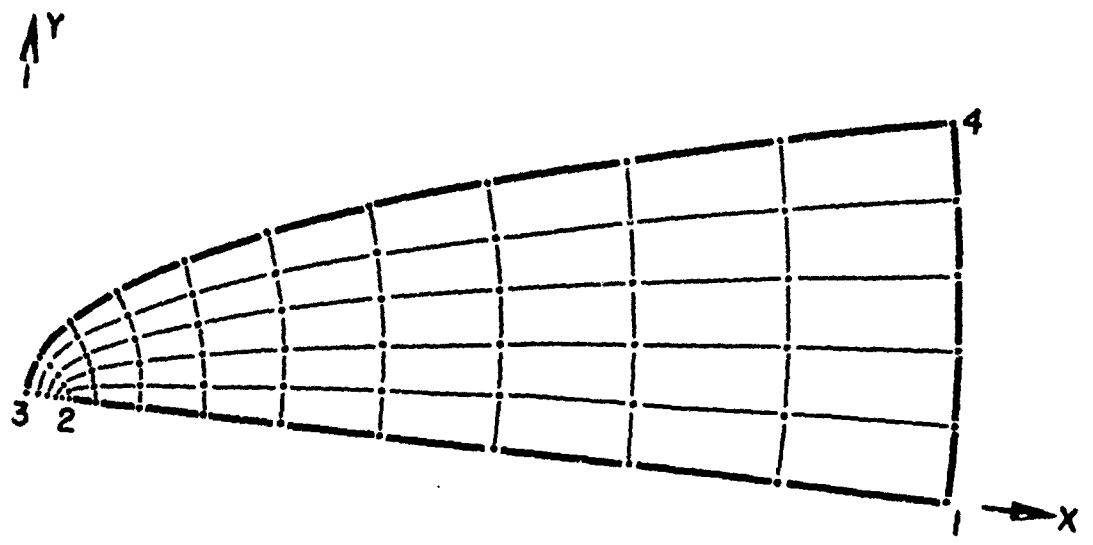

PHYSICAL COORDINATES

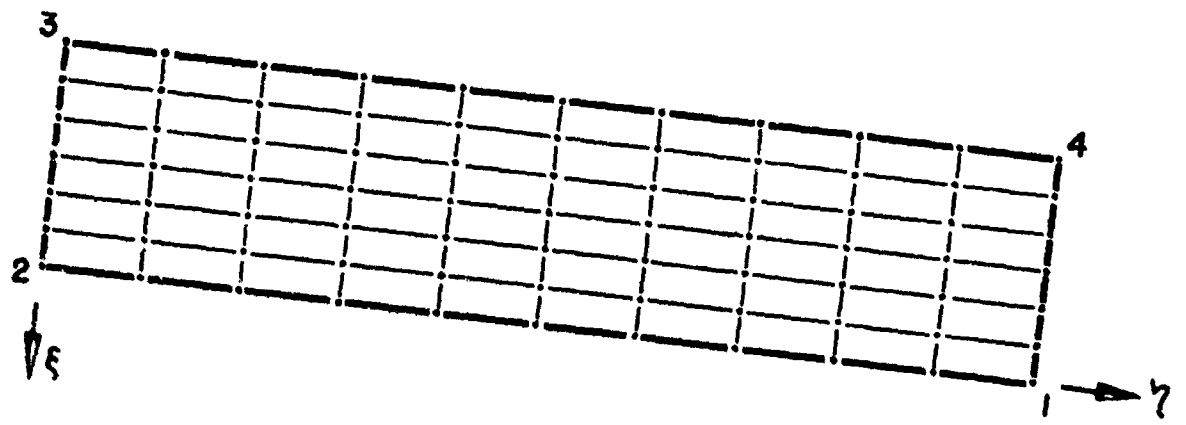

TRANSFORMED COORDINATES

Fig. 3 Finite difference grid for a hyperbolic region.

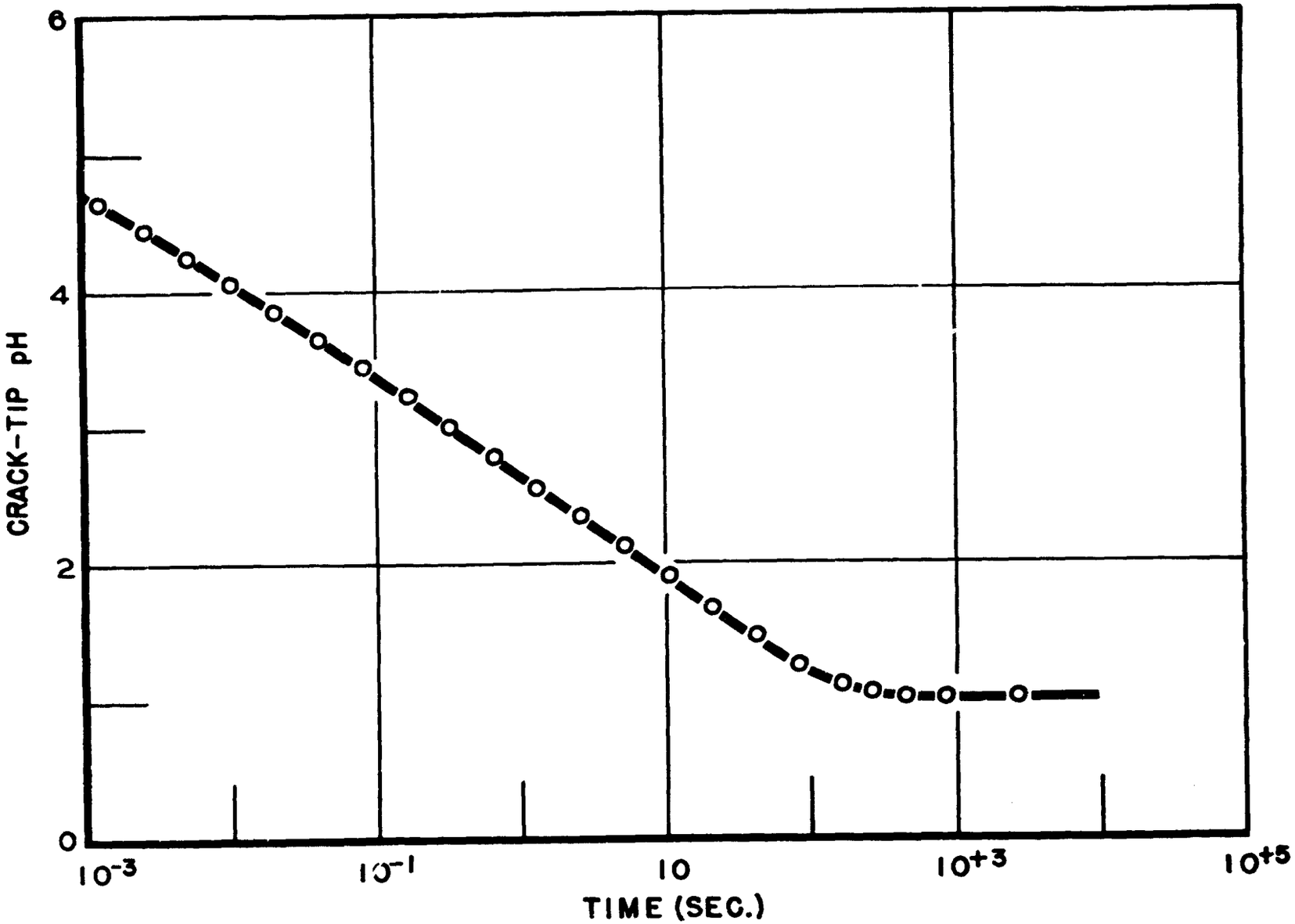

Fig. 4 Variation of the crack-tip pH with time in a hyperbolic crack with constant flux boundary conditions (transport by simple diffusion).

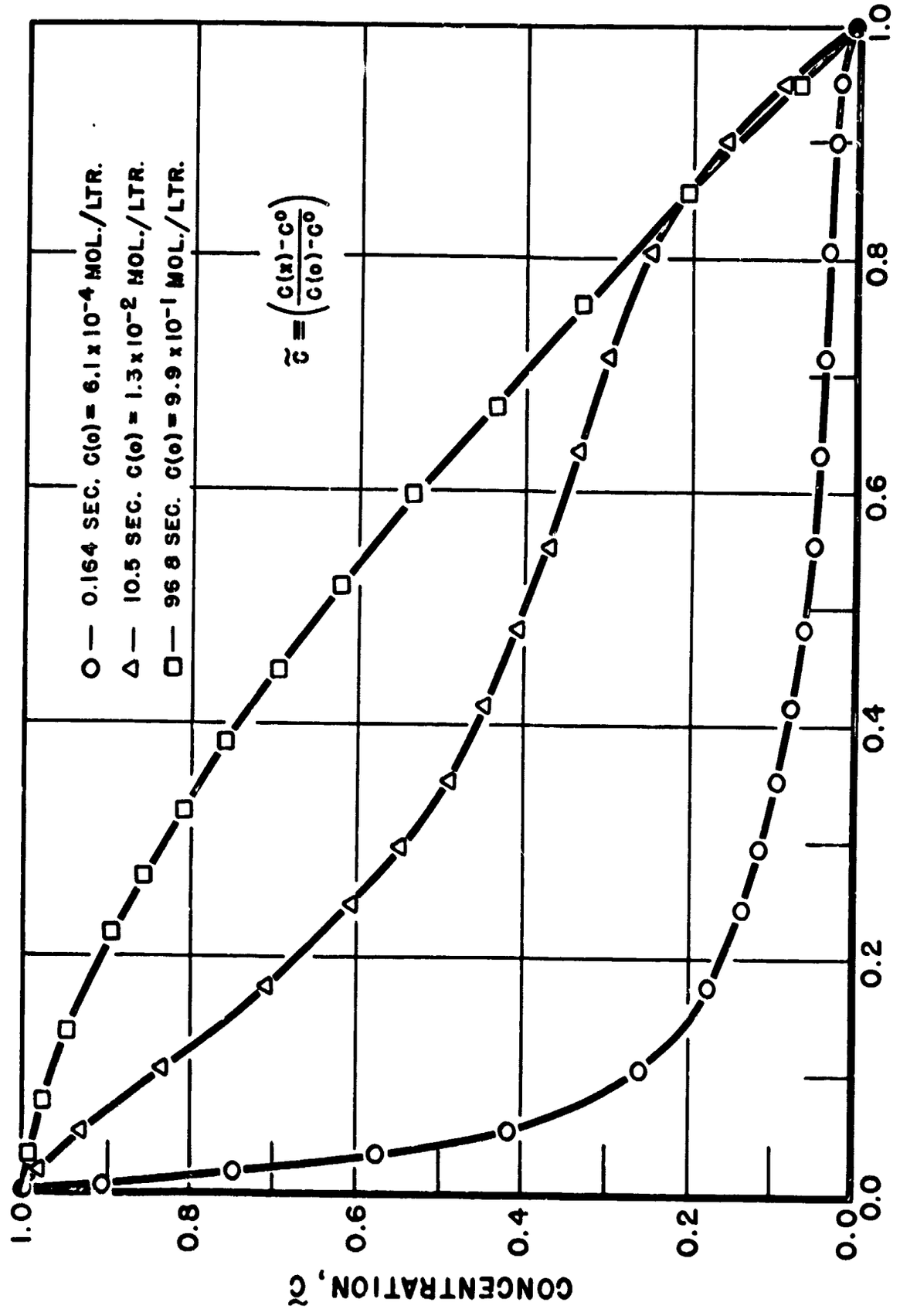

Fig. 5 Longitudinal concentration profiles in a hyperbolic crack at three different times (transport by simple diffusion).

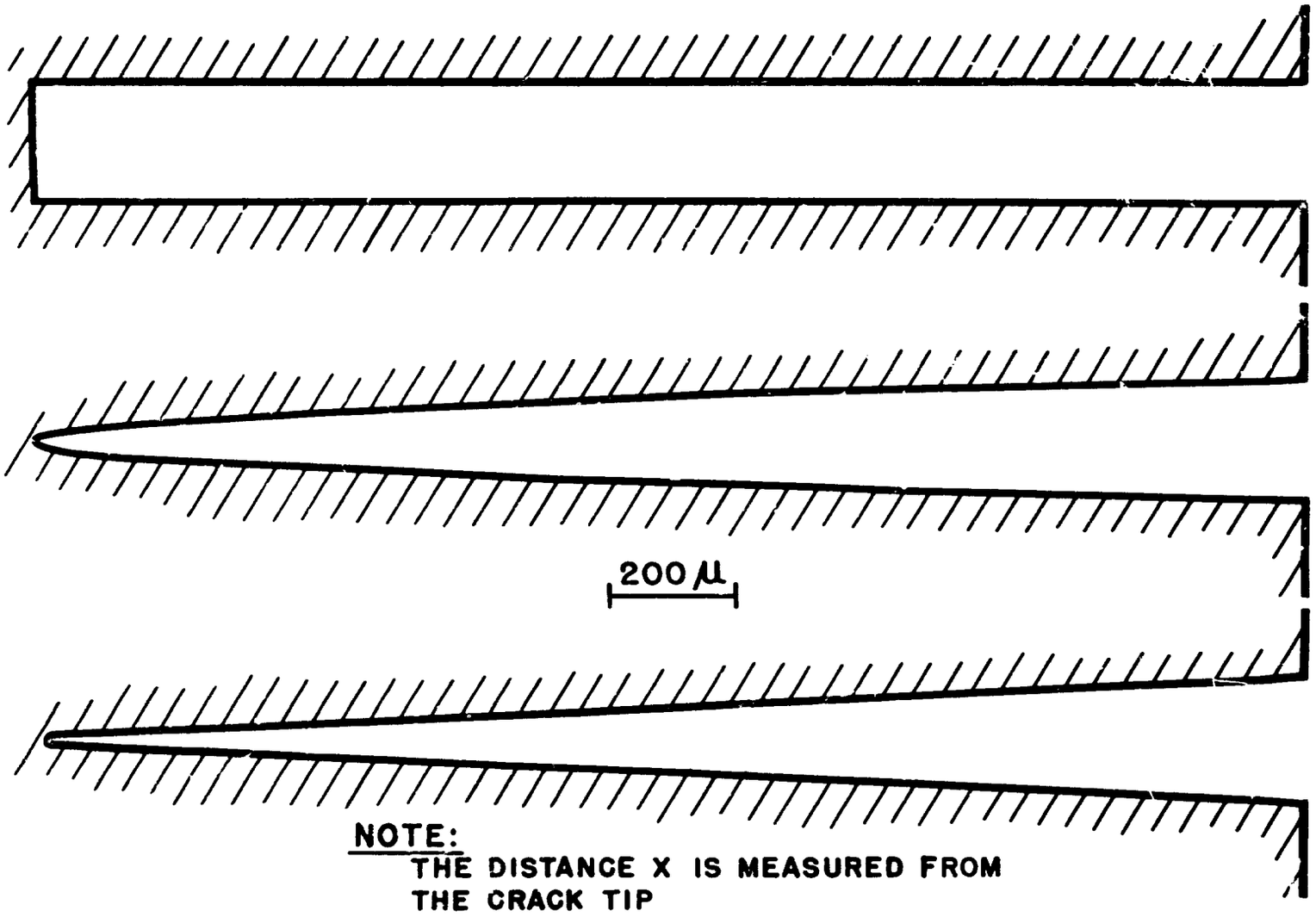

Fig. 6 Geometry of the cracks used to investigate the influence of crack shape.

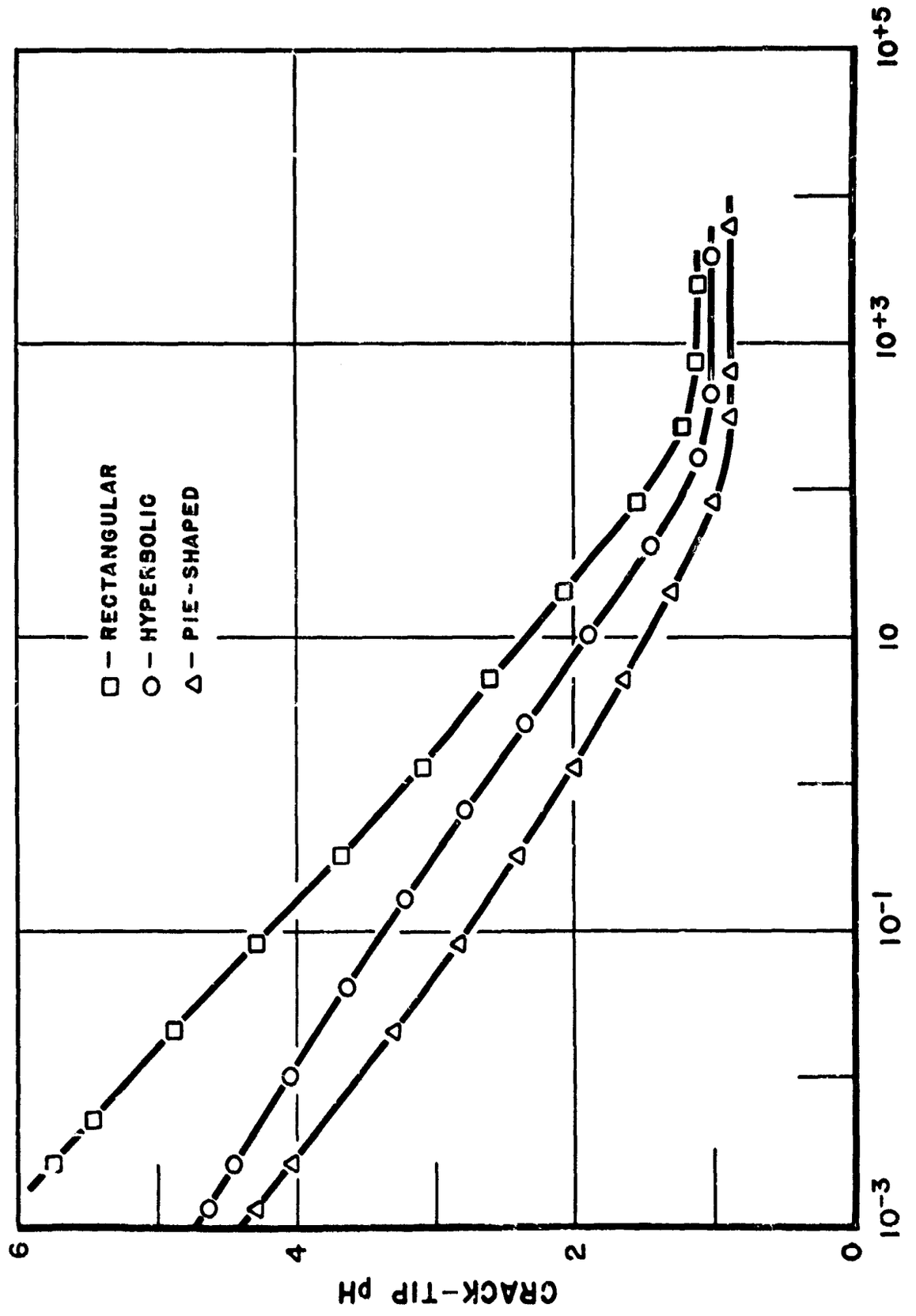

Fig. 7 Variation of the crack-tip pH with time for three different crack shapes (transport by simple diffusion).

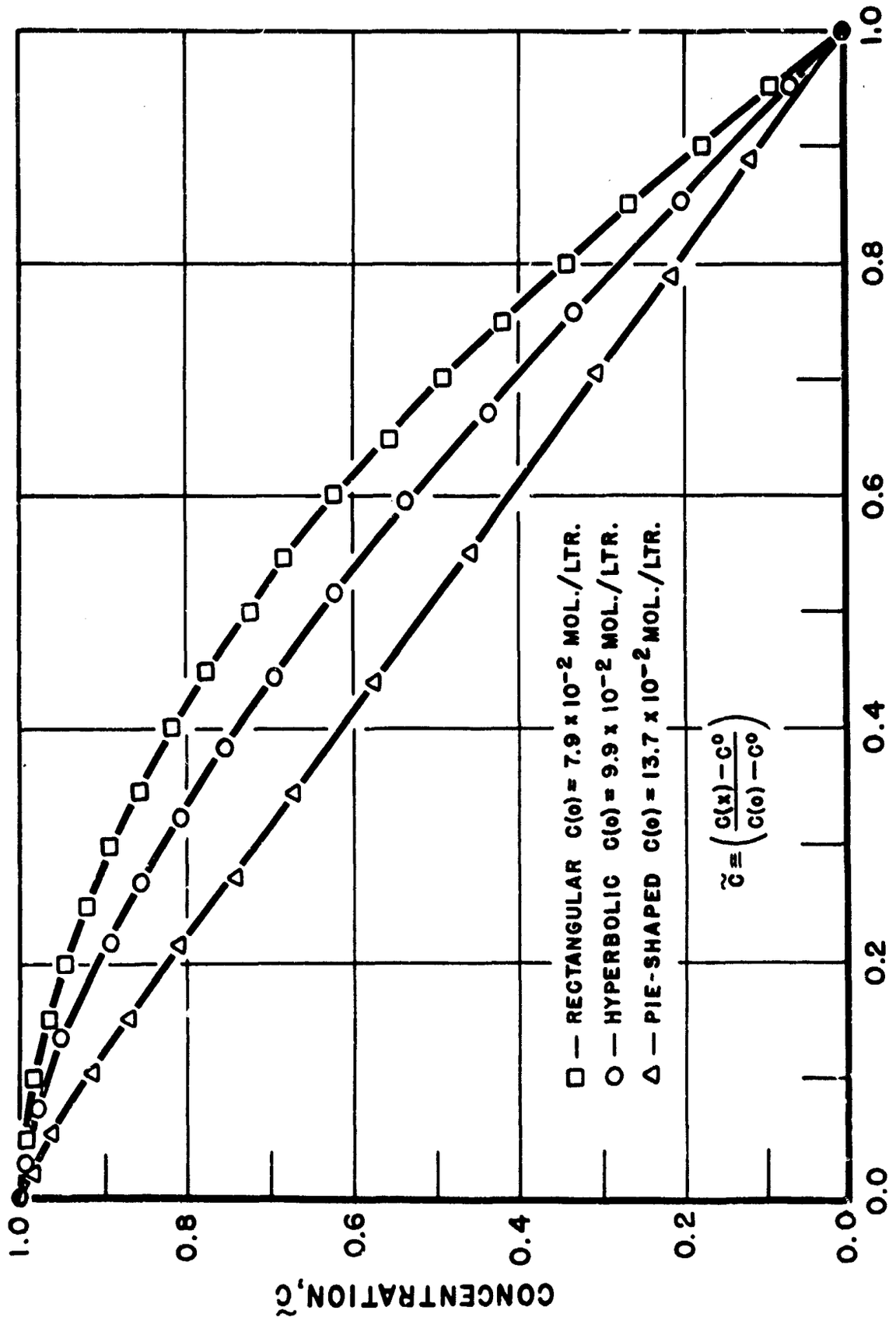

Fig. 8 Steady-state longitudinal concentration profiles in cracks of three different crack shapes (transport by simple diffusion).

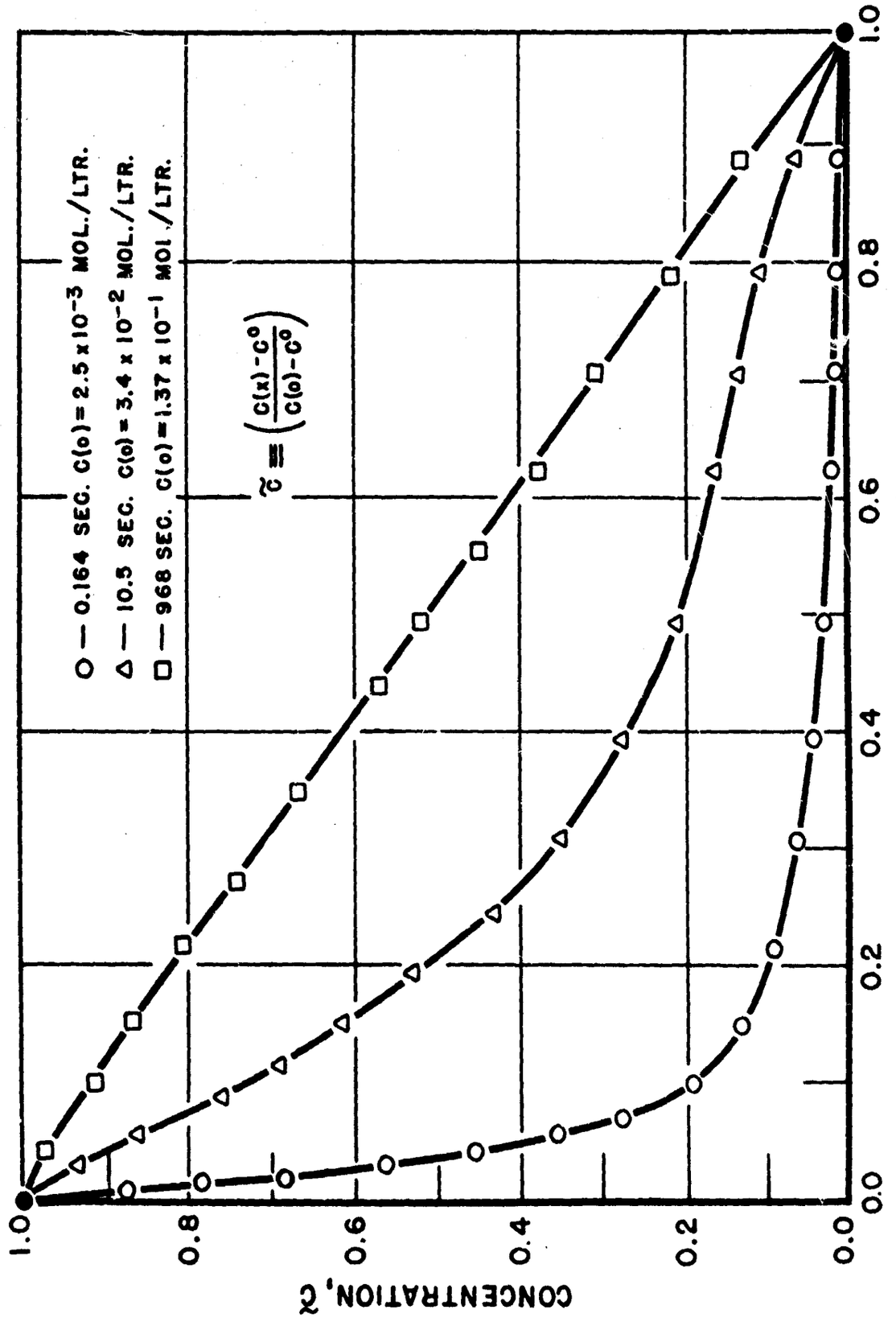

Fig. 9 Longitudinal concentration profiles in a pie-shaped crack at three different times (transport by simple diffusion).

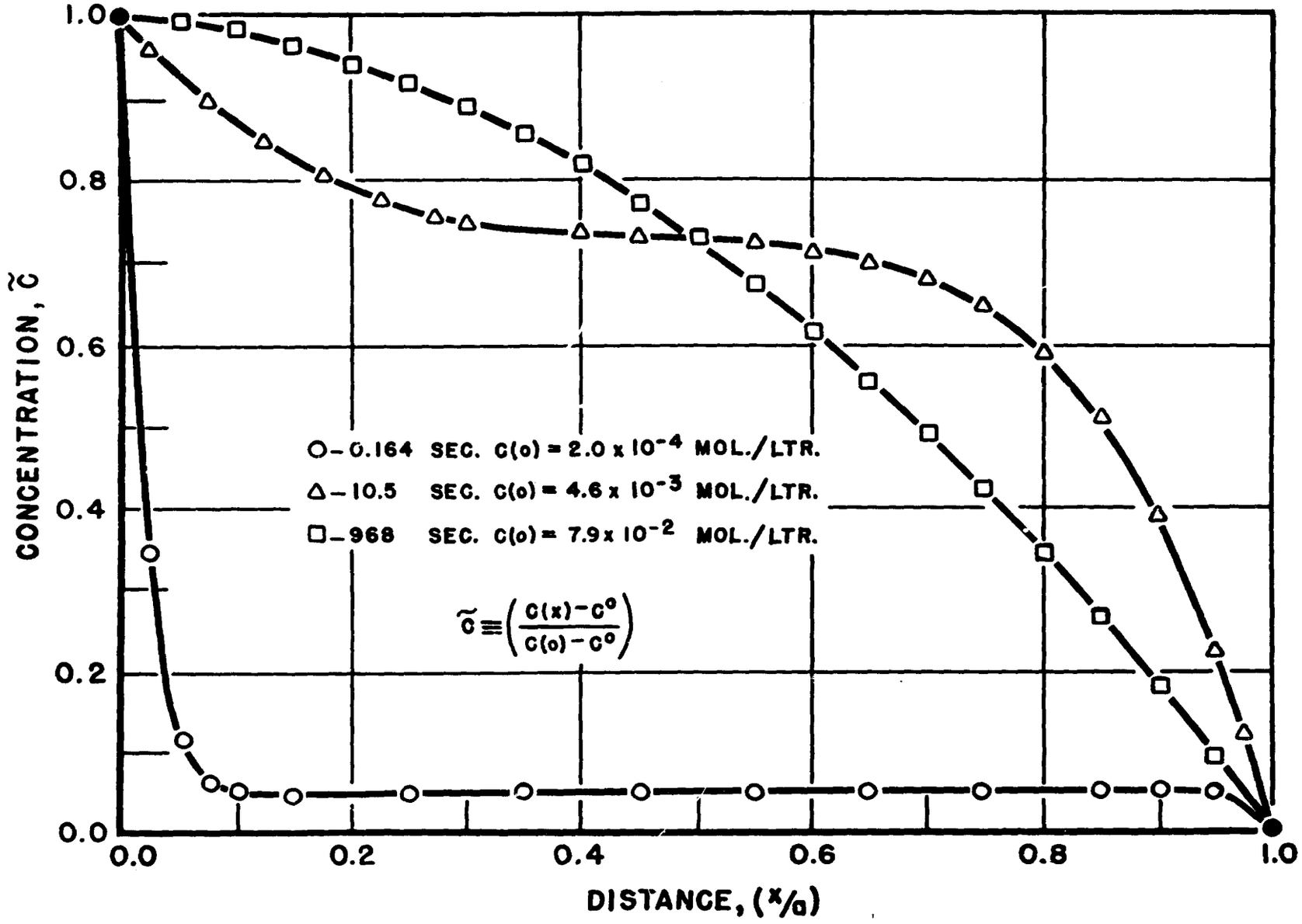

Fig. 10 Longitudinal concentration profiles in a rectangular crack at three different times (transport by simple diffusion).

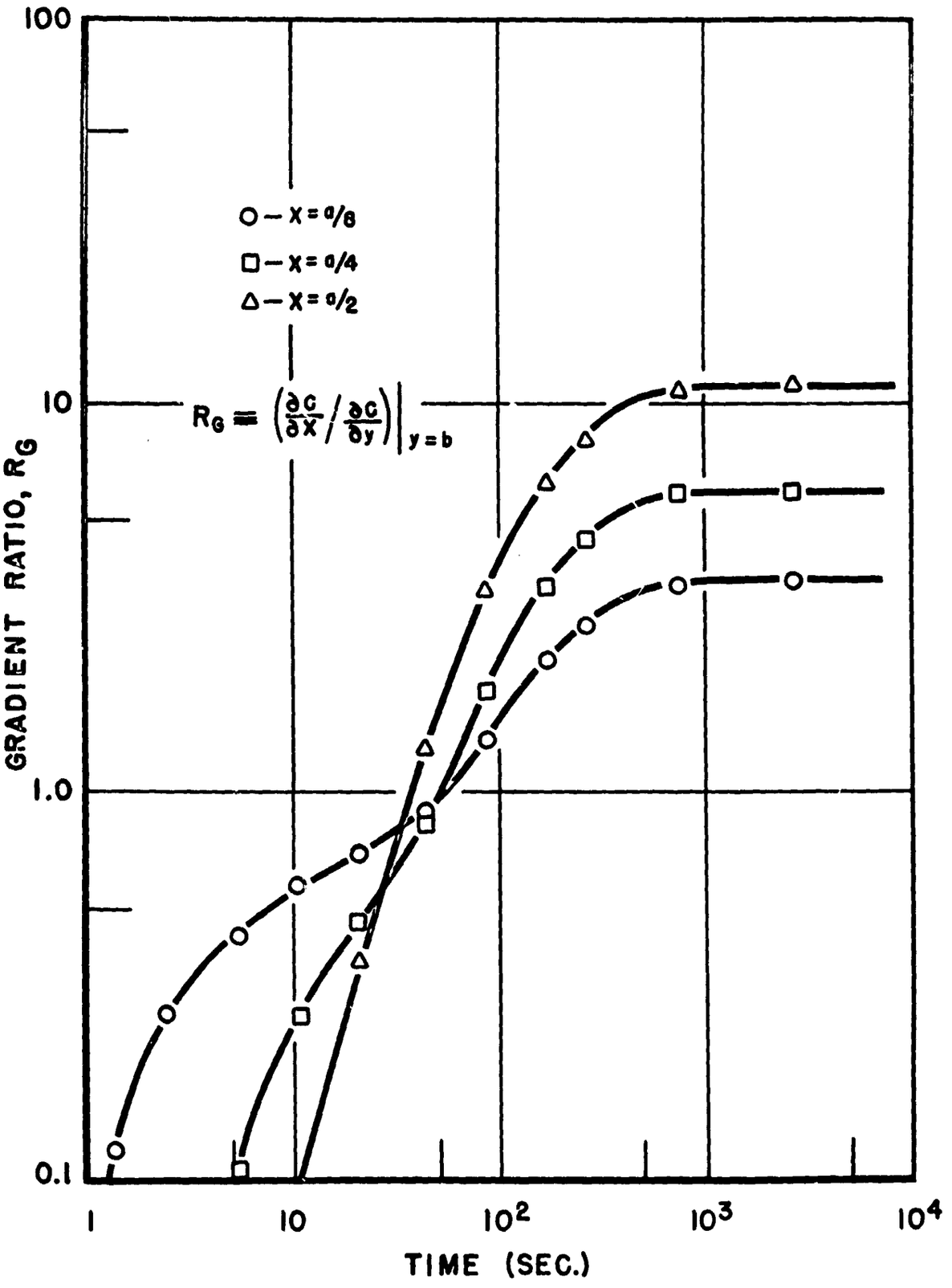

Fig. 11 Change with time in the ratio of the longitudinal to the transverse concentration gradient at three points in a rectangular crack (transport by simple diffusion).

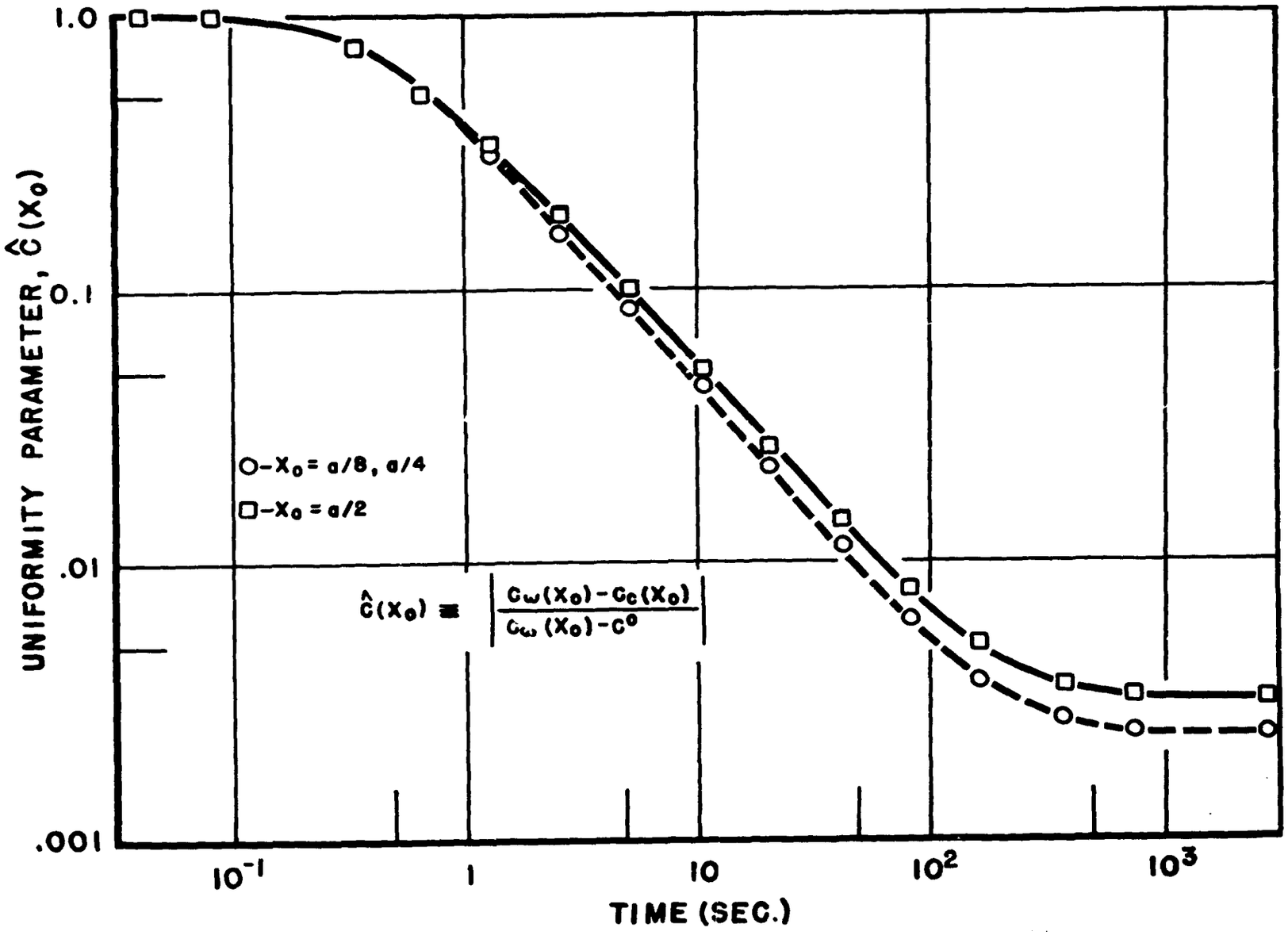

Fig. 12 Change with time in the concentration difference at three transverse sections in a rectangular crack (transport by simple diffusion).

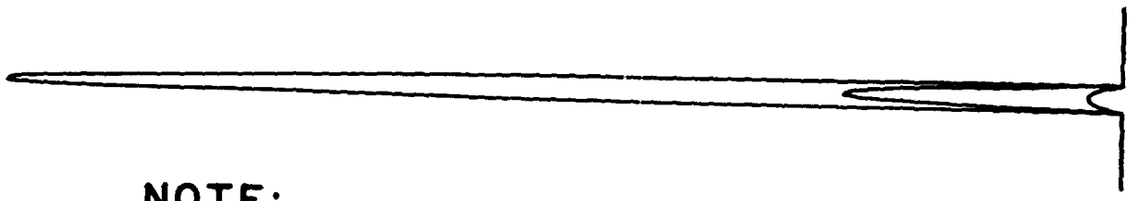

NOTE:

SCALE IN LENGTH AND WIDTH DIRECTIONS THE SAME (10X)

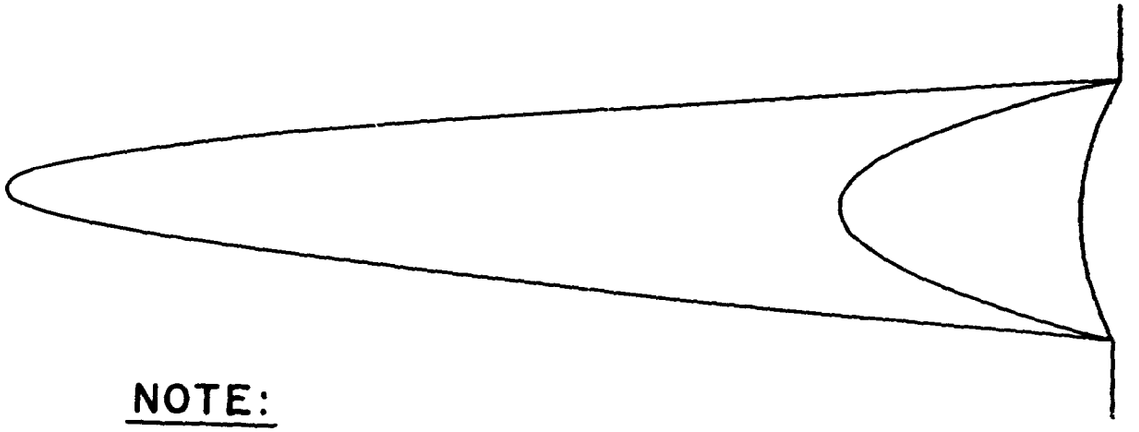

NOTE:

SCALE IN WIDTH DIRECTION TEN TIMES SCALE IN LENGTH DIRECTION

Fig. 13 Geometry of three hyperbolic cracks showing the range of sizes included in the investigation of crack length.

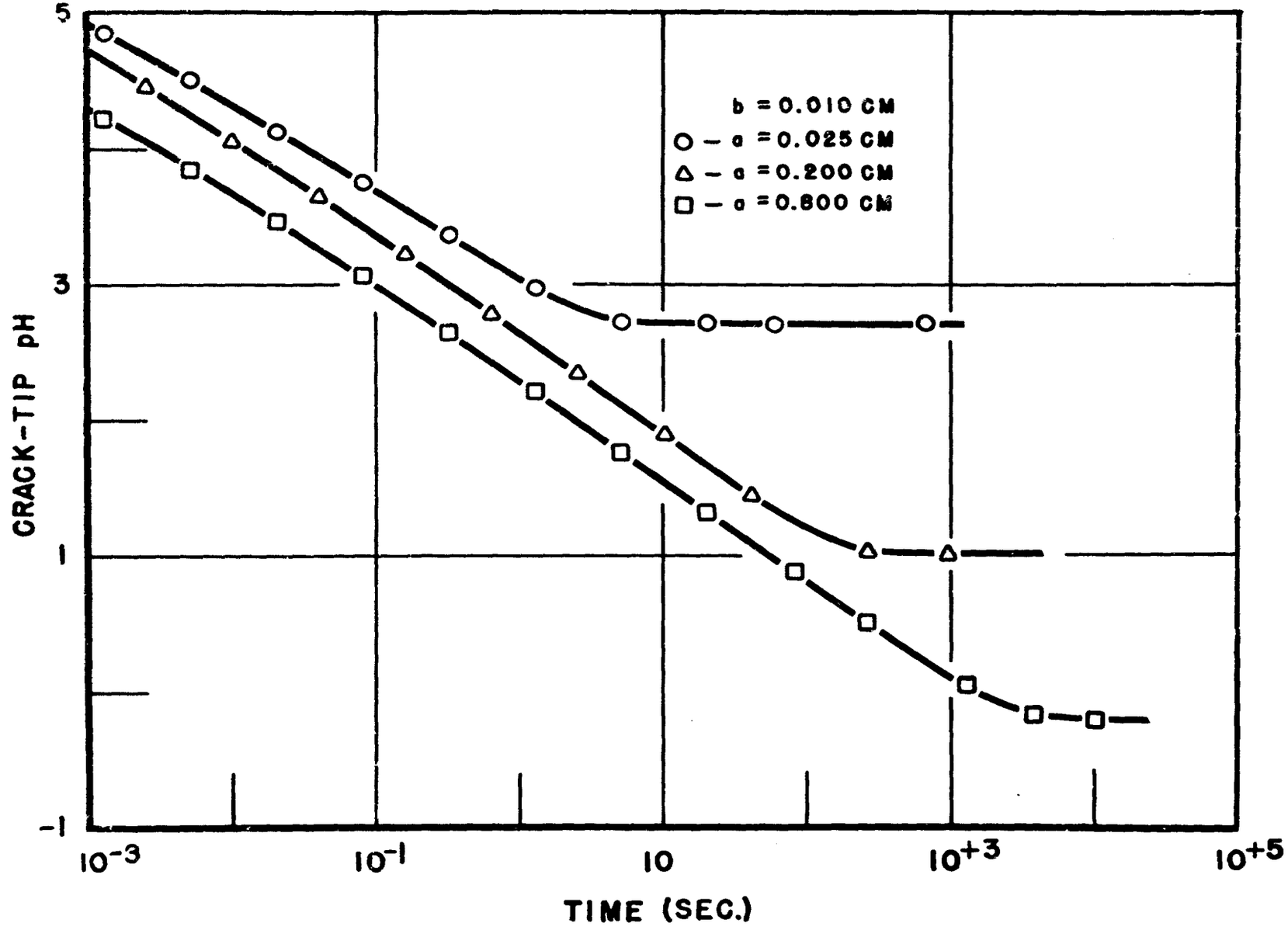

Fig. 14 Variation of the crack-tip pH with time for three hyperbolic cracks (transport by simple diffusion).

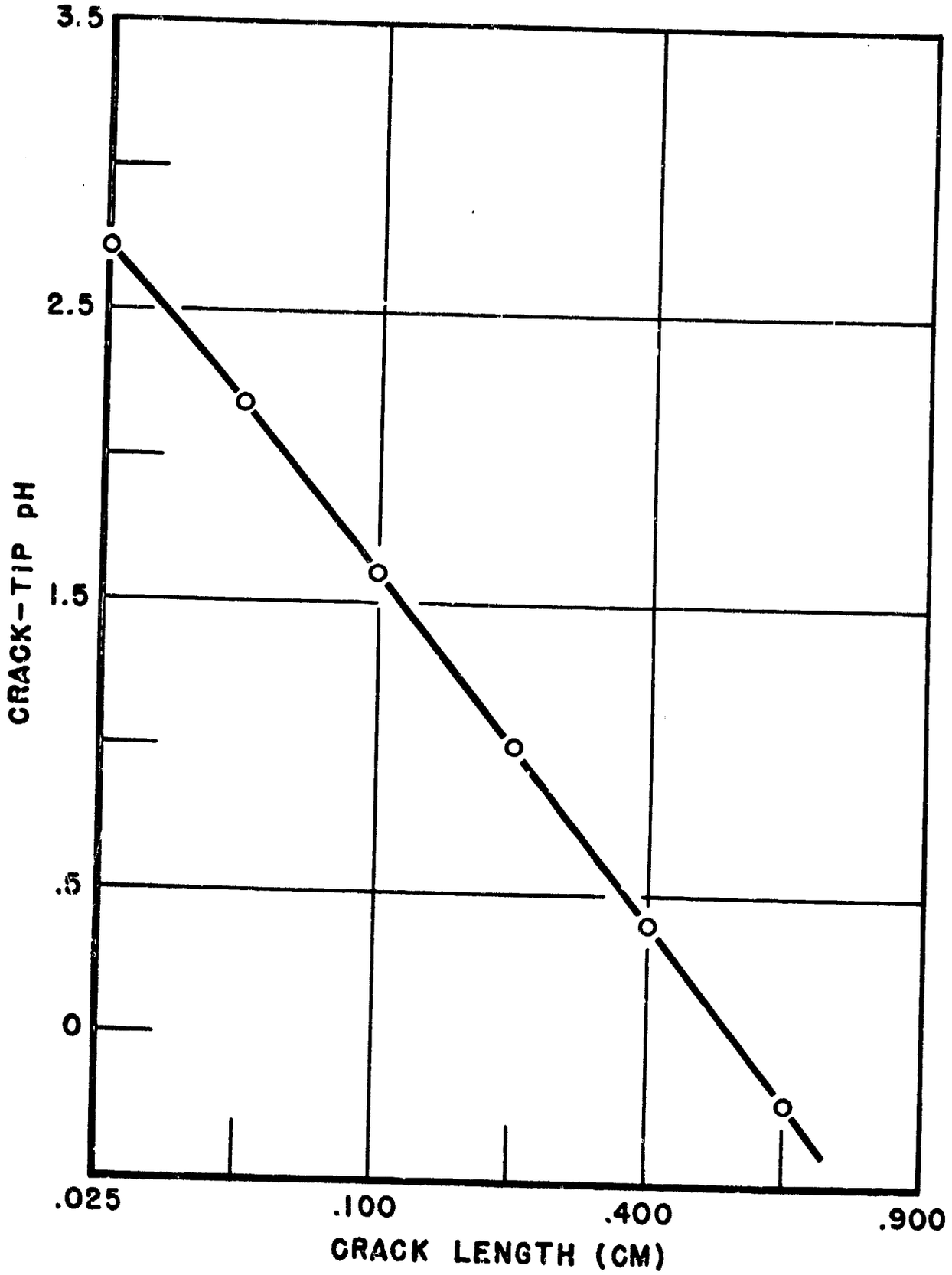

Fig. 15 Dependence on crack length of the steady-state crack-tip pH for 0.02-centimeter-wide hyperbolic cracks (transport by simple diffusion).

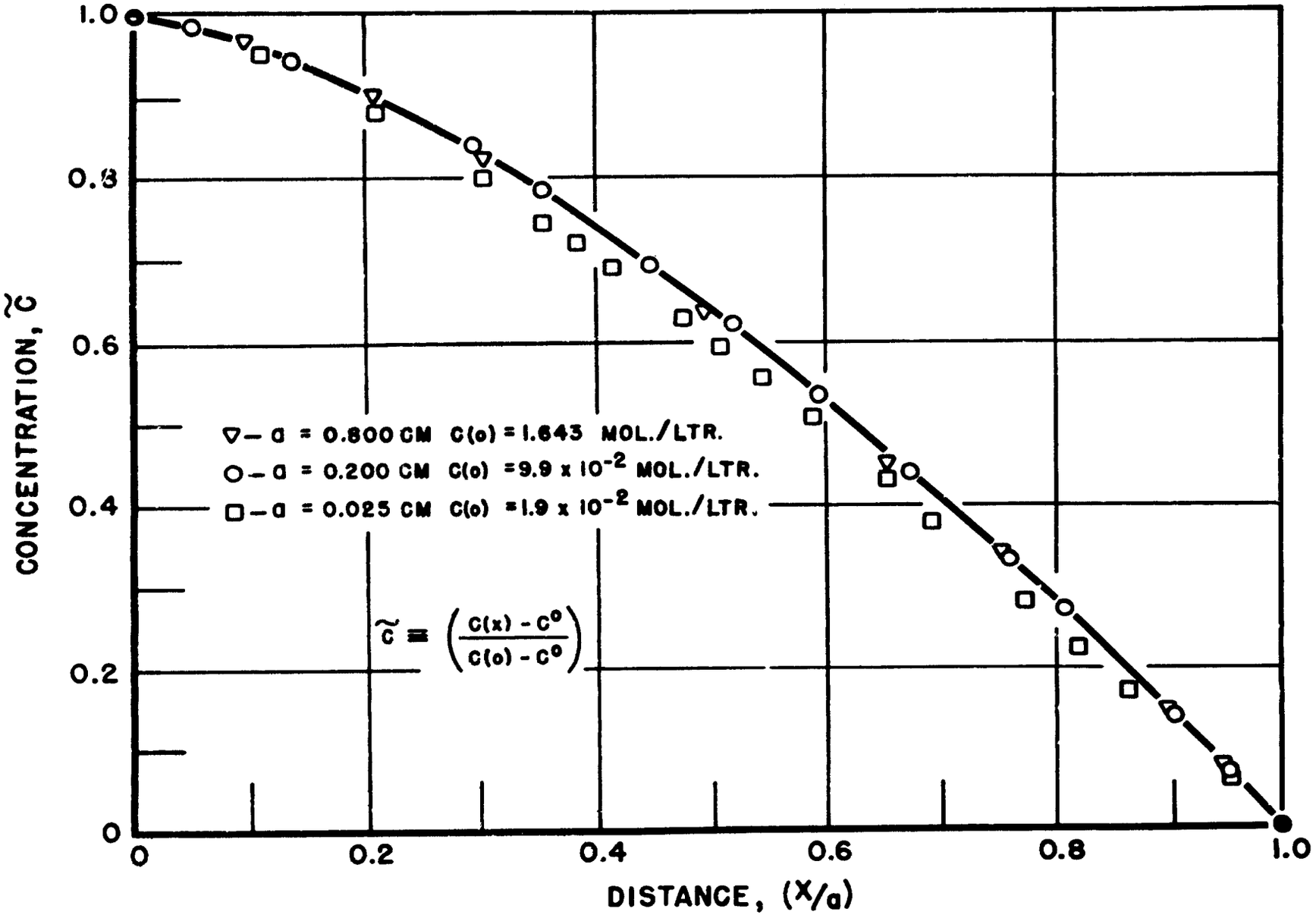

Fig. 16 Steady-state longitudinal concentration profiles in three hyperbolic cracks (constant flux boundary conditions and transport by simple diffusion).

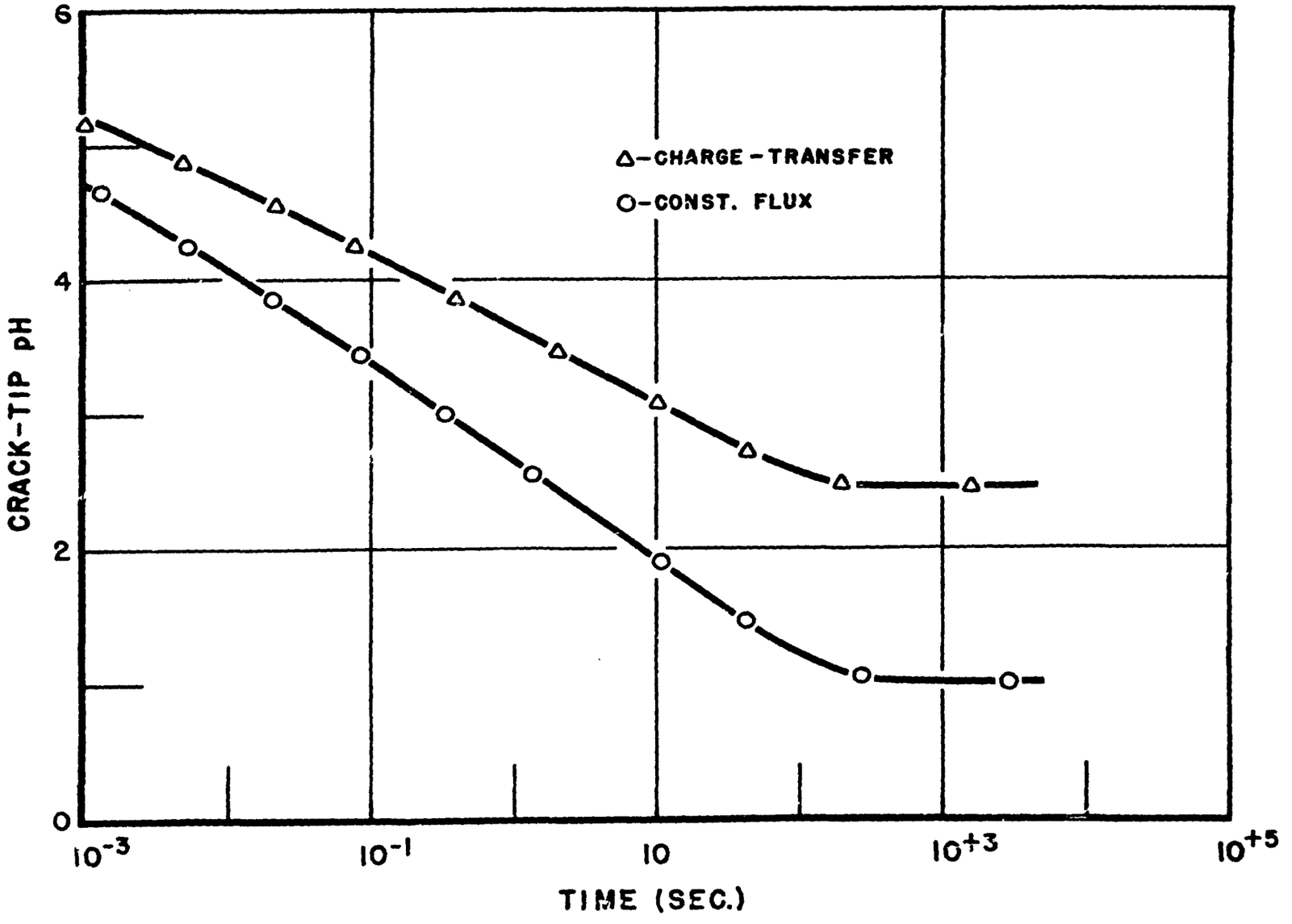

Fig. 17 Variation of the crack-tip pH with time in a hyperbolic crack with concentration-dependent boundary conditions (transport by simple diffusion).

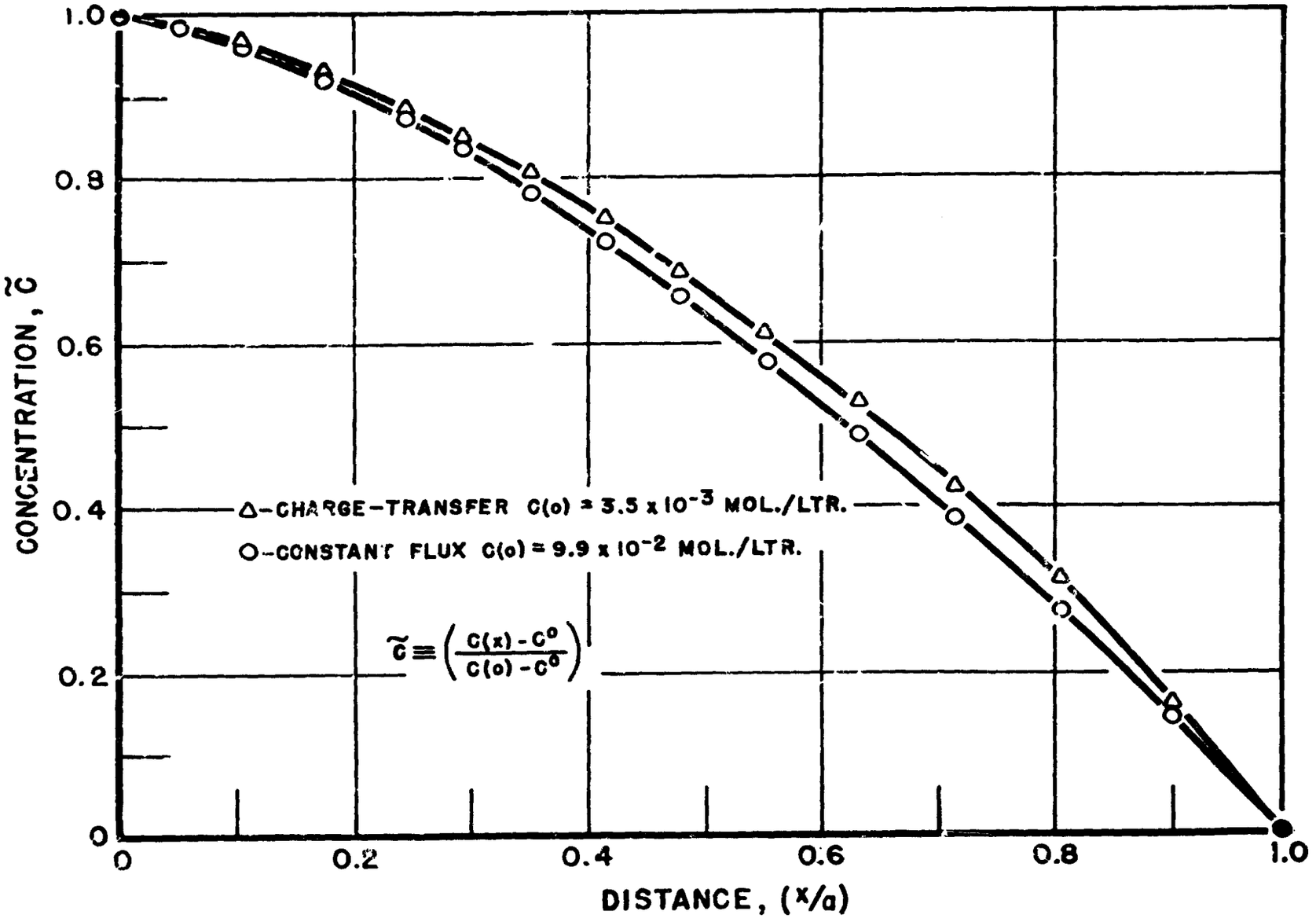

Fig. 18 Steady-state longitudinal concentration profile in a hyperbolic crack with concentration-dependent boundary conditions (transport by simple diffusion).

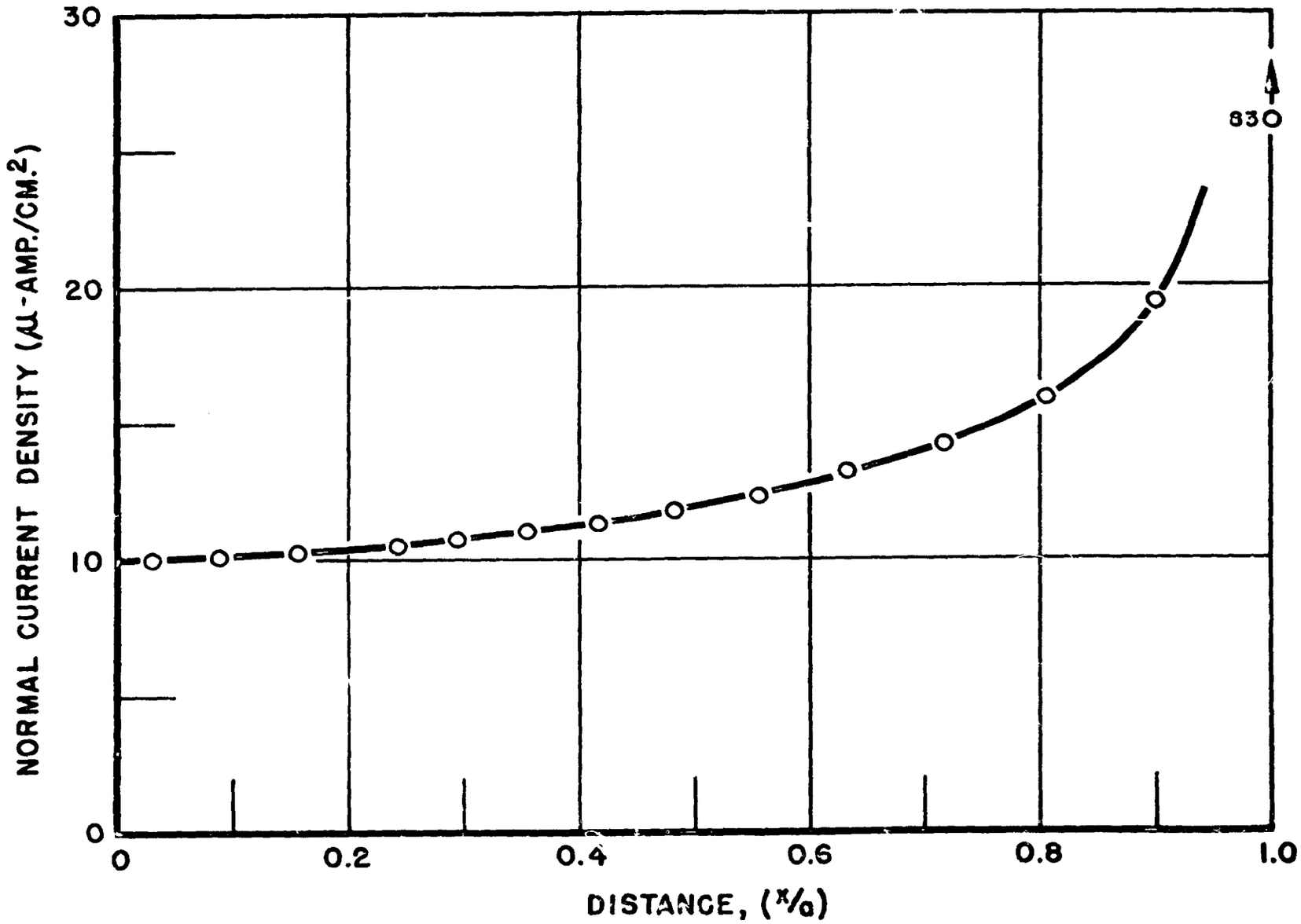

Fig. 19 Variation of the normal flux (current density) along the crack wall with concentration-dependent boundary conditions (transport by simple diffusion).

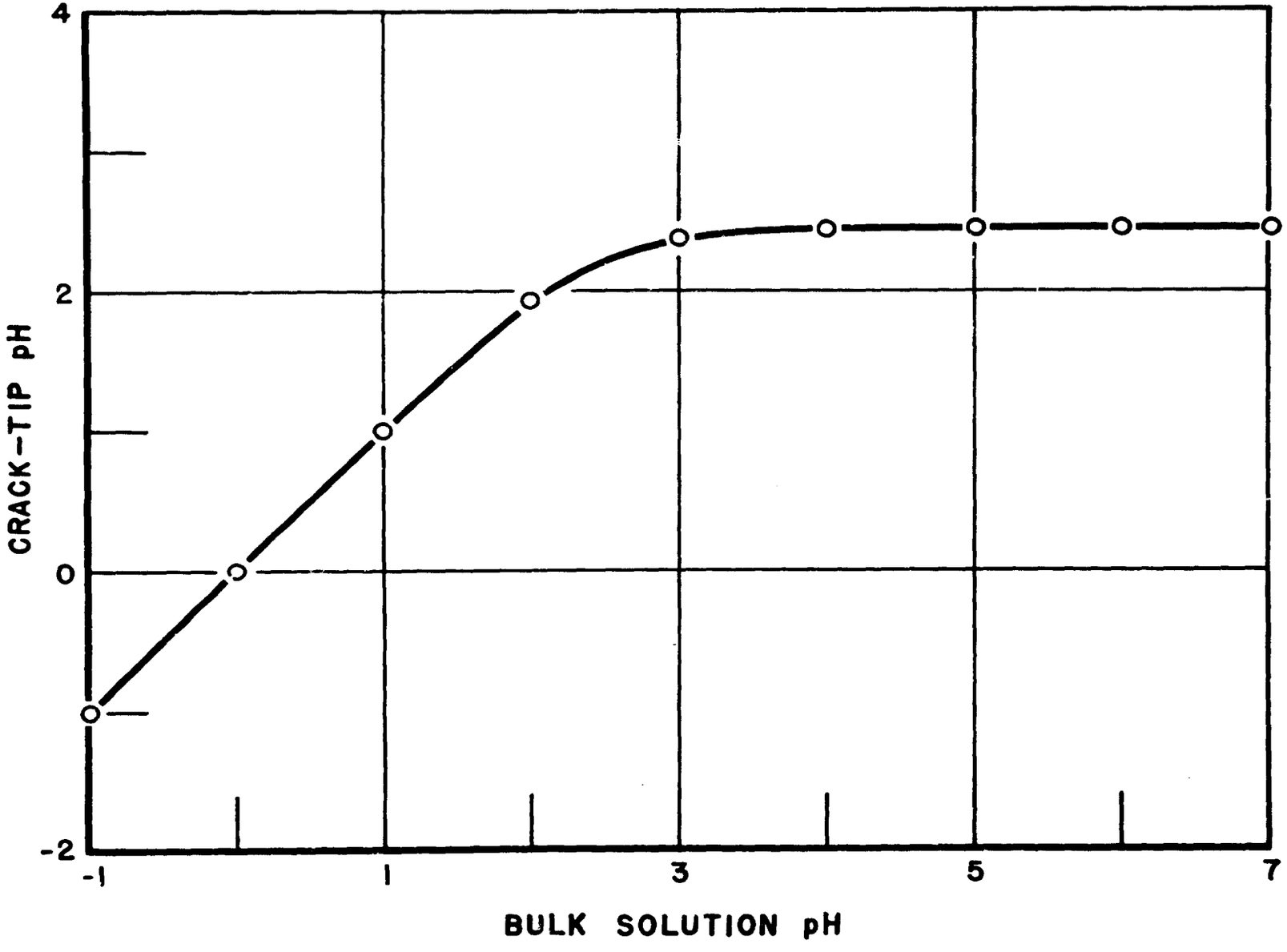

Fig. 20 Relation between crack-tip pH and bulk-solution pH for a hyperbolic crack with concentration-dependent boundary conditions.

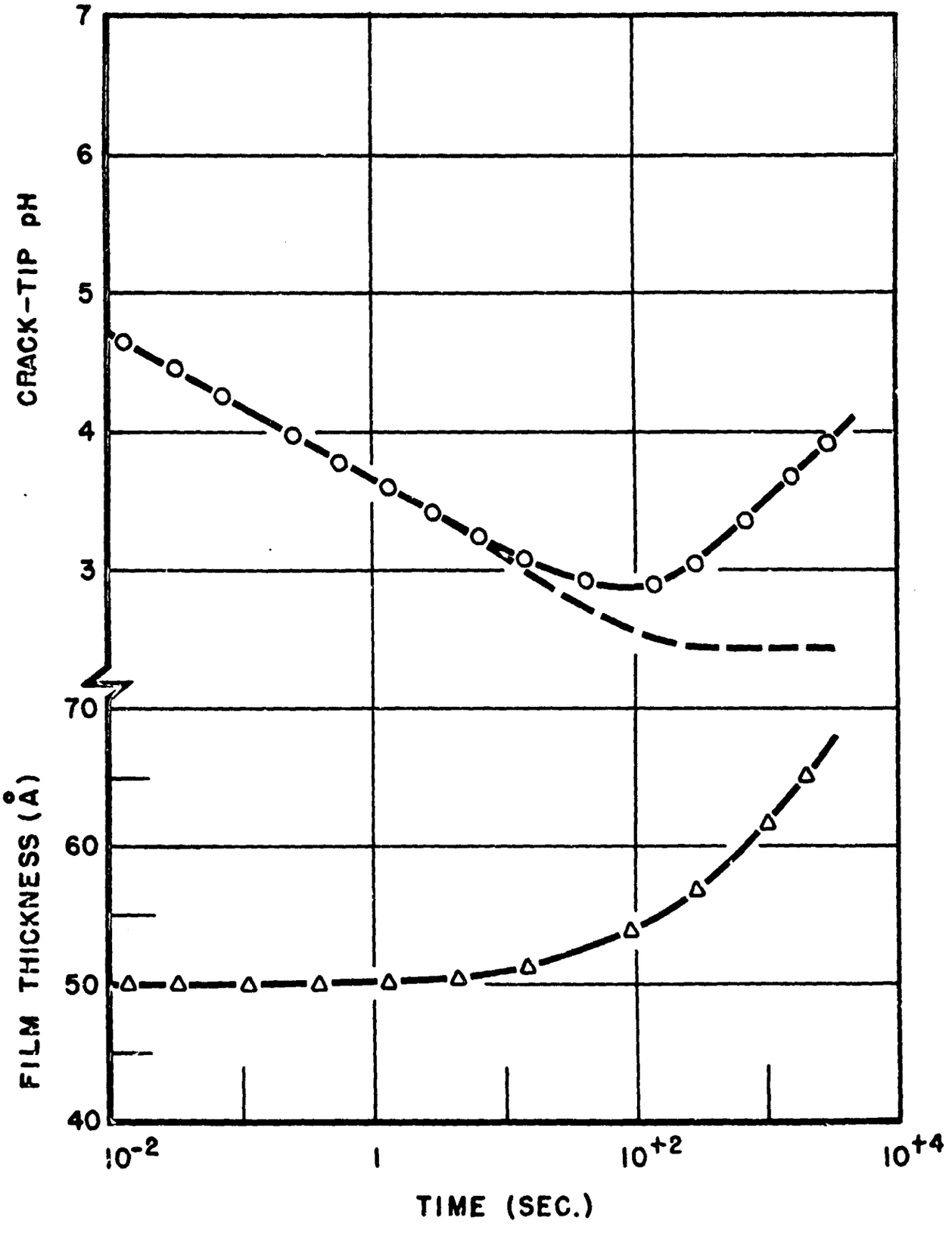

Fig. 21 Variation of the crack-tip pH and oxide-film thickness with time for a hyperbolic crack with charge-transfer boundary conditions (transport by simple diffusion).

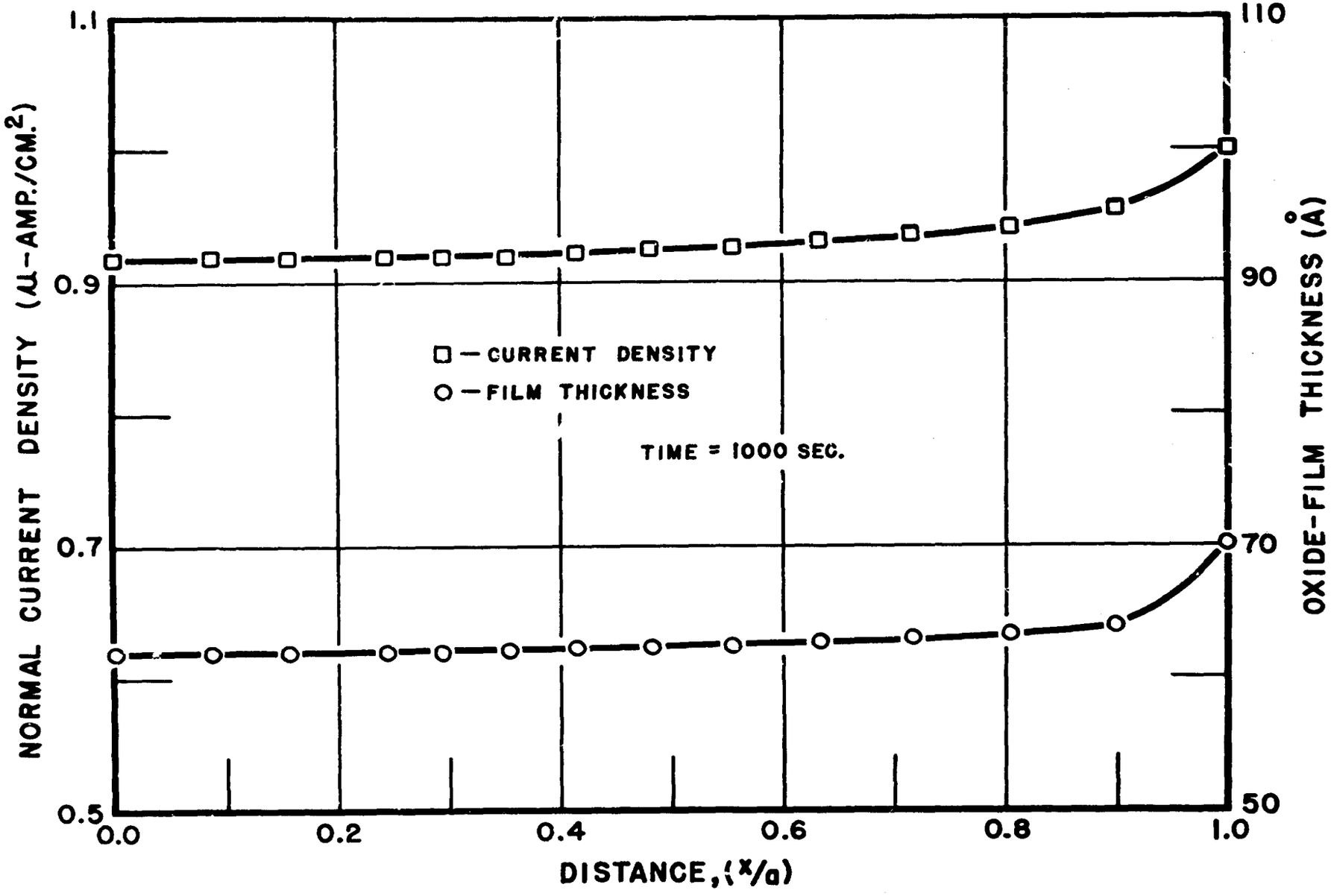

Fig. 22 Variation of the normal flux (current density) along the crack wall with the charge-transfer boundary conditions showing the effects of oxide-film growth (transport by simple diffusion).

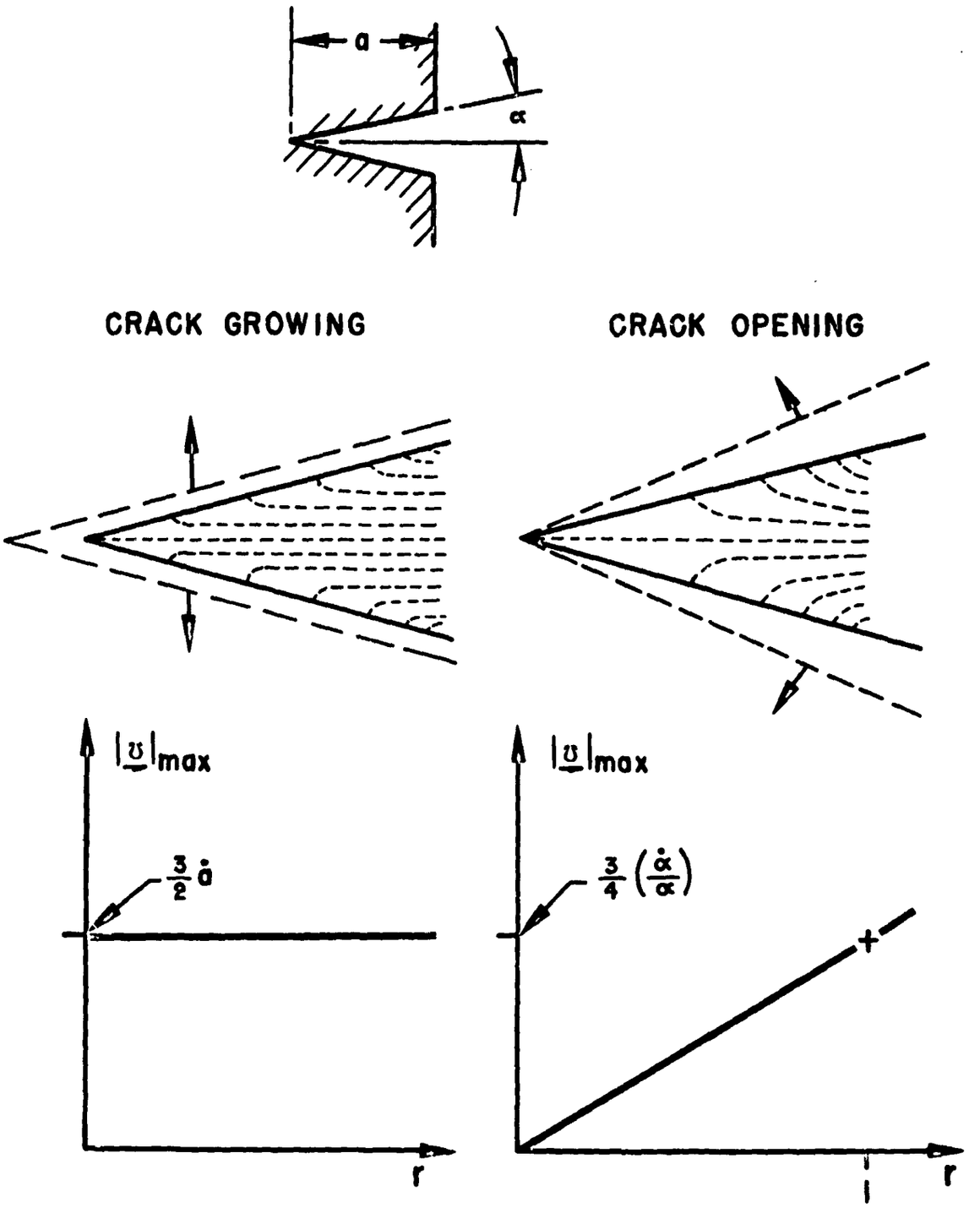

Fig. 23 Convection in a pie-shaped crack.

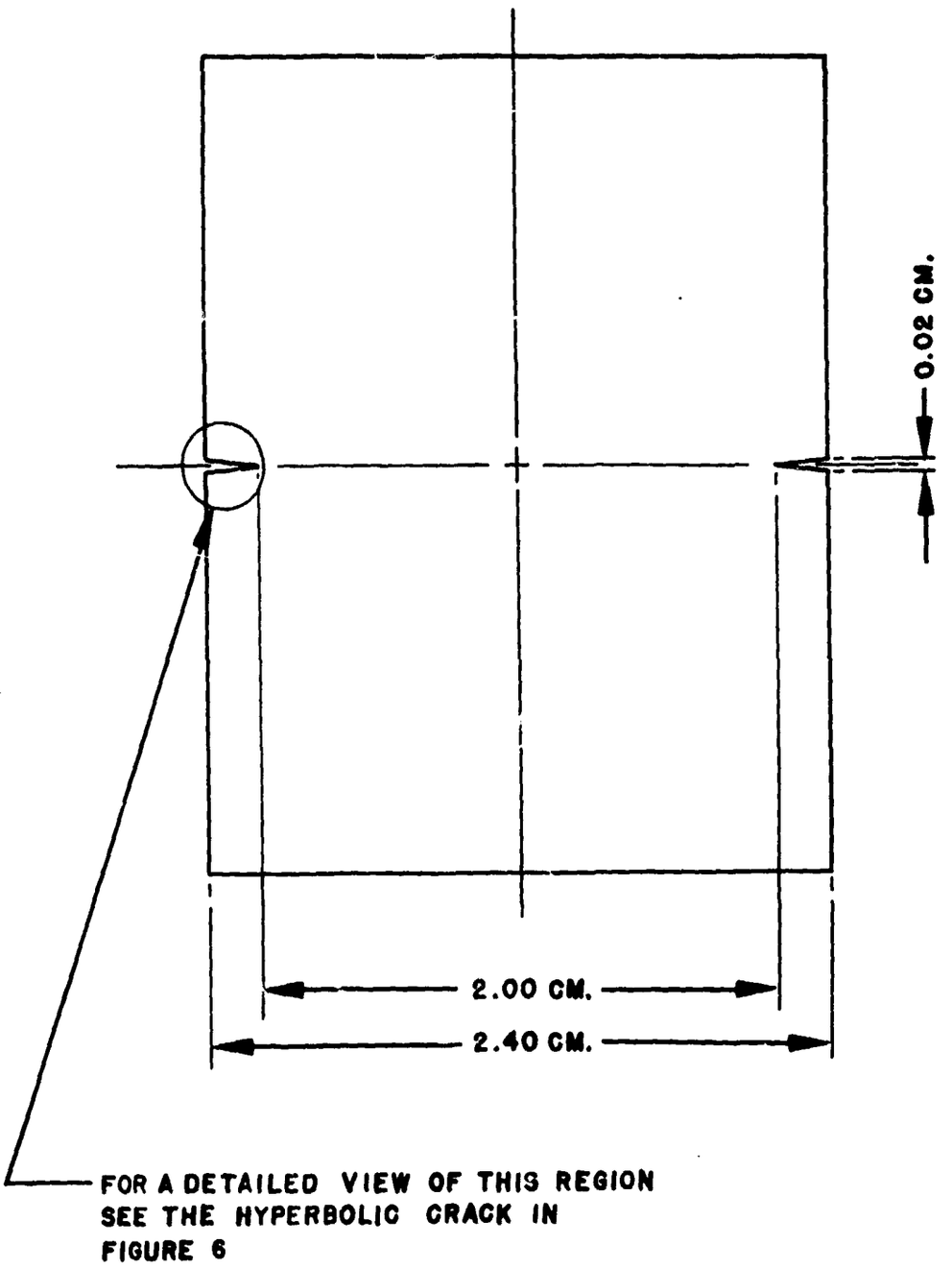

Fig. 24 Double edge-notched plate tension specimen used to investigate the effects of solvent convection.

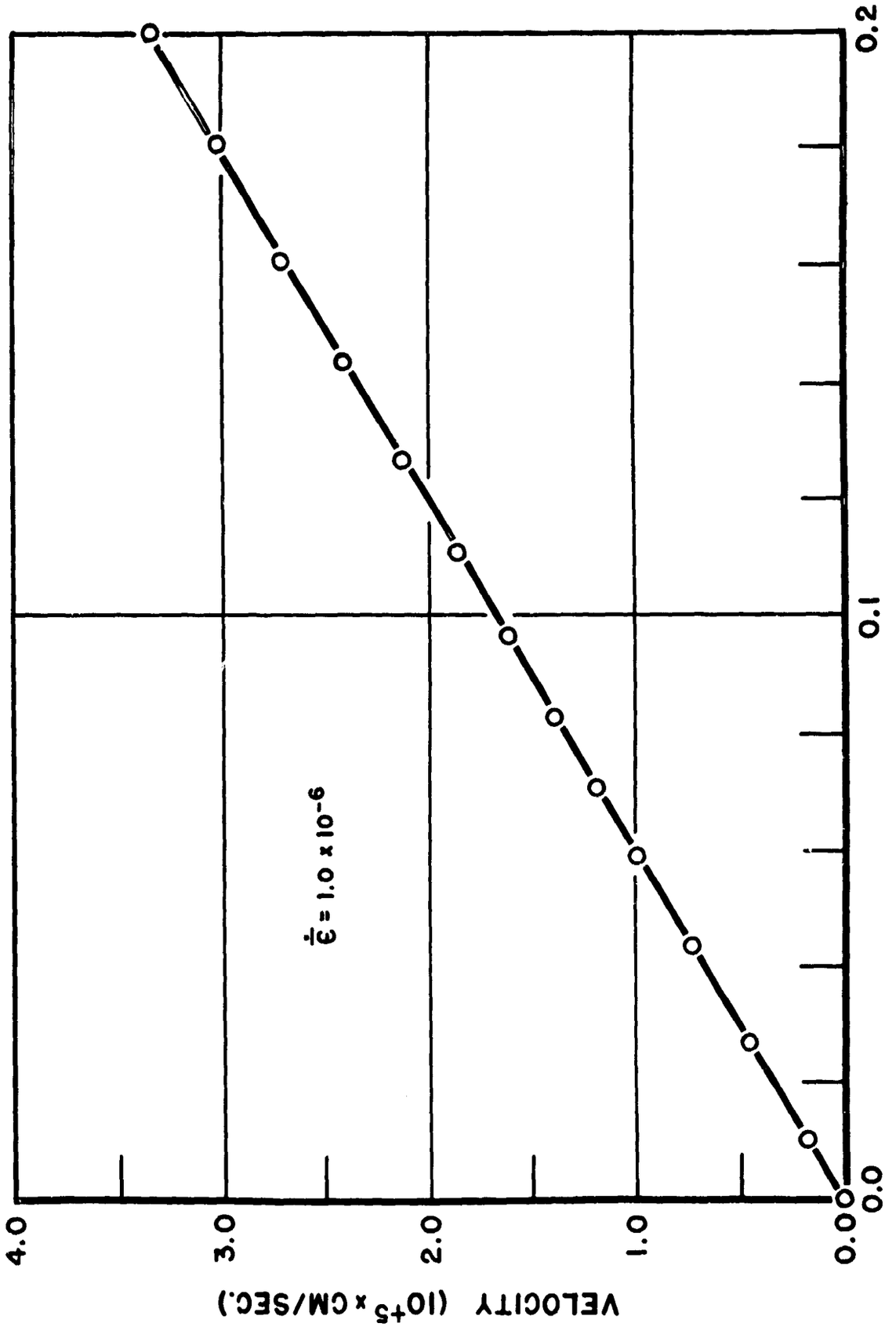

Fig. 25 Variation of the average longitudinal solvent velocity with distance for a hyperbolic crack in a double edge-notched plate specimen.

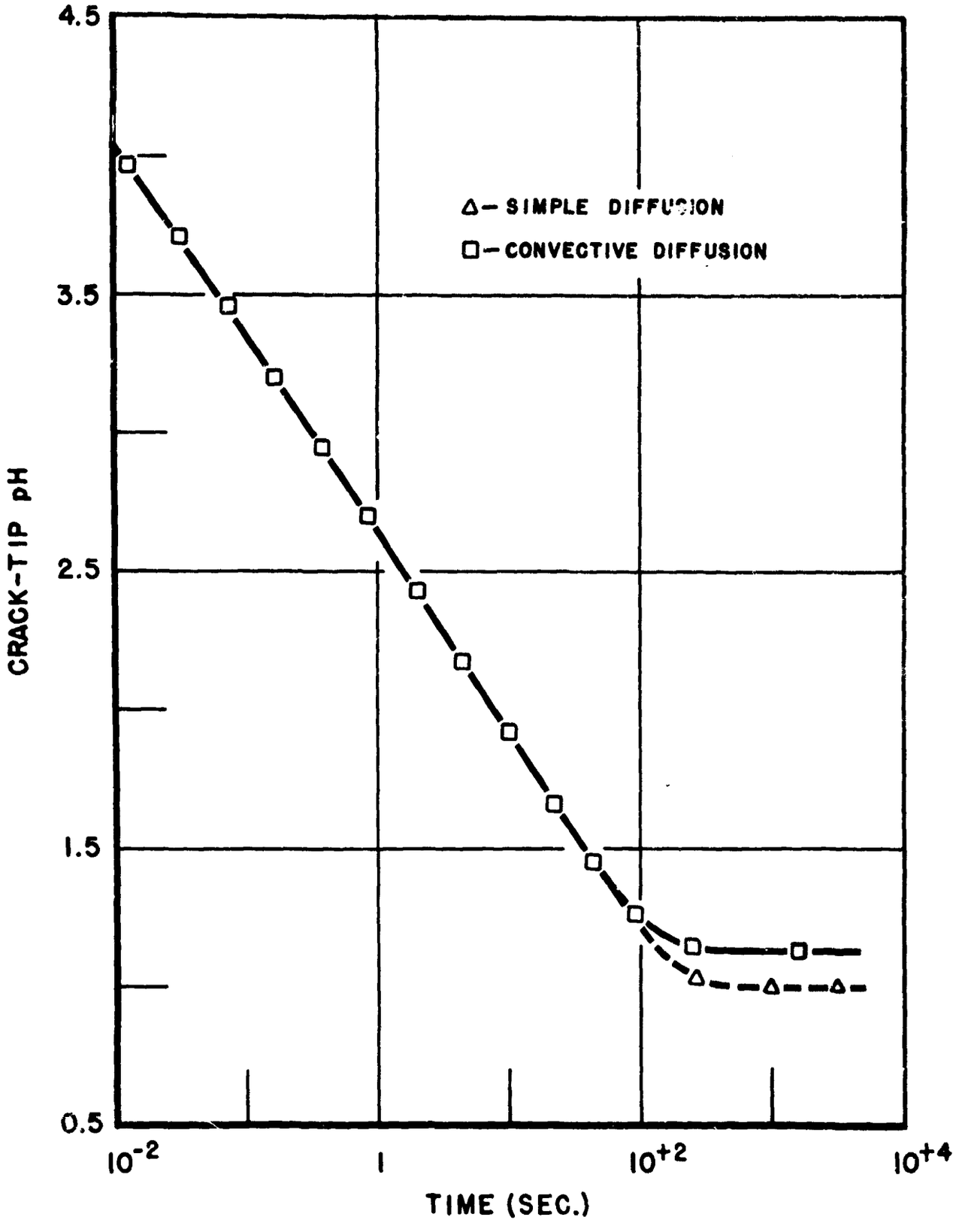

Fig. 26 Variation of the crack-tip pH with time in a hyperbolic crack showing the effect on convective transport.

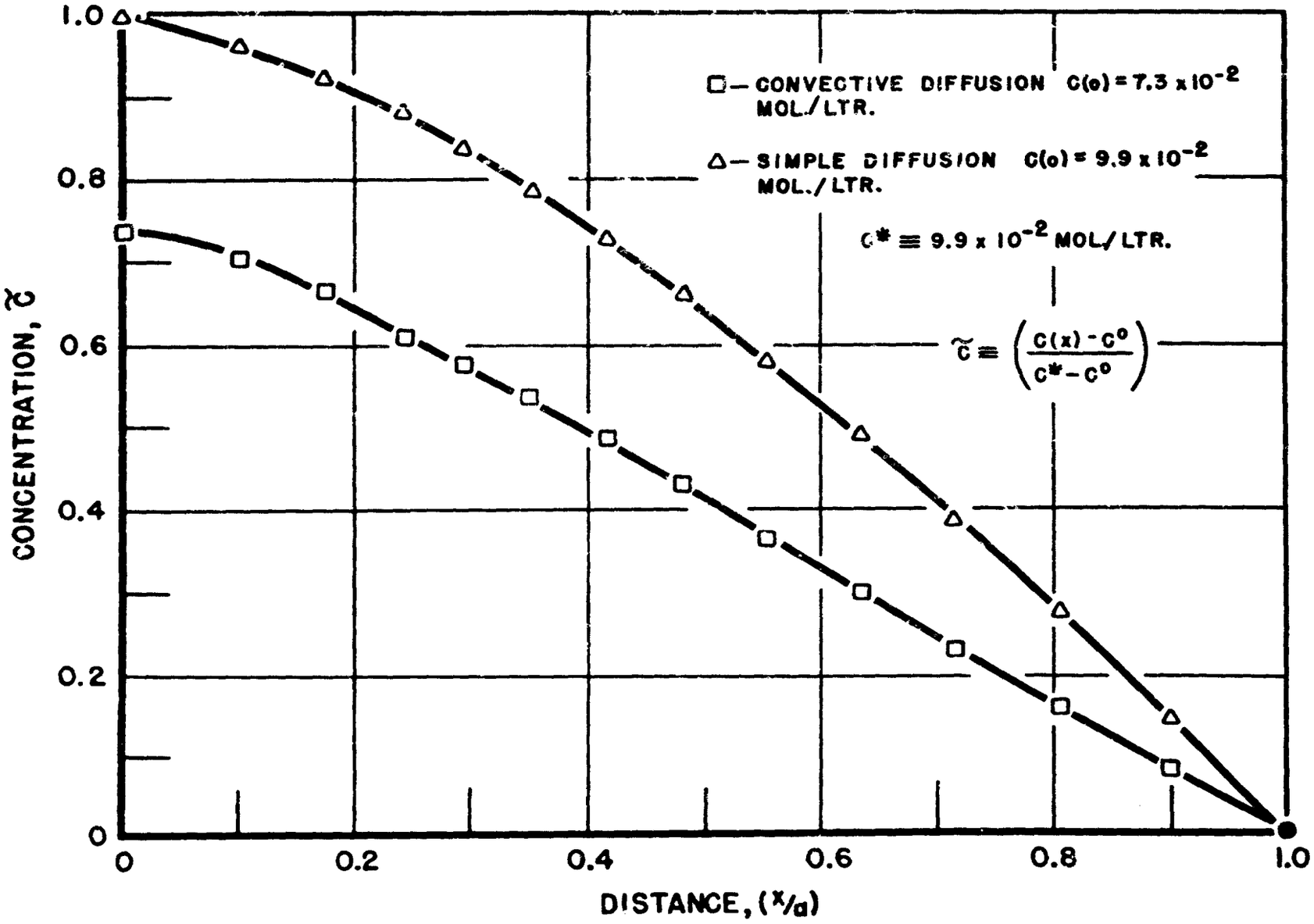

Fig. 27 'Steady-state' longitudinal concentration profile in a hyperbolic crack showing the influence of convective transport.

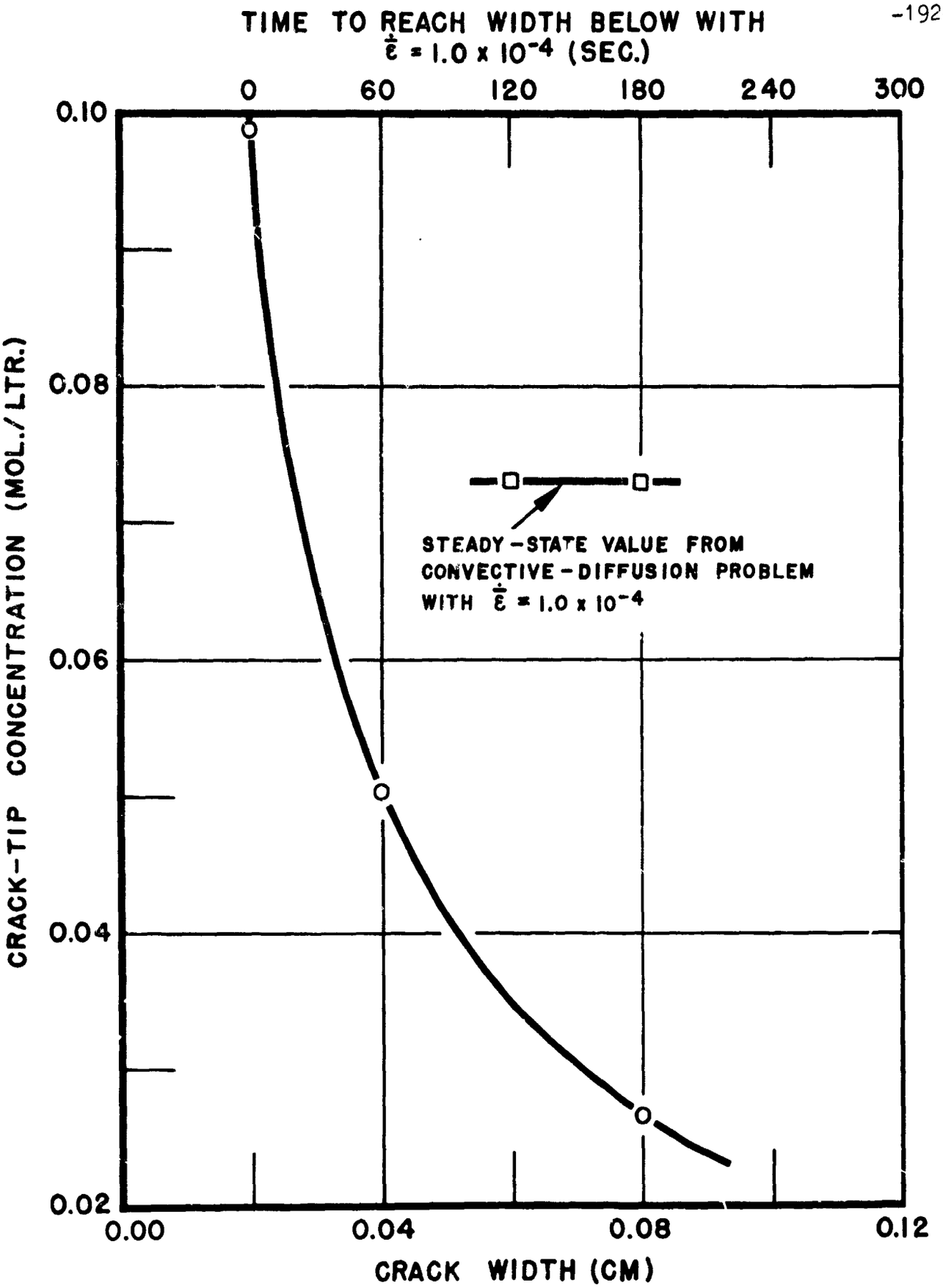

Fig. 28 Dependence on crack width of the steady-state crack-tip concentration for 0.20-centimeter-long hyperbolic cracks (transport by simple diffusion).

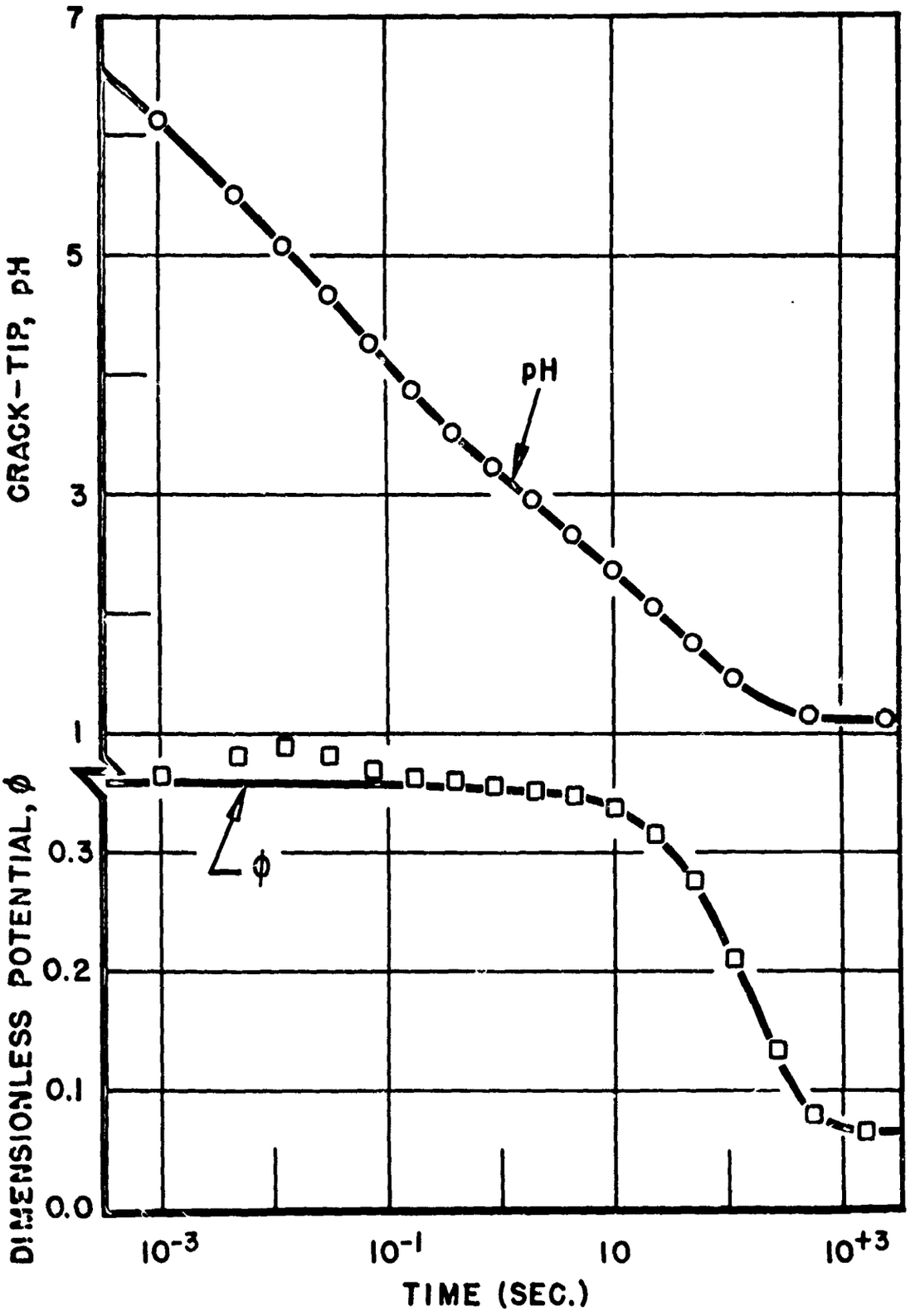

Fig. 29 Variation of the crack-tip pH and potential with time in a rectangular crack (transport by diffusion and migration).

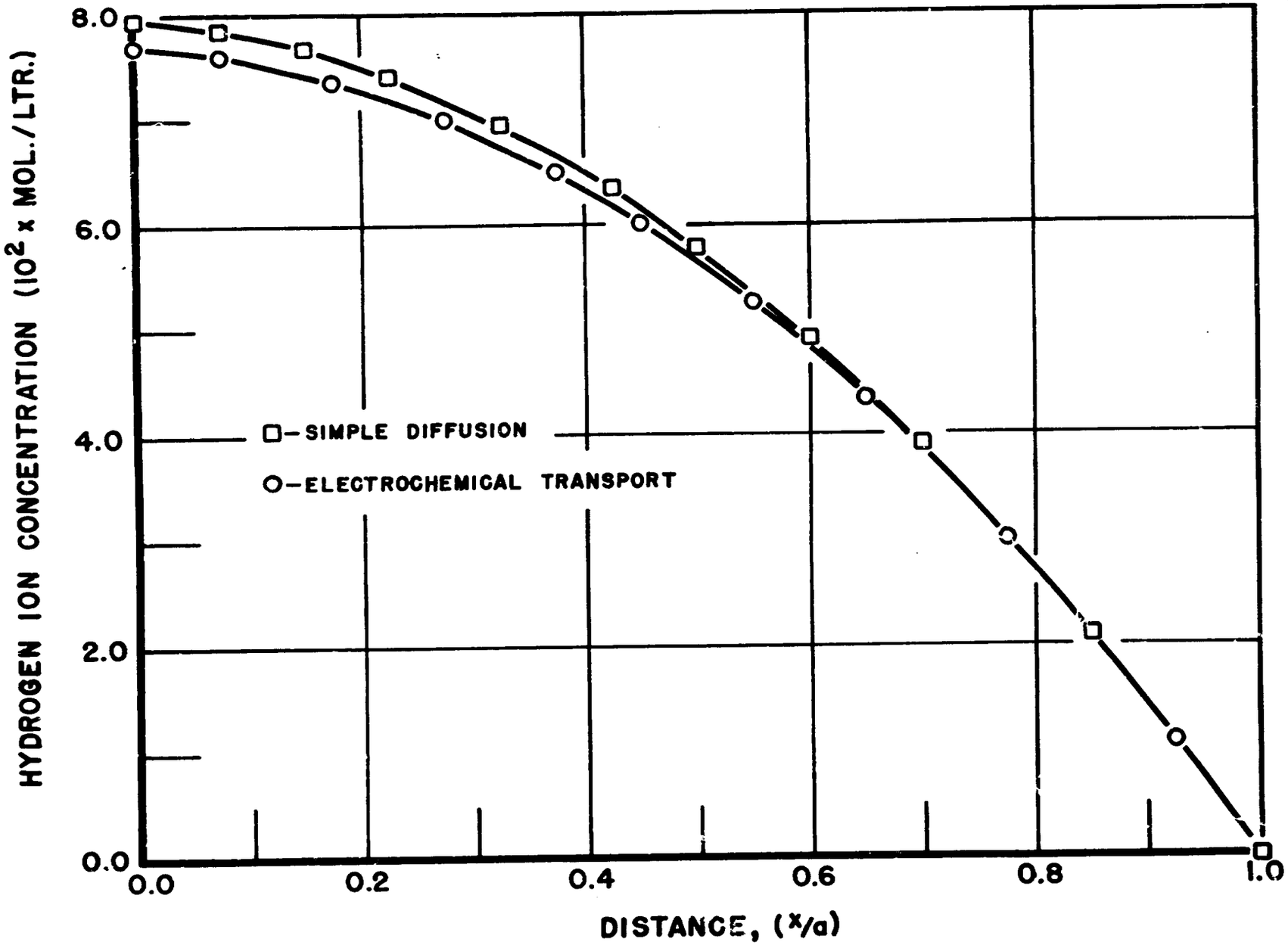

Fig. 30 Steady-state longitudinal concentration profiles for the hydrogen ion in a rectangular crack showing the influence of transport by migration.

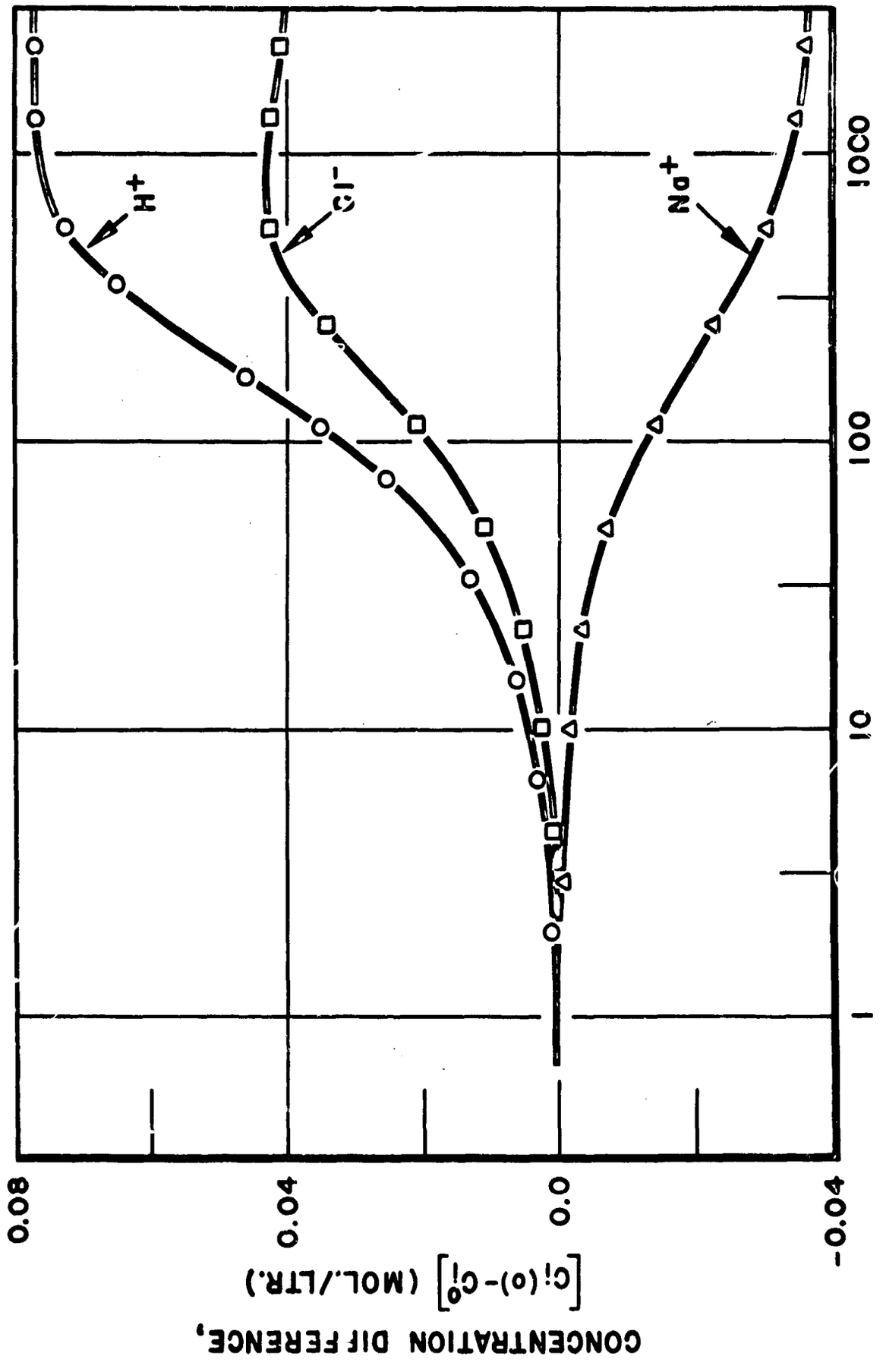

Fig. 31 Variation of the ion concentrations with time in a rectangular crack (transport by diffusion and migration).

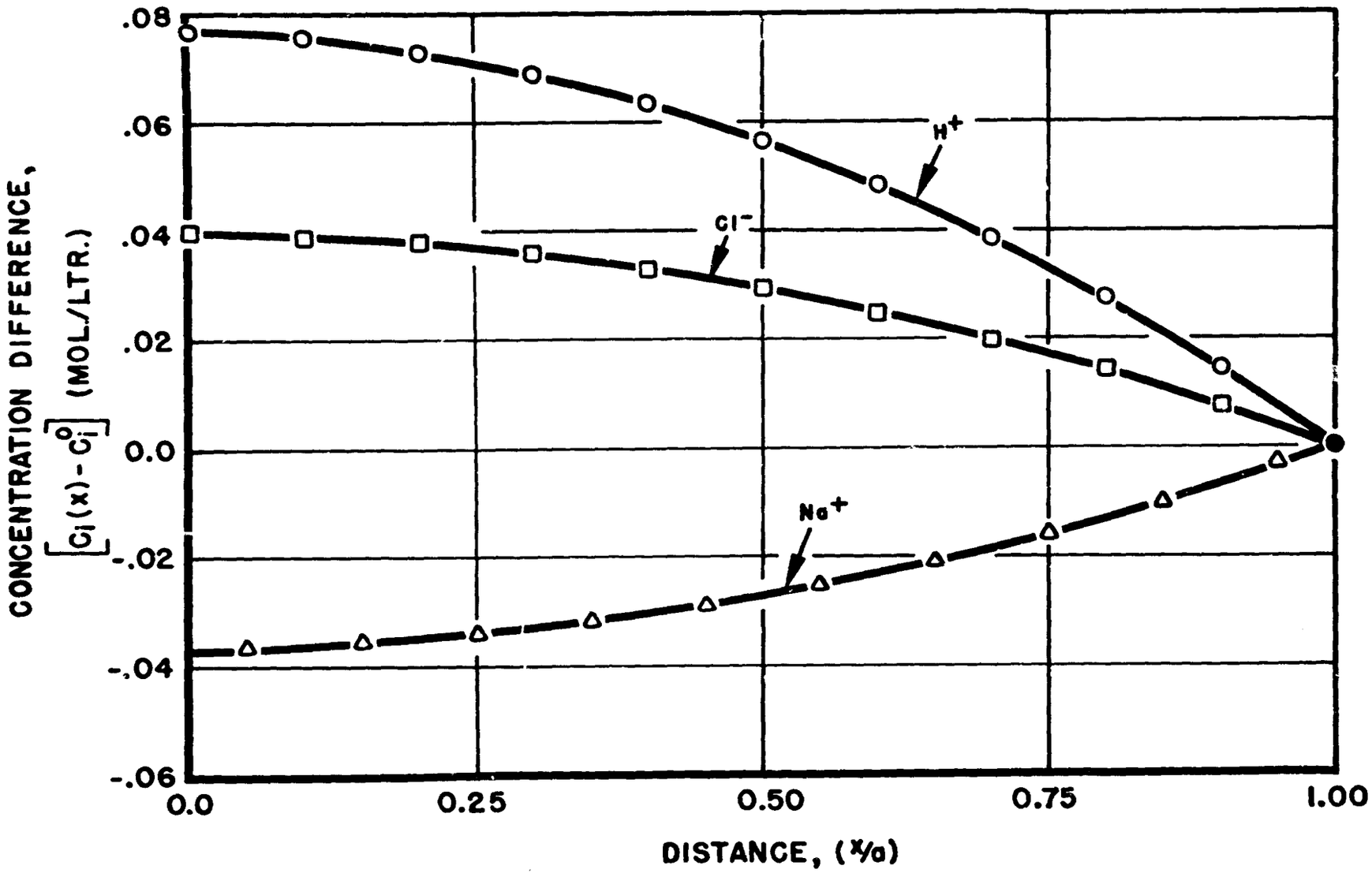

Fig. 32 Steady-state longitudinal concentration profiles for all three ions in a ternary electrolyte contained in a rectangular crack (transport by diffusion and migration).

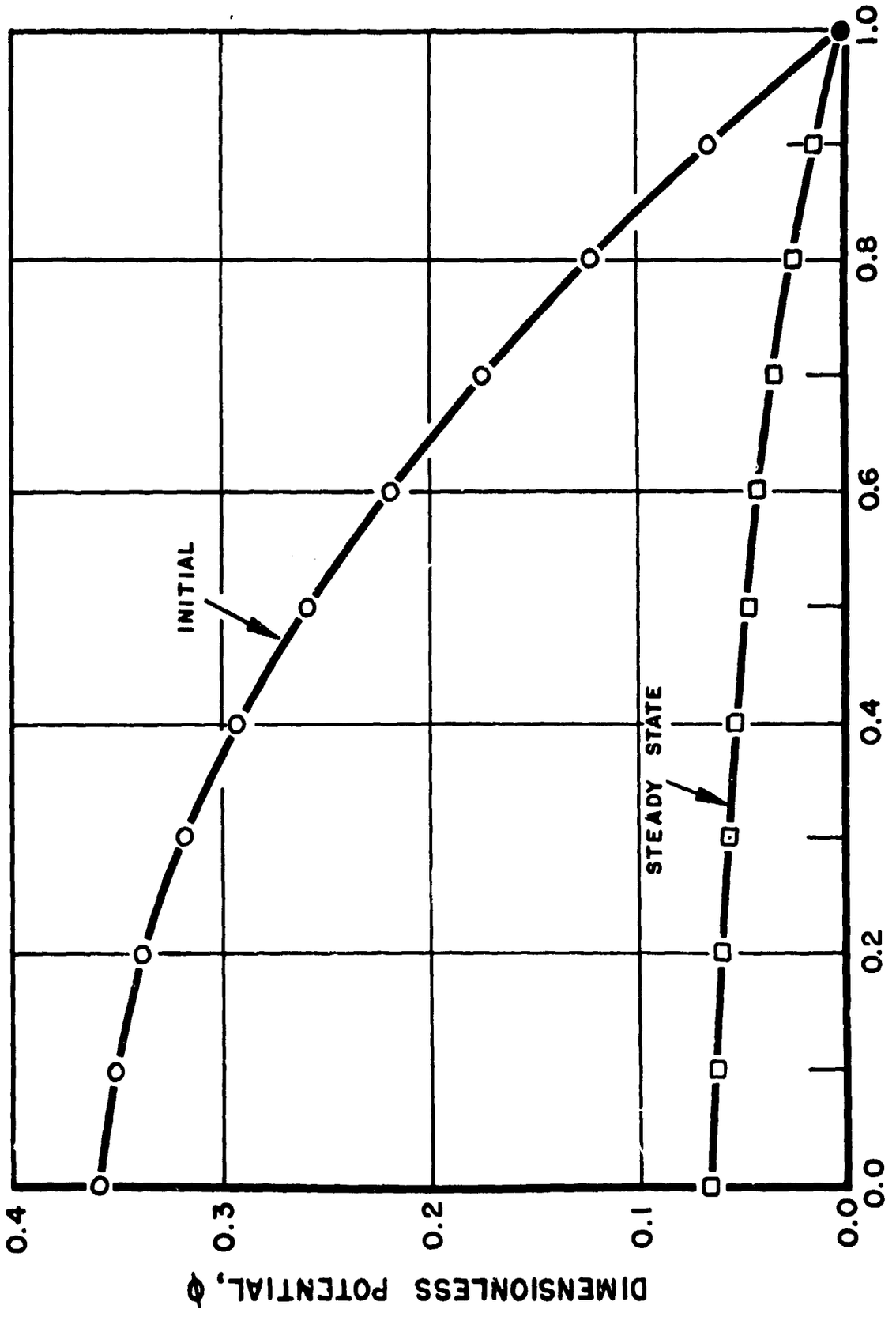

Fig. 33 Longitudiral variation of the initial and steady-state values of the electrostatic potential in a rectangular crack.

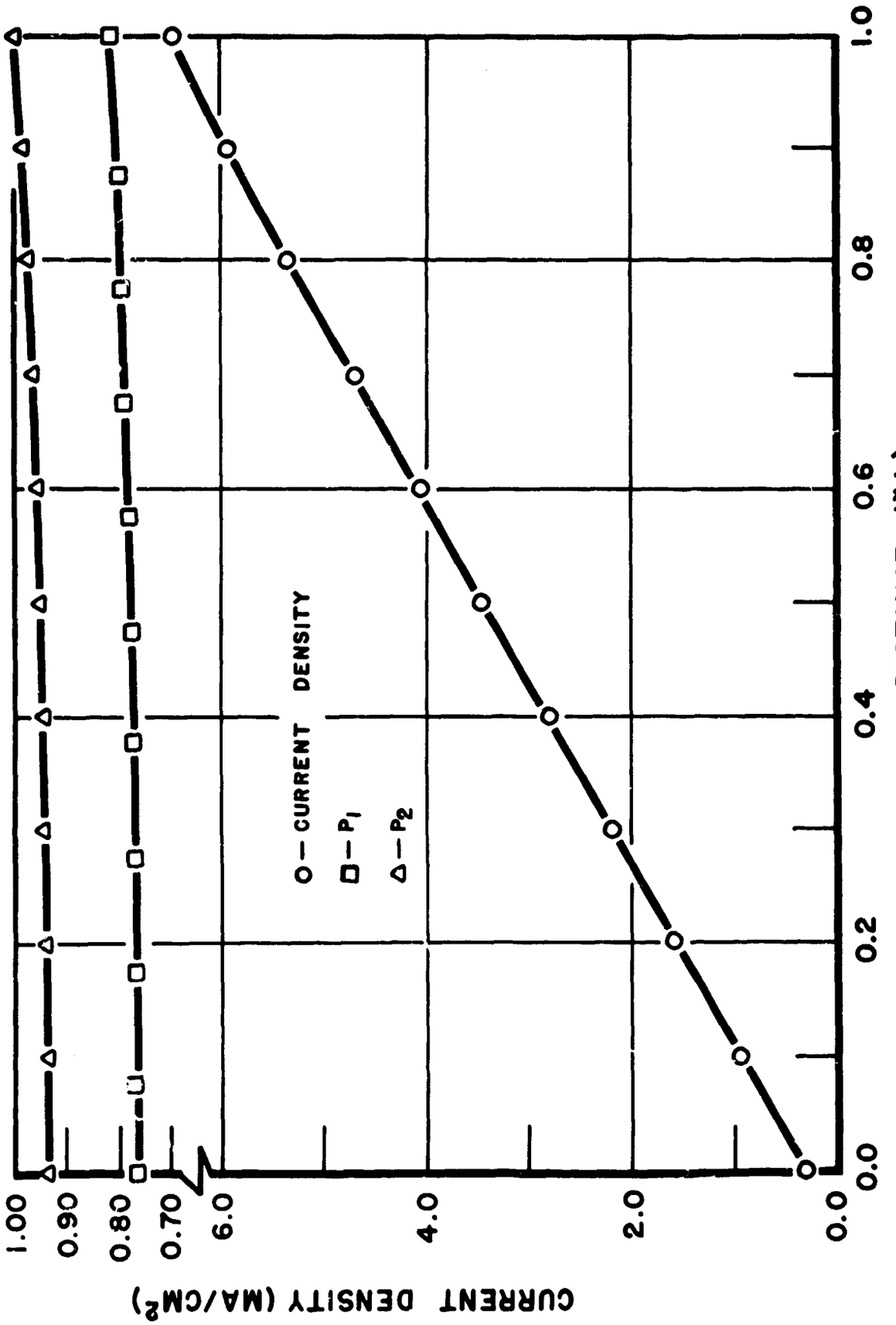

Fig. 34 Behavior of the steady-state current in a rectangular crack.

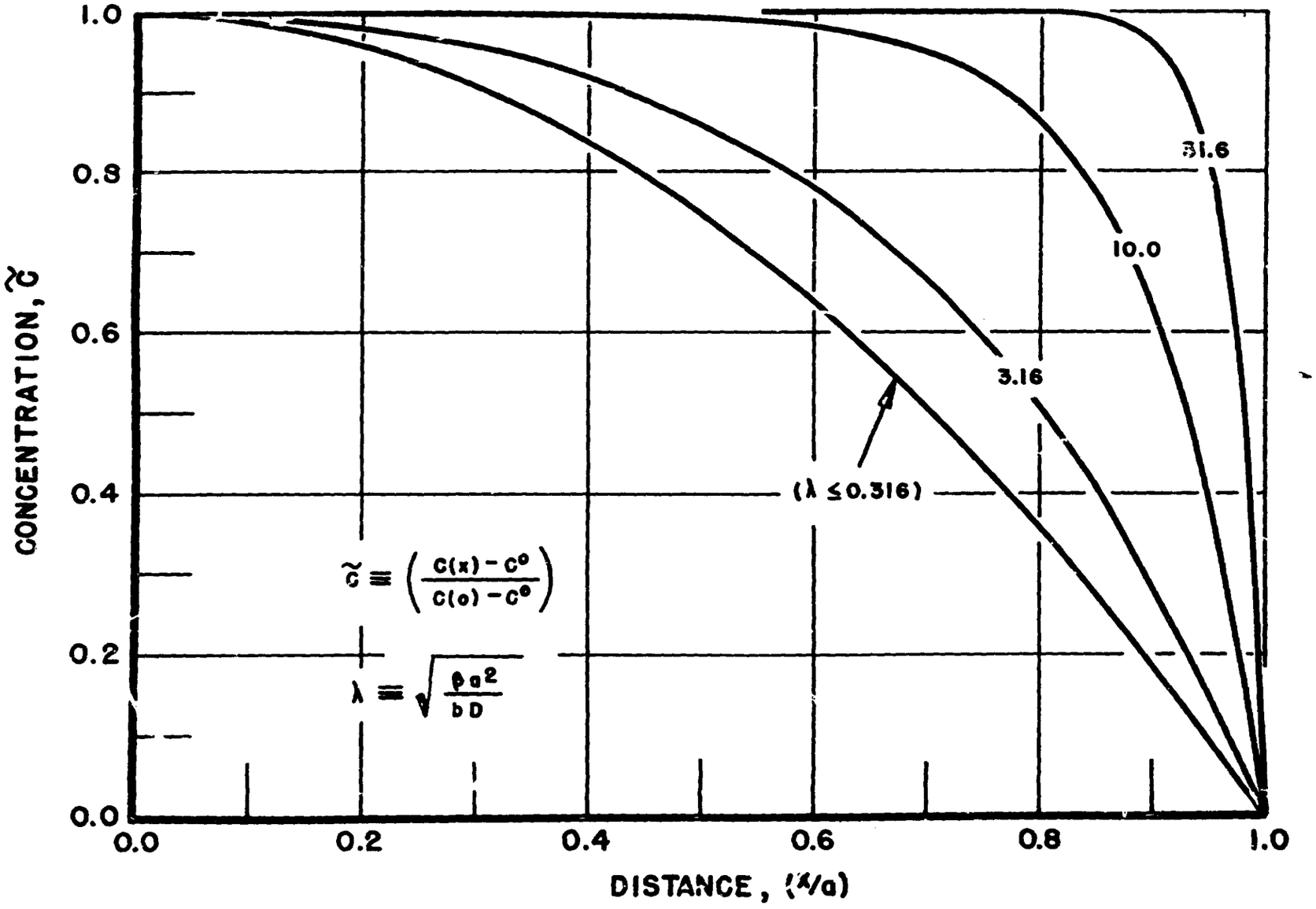

Fig. 35 Steady-state longitudinal concentration profiles in a rectangular crack for several values of the flux parameter λ (transport by simple diffusion).

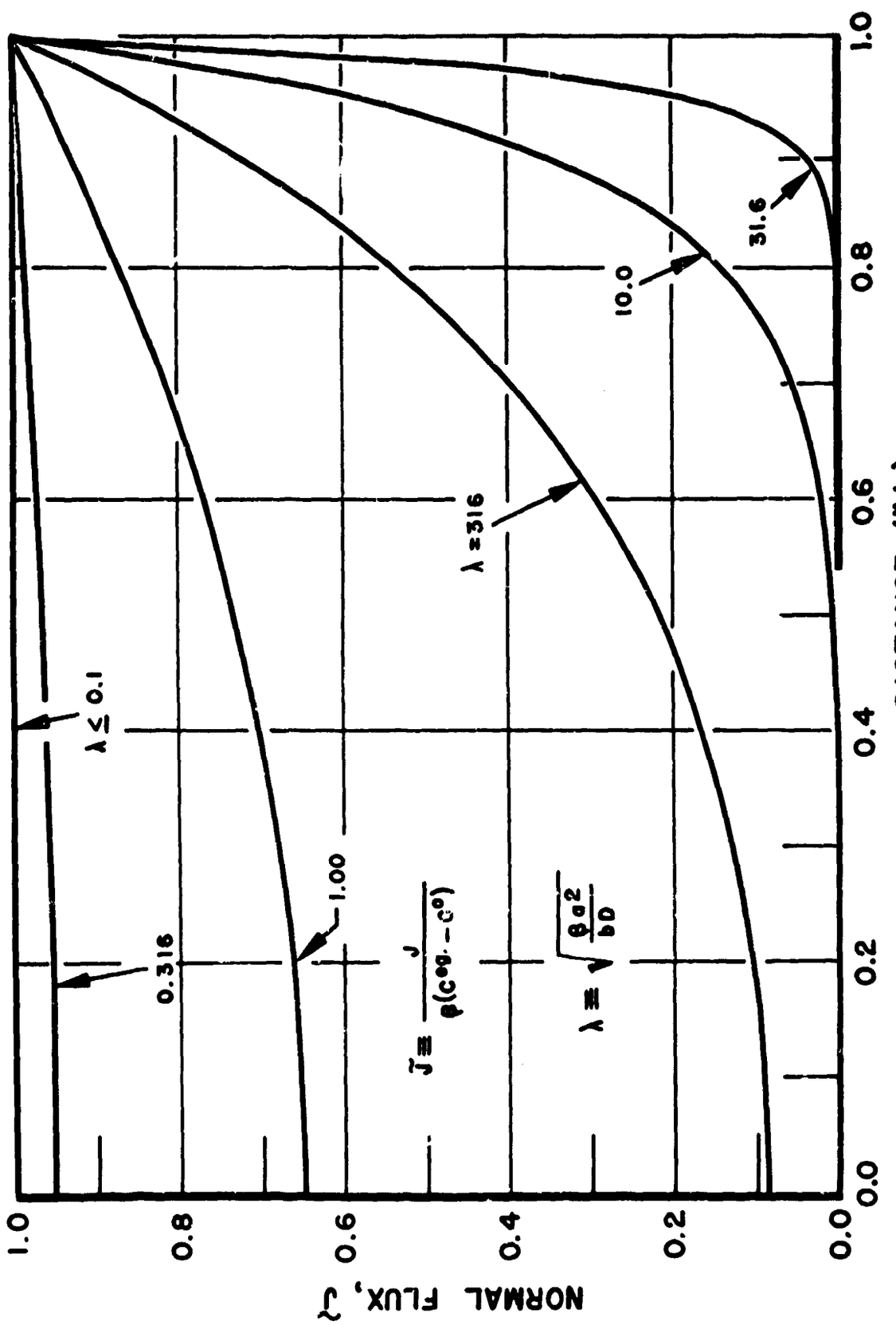

Fig. 36 Variation of the normal flux along the wall of a rectangular crack for several values of the flux parameter λ (transport by simple diffusion).

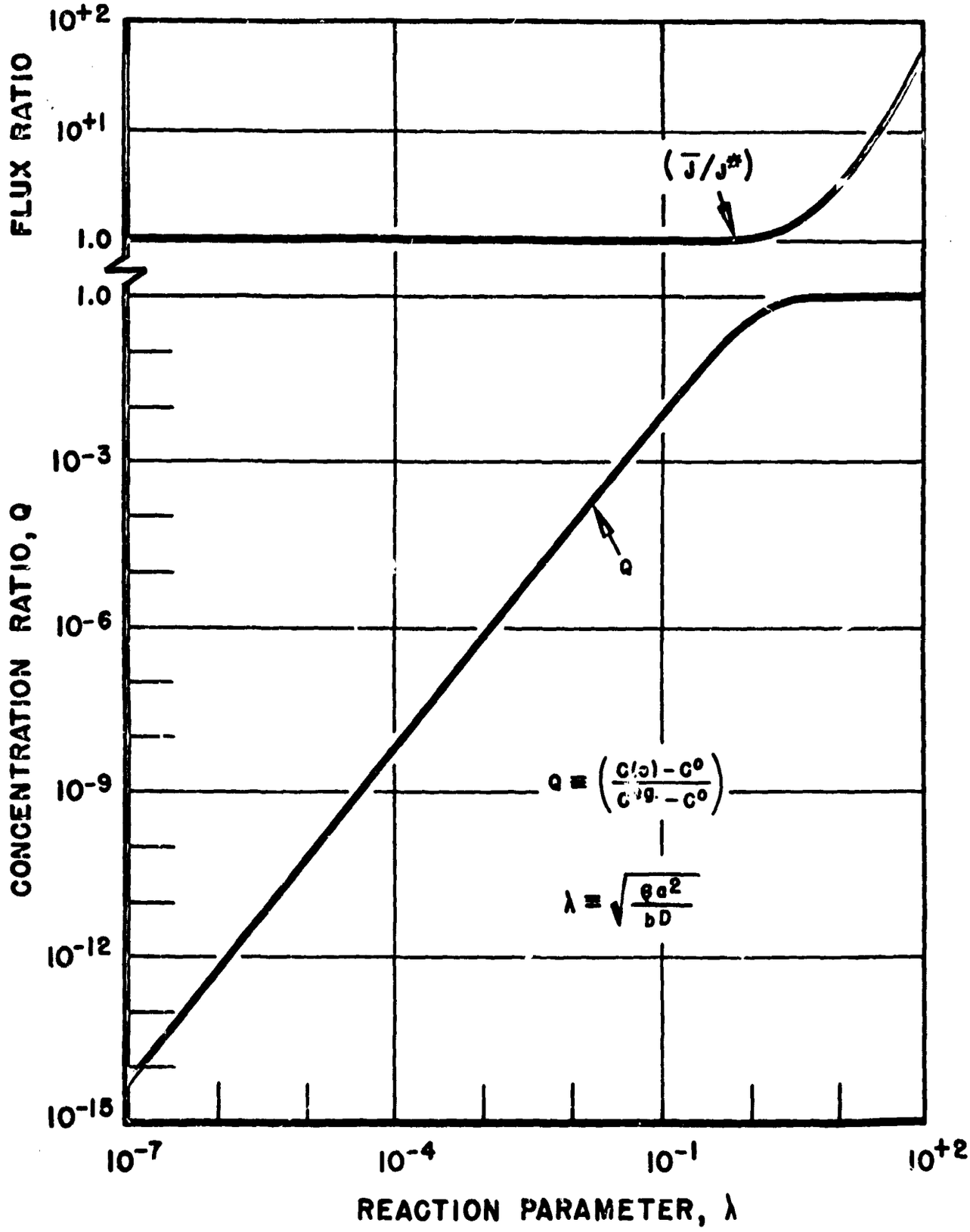

Fig. 37 Dependence of the concentration and flux in a rectangular crack on the flux parameter (transport by simple diffusion).

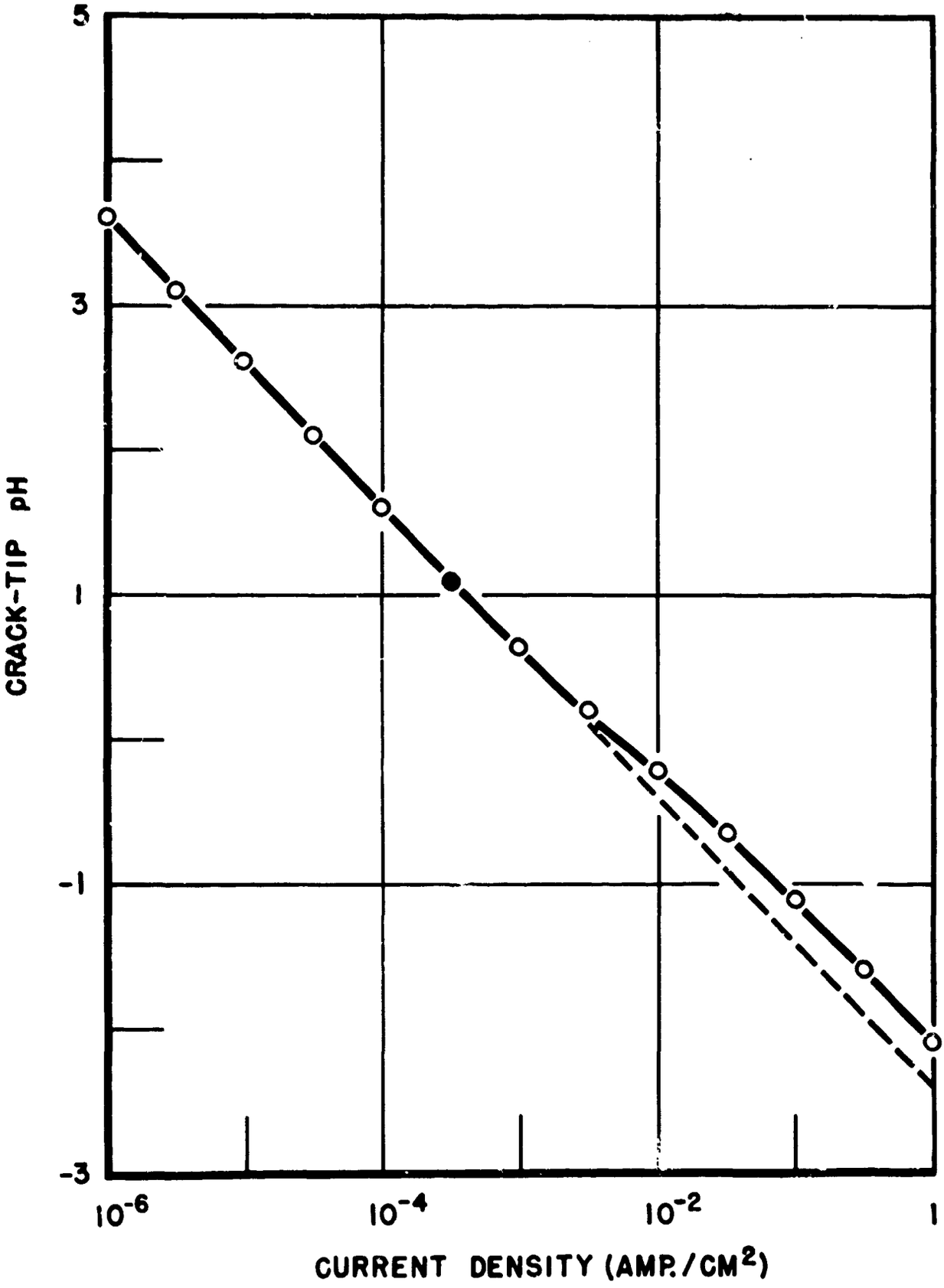

Fig. 38 Variation of the steady-state crack-tip pH with normal current density for a rectangular crack showing the effect of transport by migration.

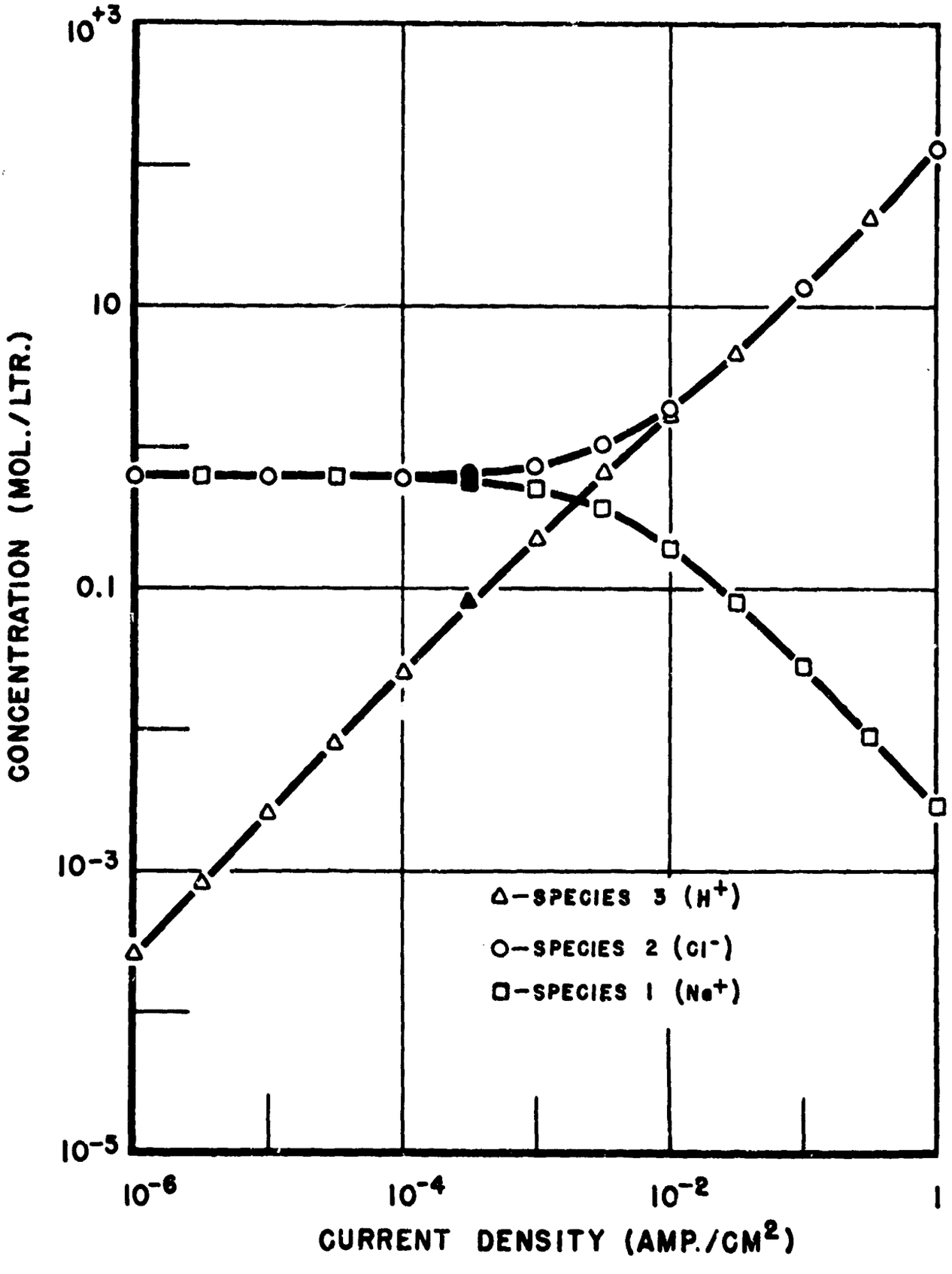

Fig. 39 Variation with normal current density of the steady-state crack-tip composition for a ternary electrolyte in a rectangular crack.

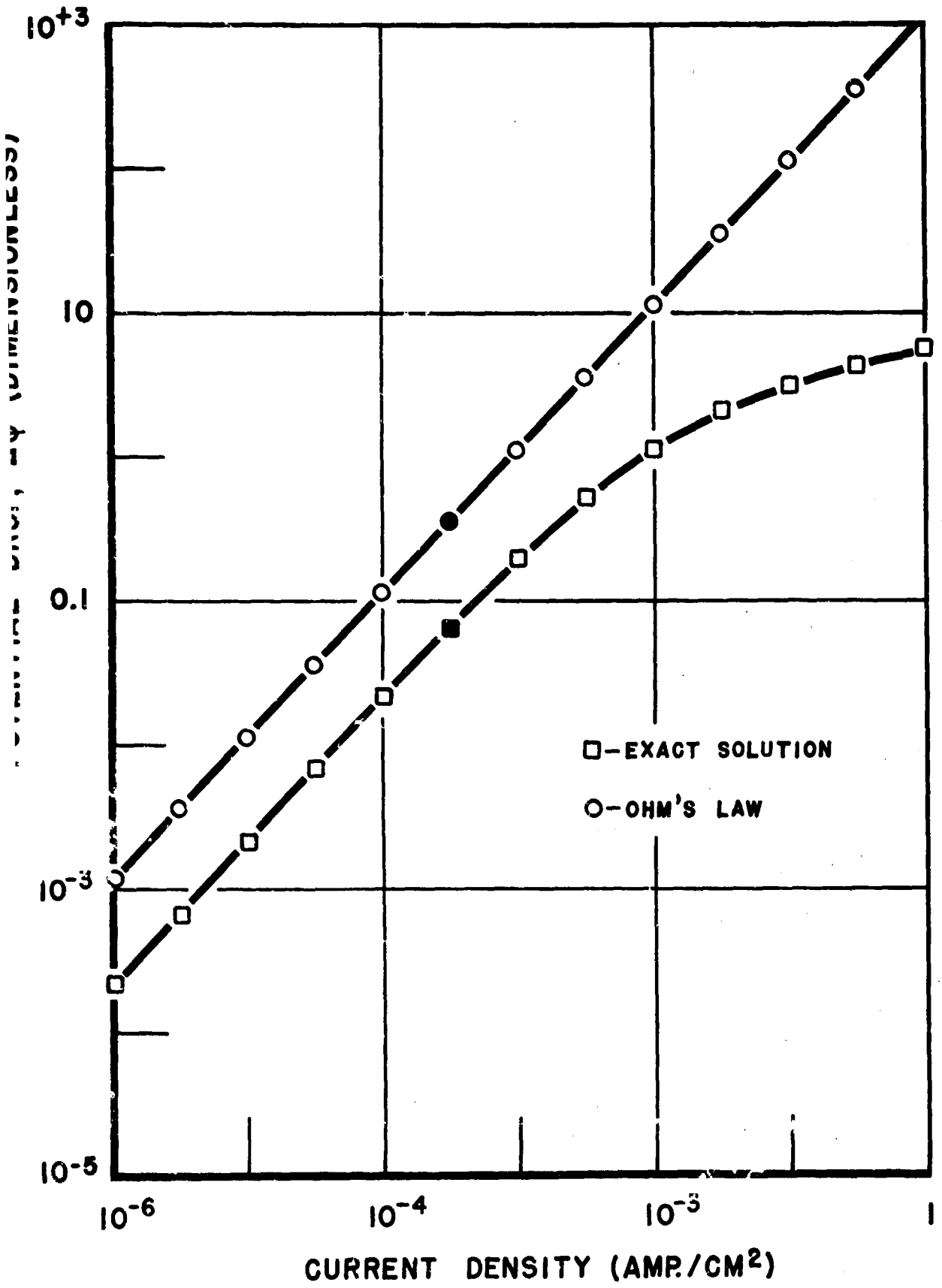

Fig. 40 Variation with normal current density of the potential drop for a ternary electrolyte contained in a rectangular crack.

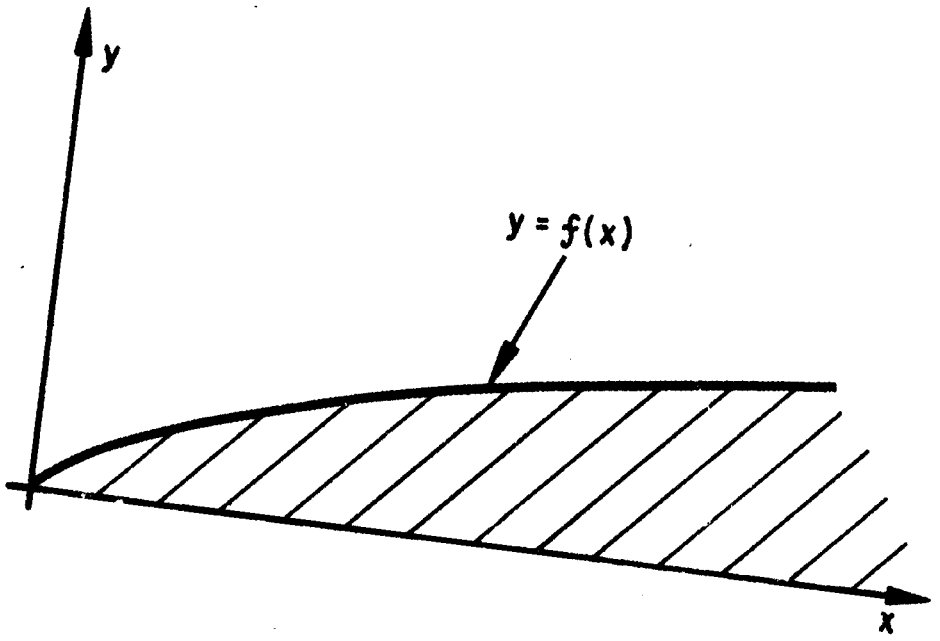

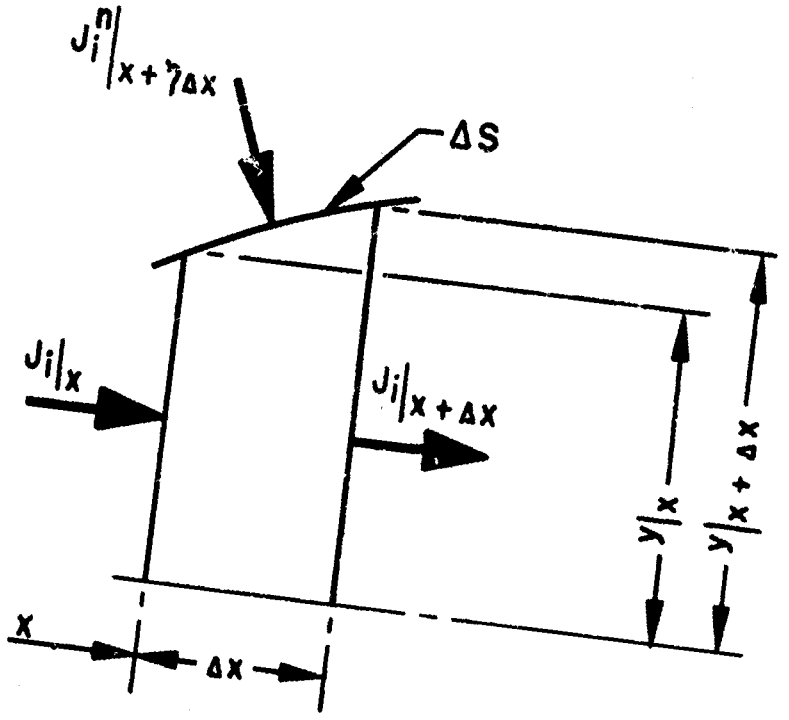

Fig. 41 Crack domain and control volume for the one-dimensional transport analysis.